SERDP

FINAL REPORT

Novel Swellable Ionomers for Enhanced PFAS Sorption and Destruction

Seetha Coleman-Kammula
Brian Coleman
Charles Powley
Science, Technology and Research Institute of Delaware

Pei Chiu
University of Delaware

March 2024

SERDP Project ER22-3415

REPORT DOCUMENTATION PAGE

Form Approved
OMB No. 0704-0188

1. REPORT DATE *(DD-MM-YYYY)*	**2. REPORT TYPE**	**3. DATES COVERED** *(From - To)*
03-15-2024	SERDP Final Report	5/2/2022 - 4/29/2024

4. TITLE AND SUBTITLE
Novel Swellable Ionomers for Enhanced PFAS Sorption and Destruction

5a. CONTRACT NUMBER 22-P-0058

5b. GRANT NUMBER

5c. PROGRAM ELEMENT NUMBER

6. AUTHOR(S) Coleman-Kammula, Seetha; Lyke, Stephen E.; Powley, Charles; Coleman, Brian; Anton, Jessica; Qin, Xiaohuan - STRIDE
Chiu, Pei; Murillo-Gelvez, Jimmy; Buitrago, A. Felipe – University of Delaware

5d. PROJECT NUMBER ER22-3415

5e. TASK NUMBER

5f. WORK UNIT NUMBER

7. PERFORMING ORGANIZATION NAME(S) AND ADDRESS(ES)
Science, Technology & Research Institute of Delaware (STRIDE)
272 Quigley Blvd.
New Castle, Delaware
University of Delaware,
Newark, Delaware

8. PERFORMING ORGANIZATION REPORT NUMBER ER22-3415

9. SPONSORING / MONITORING AGENCY NAME(S) AND ADDRESS(ES)
Office of the Deputy Assistant Secretary of Defense (Energy Resilience & Optimization)
3500 Defense Pentagon, RM 5C646
Washington, DC 20301-3500

10. SPONSOR/MONITOR'S ACRONYM(S) SERDP

11. SPONSOR/MONITOR'S REPORT NUMBER(S) ER22-3415

12. DISTRIBUTION / AVAILABILITY STATEMENT
DISTRIBUTION STATEMENT A. Approved for public release: distribution unlimited.

13. SUPPLEMENTARY NOTES

14. ABSTRACT Cost-effective treatment of per- and polyfluoroalkyl substance (PFAS)-impacted matrices, such as groundwater, would be facilitated if a rapid, high-capacity sorbent could be developed that is regenerable on-site for re-use, producing an aqueous PFAS concentrate that is compatible with an efficient PFAS destruction technology. Preliminary data indicated that ionomers, a class of novel and water-swellable sorbents, might have the required characteristics when combined with hydrothermal alkaline treatment (HALT) for PFAS mineralization to fluoride. This limited-scope project was designed to (1) determine the ionomer's PFAS sorption kinetics and capacity relative to existing commercial sorbents, and (2) evaluate the efficiencies of PFAS desorption from ionomers and their destruction in the resulting concentrate by HALT. Our data strongly support the use of ionomers for sorption and on-site regeneration and destruction of PFAS in contaminated waters. The proposed treatment occurs entirely in water (no alcohol). We recommend a larger-scale study to further develop the ionomer-HALT process for specific above-ground and in situ applications.

15. SUBJECT TERMS Circular Economy, Treatment Train, PFBA, PFBS, PFOA, PFOS, Ionomer, All-aqueous Desorption, Adsorption and Desorption Isotherms, Regeneration, Concentration, Hydrothermal Alkaline Treatment, PFAS destruction

16. SECURITY CLASSIFICATION OF:			**17. LIMITATION OF ABSTRACT**	**18. NUMBER OF PAGES**	**19a. NAME OF RESPONSIBLE PERSON**
a. REPORT	**b. ABSTRACT**	**c. THIS PAGE**			Seetha Coleman-Kammula
UNCLASS	UNCLASS	UNCLASS	UNCLASS	82	**19b. TELEPHONE NUMBER** *(302) 981-5841*

Standard Form 298 (Rev. 8-98)
Prescribed by ANSI Std. Z39.18

KEYWORDS:

Circular Economy, Treatment Train, PFBA, PFBS, PFOA, PFOS, Ionomer, All-aqueous Desorption, Adsorption and Desorption Isotherms, Regeneration, Concentration, Hydrothermal Alkaline Treatment, PFAS destruction

Table of Contents

List of Figures

List of Tables

Abstract

Cost-effective treatment of per- and polyfluoroalkyl substance (PFAS)-impacted matrices, such as groundwater, would be facilitated if we can develop a high-efficiency, high-capacity sorbent that is regenerable on-site for re-use, producing an aqueous concentrate compatible with a practical treatment for complete PFAS destruction. Preliminary data had indicated that ionomers, a class of novel and water-swellable sorbents, might have the required characteristics and can be combined with hydrothermal alkaline treatment (HALT) for PFAS mineralization. This limited-scope project was designed to determine ionomer's PFAS sorption kinetics and capacity relative to commercial sorbents, and to evaluate the desorption and destruction of PFAS in the resulting concentrate.

The ionomers studied contain a high density of cationic amine groups distributed along a cross-linked polymer backbone that controls their swelling. A single ionomer formula was used for most of the testing in this project, while other formulas with different extents of cross-linkage may also be tailor-designed for specific applications. Batch and column sorption and desorption kinetic and equilibrium tests were coupled with HALT experiments using aqueous solutions containing single or multiple model PFAS. Sorption performance of ionomer was compared to those of commercial PFAS sorbents, such as granular activated carbon (GAC) and ion exchange resin (IX), and with literature data for other novel sorbents. Modeling results, supported by short column tests, suggest that repeated cycles of sorption-regeneration operations would be feasible.

Sorption kinetic tests, using PFOA and a mixture of PFBA, PFBS, PFOA and PFOS, showed that sorption to ionomer was significantly faster than to GAC and IX. Sorption of PFOA to ionomer followed a Langmuir isotherm, with a maximum sorption capacity greater than those reported for the other sorbents. Tests using a PFAS mixture showed the sorption capacity of ionomer exceeded that of GAC for all four PFAS and that of an IX resin for PFOA and PFOS. A novel dilute (<1%, w/w) aqueous regenerant was found to be effective at desorbing and recovering the four model PFAS from used ionomer, producing an aqueous concentrate that was conducive to PFAS destruction by HALT. Modeling based on these sorption and desorption data supports repeated sorption-regeneration cycles at high efficiency, with a concentration factor potentially exceeding 1,000. A series of 5-cycle column sorption-regeneration tests showed that ionomer could be re-used effectively after desorption. HALT was applied directly to treat mixed PFAS concentrates and achieved high degrees of mineralization (*ca*. 80 to >95% fluoride recovery) under subcritical conditions. Higher temperatures were required to achieve extensive defluorination than to destroy the parent PFAS, suggesting the formation of a recalcitrant fluorinated intermediate(s).

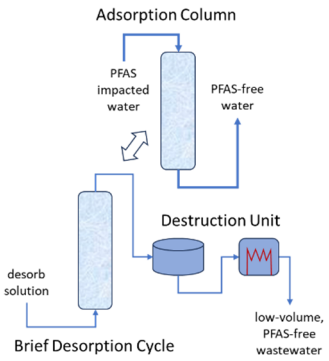

Our results strongly support the use of ionomers for sorption, on-site desorption, and destruction of PFAS in contaminated waters. The proposed treatment can take place entirely in water without the use of alcohol. We recommend that a larger-scale study be conducted to further develop the ionomer-HALT technology for targeted above-ground and/or *in situ* applications.

ABBREVIATIONS AND ACRONYMS:

4:2FTS	4:2 fluorotelomersulfonate
5:3FTCA	2H,2H,3H,3H-perfluorooctanoic acid
6:2FTS	6:2 fluorotelomersulfonate
8:2FTS	8:2 fluorotelomersulfonate
AFFF	aqueous film-forming foams
DFB-CDP	decafluorobiphenyl-cyclodextrin polymer
DNREC	Department of Natural Resources and Environmental Control
DoD	Department of Defense
DOC	dissolved organic carbon
DOM	dissolved organic matter
Ea	activation energy
EPA	Environmental Protection Agency
ESTCP	Environmental Security Technology Certification Program
GAC	granular activated carbon
HALT	hydrothermal alkaline treatment
HFPO-DA	hexafluoropropylene oxide dimer acid
HPLC	high performance liquid chromatography
IDW	investigation-derived waste
IX	ion exchange resin(s)
LC	liquid chromatography (or liquid chromatograph)
MS	mass spectrometry (or mass spectrometer)
NELAP	national environmental laboratory accreditation program
NMR	nuclear magnetic resonance
PDP	proprietary desorption promoters
PEI-f-CMC	poly(ethylenimine)-functionalized cellulose microcrystals
PFAS	per- and poly-fluoroalkyl substances
PFBA	perfluorobutanoic acid
PFBS	perfluorobutane sulfonic acid
PFDA	perfluorodecanoic acid
PFHpA	perfluoroheptanoic acid
PFHpF	perfluoroheptanoyl fluoride
PFHpS	perfluoroheptanesulfonic acid
PFHxA	perfluorohexanoic acid
PFHxS	perfluorohexane sulfonic acid
PFMBA	perfluoro-4-methoxybutanoic acid
PFMPA	perfluoro-3-methoxypropanoic acid
PFNA	perfluorononanoic acid
PFOA	perfluorooctanoic acid
PFOS	perfluorooctanesulfonic acid
PFPeA	perfluoropentanoic acid
PFPeS	perfluoropentanesulfonic acid
PFUnA	perfluoroundecanoic acid
ppb	parts per billion (or µg/L [ng/mL] for aqueous concentrations)
ppt	parts per trillion (or ng/L for aqueous concentrations)
QA	quality assurance

QC	quality control
SERDP	Strategic Environmental Research and Development Program
SON	Statement of Needs
STRIDE	Science, Technology and Research Institute of Delaware
TDS	total dissolved solids
TOC	total organic carbon
UD	University of Delaware

ACKNOWLEDGEMENTS

The authors acknowledge support for this project from the U.S. Department of Defense Strategic Environmental Research and Development Program (SERDP).

Executive Summary

Goal

The Strategic Environmental Research and Development Program (SERDP) has identified under the 2022 Broad Agency Announcement research needs ERSON-22-C4 titled *Treatment of Per- and Polyfluoroalkyl Substance-Impacted Matrices*. The goal of this ***Limited Scope Project*** is to determine whether a class of novel sorbents – swellable ionomers – outperforms conventional sorbents in removing a broad range of PFAS ***and*** can be regenerated on-site for reuse to produce a concentrate that is conducive to PFAS destruction. The proposed treatment can minimize the adverse environmental impacts and maintain the highest value of all resources used from cradle to cradle for as long as possible, following the definition of Circular Economy (U.S. EPA, 2023).

Introduction

Hundreds of DoD sites in the U.S. are impacted by per- and poly-fluoroalkyl substances (PFAS) due to historic use of aqueous film-forming foams (AFFF) for fire suppression since the 1970's. To treat PFAS-impacted waters, such as AFFF-polluted groundwater and aqueous investigation derived wastes (IDW), the standard methods typically involve sorption using granular activated carbon (GAC) or anion exchange resins (IX). While these sorbents are mature and field-proven technologies, they can have slow sorption rates and thus may require long contact/operation times. Furthermore, technologies for the regeneration of these sorbents and destruction of PFAS have multiple drawbacks, ranging from high energy input and greenhouse gas emissions to production of secondary wastes that require additional treatment and/or disposal.

Our project aims to address some of these drawbacks by applying ionomers, a new class of water-swellable polyamine polyelectrolytes that are designed to have granular forms and consist of amine functional groups distributed along a cross-linked organic polymer backbone. We hypothesized that, because the entire molecular structure of a swollen ionomer is accessible to and can interact with PFAS molecules through hydrophobic, van der Waals, and charge interactions, ionomers will exhibit faster kinetics and higher capacities than GAC and IX for PFAS sorption. Additionally, we aimed to develop an alcohol-free method to desorb PFAS for destruction and regenerate ionomers for reuse, without the secondary problems that often plague GAC and IX resins. We selected hydrothermal alkaline treatment (HALT) for PFAS destruction for its non-selective defluorination at high yields and its compatibility with the ionomer operation.

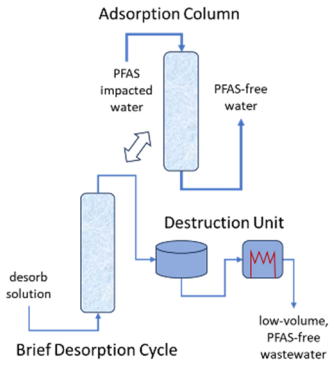

Objectives

To demonstrate ionomers can (1) remove long- and short-chain PFAS from water more effectively than GAC and IX, (2) be regenerated for reuse *in situ* to release sorbed PFAS without using heat or alcohol, and (3) produce an aqueous concentrate that is conducive to HALT for efficient PFAS mineralization.

Technical Approach

We conducted a series of sorption, desorption and defluorination experiments. Sorption and desorption studies and PFAS analysis were conducted at the STRIDE Center for PFAS Solutions (Center) laboratory, and destruction of PFAS in concentrates was conducted at the University of Delaware (UD). Targeted PFAS analysis was conducted using an Agilent high-performance liquid chromatograph (HPLC) triple quadrupole mass spectrometer in the Center's laboratory which is NELAP accredited for the EPA drinking water methods 537.1

and 533. Standard operating procedures adhering to the QA/QC requirements of the EPA Draft Method 1633 were applied. Fluoride was measured using an ion selective electrode.

Mixtures of PFBA, PFBS, PFOA and PFOS, representing two short chain and two long chain PFAS were used. Data were collected on sorption kinetics and capacities of two ionomer grades designated HG-1 and HG-5, the GAC Filtrasorb 400, and the IX CalRes 2301 or 2304, for side-by-side comparison. Where possible, the data were compared with literature data on other PFAS sorbents. Mostly batch, PFAS adsorption and desorption kinetic and equilibrium testing with some column experiments to study regeneration were conducted. Reaction rate constants were calculated applying applicable kinetic models and Langmuir or Freundlich isotherms were applied to capacity data for all three types of sorbents. Various aqueous desorbing reagents were investigated for desorption and concentration. Modeling, supported by short-column tests, projected ionomer performance through repeated sorption-regeneration cycles.

PFAS degradation experiments were conducted under controlled (pH, temperature, and pressure) conditions to measure the rate and extent of PFAS defluorination by HALT. All experiments were carried out using a 0.1-L, high-temperature reactor from Parr Instruments (Parr 4790) equipped with a temperature control unit, a pressure gauge, and a sampling port. Parts containing PTFE were replaced with graphite parts for this work. The reactor was set up and leak-tested in a dedicated HF-resistant fume hood in an environmental engineering laboratory at UD.

Results and Discussion

Adsorption Kinetics in Single-component PFOA Solutions (Task 1a)

PFOA adsorption kinetic tests were performed using ionomers, GAC and IX adsorbents. We found that both the GAC (Filtrasorb 400) and the IX (CalRes 2301) adsorbed 1 µg/L PFOA too slowly for practical measurement at the 10 mg/L dosing used with HG-1 and HG-5. As a result, dosing for GAC and IX resins was increased to 100 mg/L. Initially, the IX sorbed PFOA faster than the GAC but seemed to reach saturation with more PFOA remaining in solution. Even at 10 times lower dosing, both HG-1 and HG-5 removed PFOA from solution one to two orders of

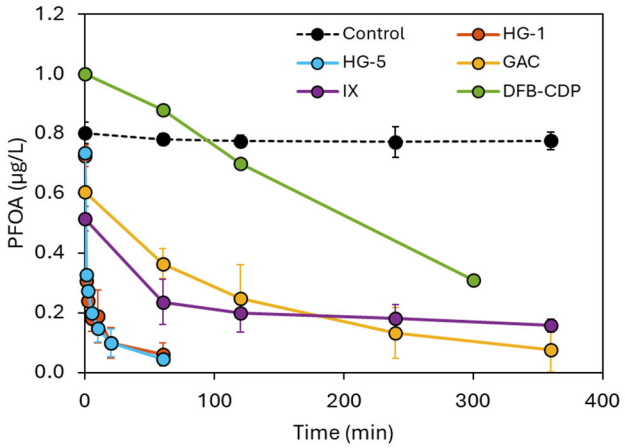

Figure 1 – PFOA adsorption kinetics for two novel ionomers (HG-1 and HG-5) and other sorbents. All sorbent loadings were 10 mg/L except for GAC and IX (100 mg/L). Data represent the average concentration ± one standard deviation of triplicate reactors. All data are from this study except for decafluorobiphenyl-cyclodextrin polymer [DFB-CDP] (Xiao, et al., 2017).

magnitude faster than the GAC and IX resin studied, as can be seen in **Error! Reference source not found.**.

Table 8 lists the parameters determined from the tests reported above along with those reported by Xiao *et al.* for their DFB-CDP, another material (sieved coconut shell activated carbon, CCAC, S_{BET} = 1085 m^2 g^{-1}) that they tested under similar conditions, and for poly(ethylenimine)-functionalized cellulose microcrystals – PEI-f-CMC (Ateia, et al., 2018). Both HG-1 and HG-5 were found to adsorb PFOA much faster than the comparison materials.

Table 1 – Pseudo-second Order Rate Parameter Comparison (conditions in text)

Material	**k_{obs}, g/mg/hr**
HG-1	1700
HG-5	1200
CCAC (Xiao, et al., 2017)	600
PEI-f-CMC (Ateia, et al., 2018)	12.8
DFB-CDP (Xiao, et al., 2017)	2.9

Adsorption Kinetics in a 4-PFAS Mixture (Task 1a)

Figure 2 a, c and d show the rates of removal of a four PFAS mixture (PFBA, PFBS, PFOA and PFOS; 10 ppb each) by 100 mg/L of ionomer HG-1, granular activated carbon Filtrasorb 400, and anion exchange resin CalRes 2304, respectively. First or second order reversible model fits are included to aid visualization. The 1st order model fits the shorter-chain PFAS data while the 2nd order reversible model is a better fit to some of the longer chain data. **Figure 2 b** shows rates of removal by 100 mg/L of ionomer from initial PFAS concentrations of 100 ppb each.

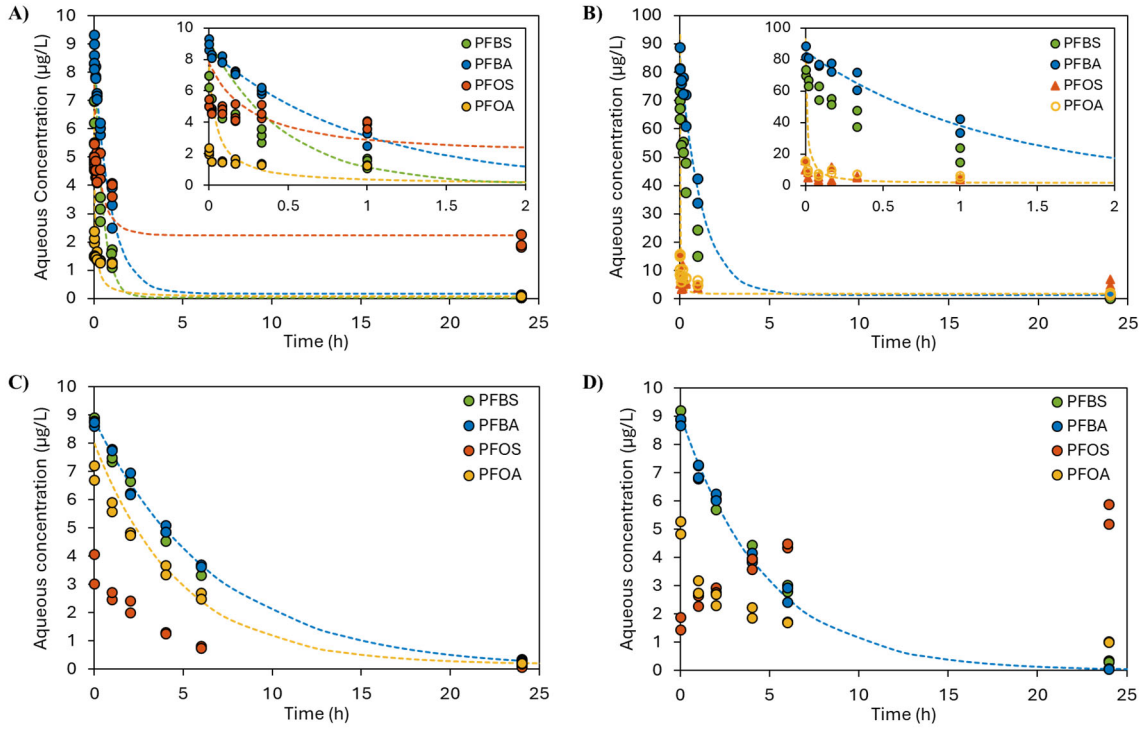

Figure 2 – Sorption kinetics of a 4-PFAS mix onto (A. and B.) HG-1, (C.) GAC and (D.) IX. *The sorbent loading was 100mg/L in all cases. The dashed lines represent the 1st and 2nd order*

reversible model fits for short- and long- chain PFAS, respectively, except for PFOA in panel C. (1st order model).

Faster adsorption kinetics of the ionomer can be seen qualitatively by comparing the plots. **Figure 3** compares first order reversible rate constants calculated from the initial 10 ppb data.

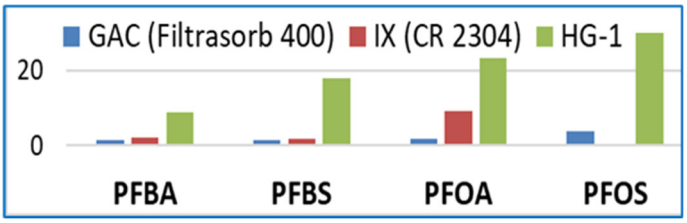

Figure 3 – First Order Reversible Rate Constants (L/g/hr) in Four PFAS Mixtures at 10 mg/L initial Concentrations.

PFOA Adsorption Capacity (Task 1b)

In addition to the adsorption kinetics comparison, a PFOA adsorption isotherm for ionomer HG-1 was determined and compared with published isotherm data. **Figure 4Error! Reference source not found.** illustrates the comparison. Over a broad concentration range, we measured adsorption capacity higher than all published reports we had located. Two sets of data show that HG-1 can sorb up to 18% its mass (175 mg/g) in PFOA, a capacity that is significantly greater than the comparison sorbents.

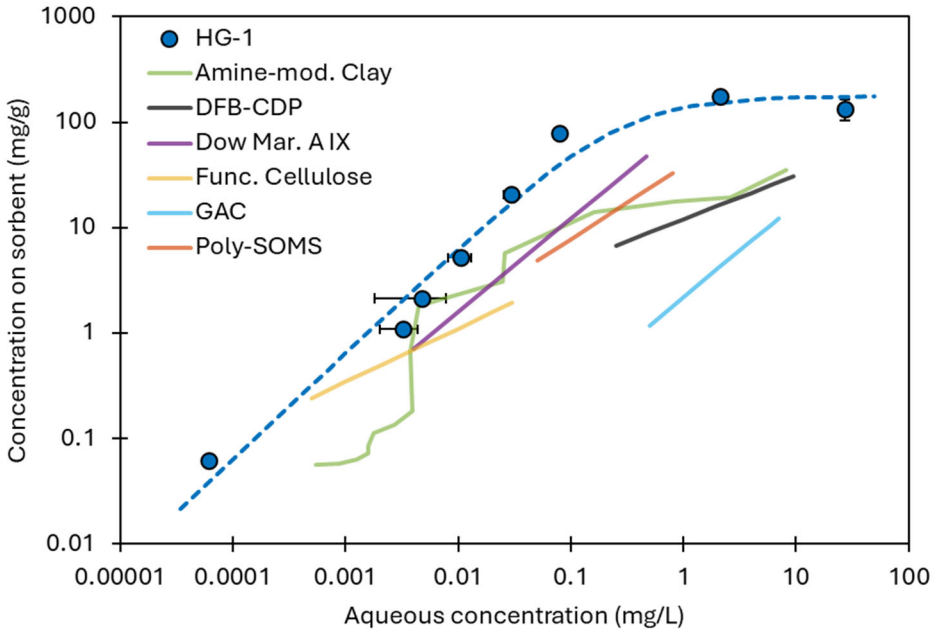

Figure 4 – **Ionomer Isotherm.** PFOA sorption isotherms for the ionomer HG-1 and other sorbents: decafluorobiphenyl-cyclodextrin polymer [DFB-CDP] *(Xiao, et al., 2017)*, granular activated carbon [GAC] *(Zhang, et al., 2016)*, functionalized cellulose *(Ateia, et al., 2018)*, surfactant amine-modified clay *(Yan, Wang, & Liu, 2021)*, polymer-infused swellable organically modified silica [poly-SOMS] *(Stebel, et al., 2019)*, Dow Marathon anion exchange resin *(Chularueangaksorn, Tanaka, Fujii, & Kunacheva, 2014)*. Data are the average ± one

standard deviation of triplicate (HG-1) experiments. The dashed line represents the Langmuir isotherm fit to the data.

Capacity for Adsorption of 4 PFAS (Task 1b)

A chloride form of HG-1 ionomer – HG-1(Cl) – was used for capacity studies in the 4 PFAS mixture. It is the same copolymer as the HG-1 used to produce previously-reported results, but with the bromide ion, that results from the bromide monomer, mostly removed, and replaced by chloride ion. HG-1(Cl) has similar fast adsorption kinetics, a higher swell factor, and more capacity than the un-exchanged ionomer, which we can designate as HG-1(Br). Results of the 4 PFAS capacity measurements for the HG-1(Cl) ionomer are presented in **Figure 5**.

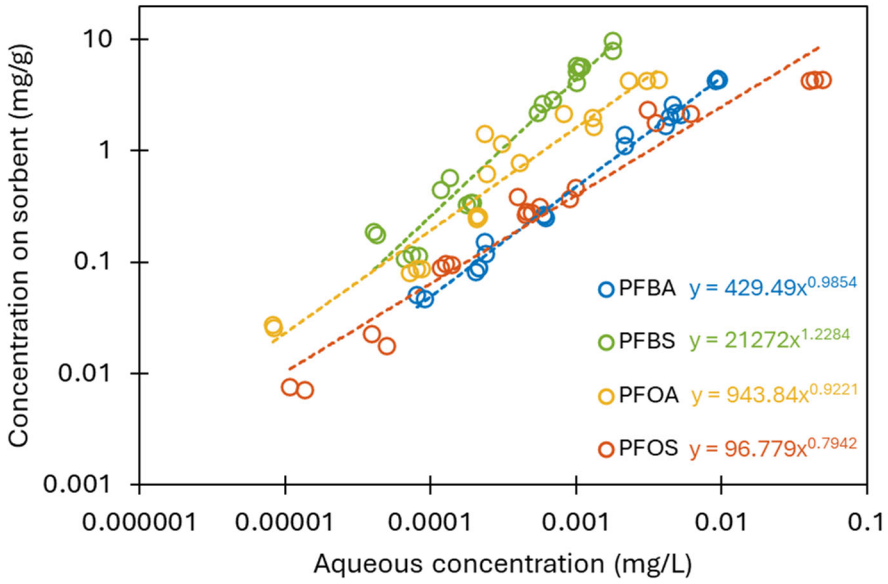

Figure 5 – Adsorption Capacity Data and Freundlich Isotherm Fits for a 4-PFAS mix.

The linear dependence of loading on concentration with a slope of ~1 on a log-log scale for each PFAS is consistent with the low concentration end of a Langmuir isotherm or with a Freundlich isotherm where n = 1. Similar plots and isotherm fits for the comparison GAC and IX sorbents allowed interpolation to quantity adsorbed at 1 ppb of each PFAS. **Table 2** compares the measured capacities of the three sorbents at 10^{-3} mg/L (1 ppb). The table shows HG-1 capacity exceeding that of the tested GAC for each PFAS in the mixture and exceeding that of the IX for PFOA and PFOS.

Table 2 – Capacity Comparison Interpolated from Isotherm Fits to 4-PFAS Data

	mg/g PFAS loading on sorbents at 10^{-3} mg/L		
	GAC F400	IX CR2304	HG-1(Cl)
PFBA	0.26	2.59	0.48
PFBS	0.60	>10	4.39
PFOA	0.35	0.17	1.62
PFOS	0.23	0.02	0.40

In summary, adsorption kinetics for ionomer was significantly faster than for commercial GAC and IX materials with PFOA alone and with mixtures of the four PFAS. PFOA adsorption on ionomer was shown to follow a Langmuir isotherm with a higher adsorption capacity than any comparable data we found in the literature. Our experiments showed ionomer adsorption capacity for the four PFAS exceeding that of GAC and exceeding that of a benchmark IX for PFOA and PFOS. Testing with AFFF-impacted well water (see full report* Figure 25 *and* Figure 26*) showed ionomer adsorbing all 16 PFAS, with adsorption of long-chain PFAS less impacted by co-contaminants than that of PFBS and PFBA.

Batch Desorption Experiments (Task 2)

Four sets of batch adsorption-desorption experiments were conducted to begin developing a technology to desorb PFAS from ionomer. Mixtures of PFBA, PFBS, PFOA, and PFOS were again used as model PFAS. Due to the negative environmental impacts and costs associated with methanol based PFAS extractants, we investigated aqueous reagents (no methanol) to desorb PFAS from our ionomers. Our investigation of several all-aqueous desorption reagents identified two proprietary desorption promoters (PDP A and PDP B) that significantly enhance the effectiveness of aqueous solutions for desorbing the PFAS mixture. The experiments identified PDP A with added NaCl as a preferred desorption solution for effectively removing PFAS from HG-1. Results of two such experiments are presented in **Table 3**.

Table 3 – Desorption of 4-PFAS by Aqueous Desorption Solution

		PFBA	**PFBS**	**PFOA**	**PFOS**	
Desorb solution	Sorbent type used	**Percent of PFAS desorbed based on PFAS sorbed**				**Eq. time**
0.2% PDP A + 0.5% NaCl	HG-1(Cl) – 14.3 mg (20 mL -> 20 mL)	84.5	108	73.6	51.1	1hr
		86.2	90.0	77.7	73.3	22hrs
	HG-1(Cl) – 13.1 mg (250 mL -> 20mL)	80.9	73.0	48.8	23.7	1hr
		91.7	97.4	79.6	59.3	24hrs

Flow-through Desorption Experiments (Task 2)

As part of the transition from bottle-shaking (i.e., from batch tests to small column testing), a set of experiments was conducted featuring bottle adsorption followed by flow-through desorption. Results of the experiment are presented in **Error! Reference source not found.**. For three of the PFAS, aqueous desorption efficiency in the flow-through mode was similar or higher than previous, batch desorption results, while for PFOS, desorption was somewhat less efficient compared with previously-reported 24-hour batch desorption experiments. This would indicate that desorption kinetics are slower for PFOS than for the other three PFAS tested, consistent with earlier observations comparing 1- and 22-hour batch desorption times.

Table 4 – Results of Batch Adsorb/Flow-through Desorb Tests

Sample		**PFBA**	**PFBS**	**PFOA**	**PFOS**
Name	Comment	ng/mL	ng/mL	ng/mL	ng/mL
4 PFAS starting mixture	Stock Solution	60.8	92.1	54.1	60.2
		percent adsorbed			
HG-1(Cl), 180-425µm		98.2%	99.4%	99.0%	96.4%
		percent desorbed			
HG-1(Cl), 180-425µm		99%	98%	78%	44%

Projecting Column Adsorption and Desorption Performance from Batch Data (Task 2)
The following analysis was conducted to determine whether the desorption performance found in preliminary, batch desorption data could be sufficient to realize an efficient column desorption system with aqueous regeneration into a concentrated solution for destruction. **Figure 6** includes batch adsorption isotherm data reported earlier. The figure also includes batch, aqueous desorption data from two sets of tests, such as those reported above, using PDP A aqueous desorption solution. The plot is based on the idea that after a day of batch desorption, the sorbent reaches a new equilibrium with the desorption solution which can be represented as a desorption isotherm. We have found that HG-1(Cl) adsorption isotherms have slopes close to one on this type of plot. Based on our understanding of how PDP functions, we expect a desorption isotherm with a similar slope. Although there is scatter in the desorption equilibrium data, the plot shows likely adsorption and desorption isotherm lines located to represent the PFOA data. In the plot, we can see that at the same sorbent loading, switching to the aqueous desorption solution can provide more ***than three orders of magnitude increase in equilibrium PFAS concentrations.***

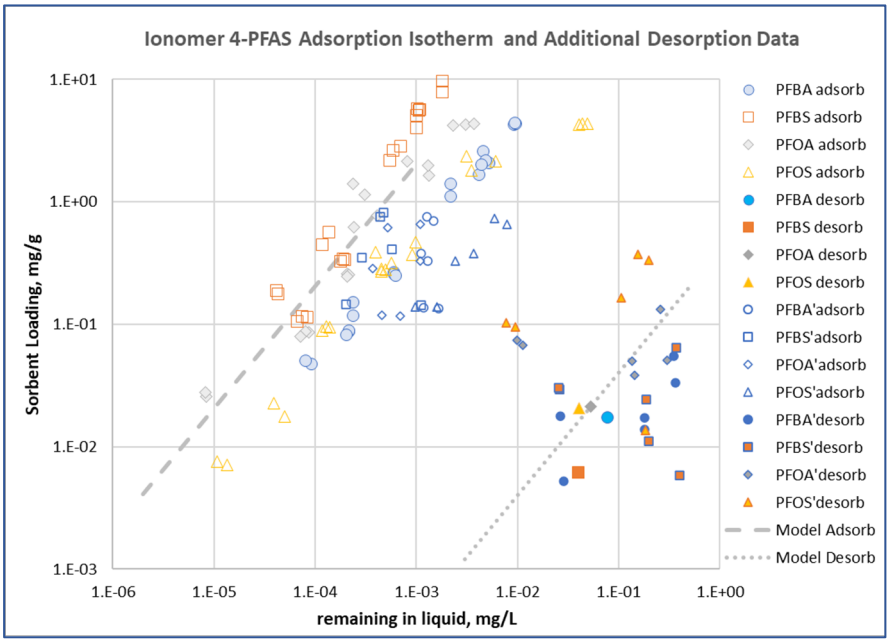

Figure 6 - Adsorption - Desorption Equilibrium Data Compared with PFOA Modeling Isotherms. *Primes in the legend indicate a second data set.*

Using the equilibrium isotherm lines shown in **Figure 32**, together with previously measured adsorption kinetics and desorption rate constants estimated from timed desorption data such as that in **Table 3**, a relatively simple model of adsorption column performance was developed (see the body of this report). The model follows the column through multiple cycles of adsorption and countercurrent regeneration by aqueous desorption solution settling to a steady state condition in a few cycles. ***The model projects a 150-day adsorption cycle before PFOA breakthrough followed by a 6-hour regeneration cycle that produces an aqueous solution concentrated by a factor approaching 3000 times the 50 ppt PFOA adsorption feed, using practical adsorption bed depth and velocities.*** Although the model results are encouraging, they represent a projection from limited, batch data, and should be considered only indicative of what might be found with future column adsorption and desorption testing and development.

In summary, the presented analysis shows that adsorption and all-aqueous desorption performance measured in batch experiments appears sufficient to project a flow system comprising a regenerable adsorption column, operable in a cycle, efficiently removing PFAS and producing concentrate for destruction. More precise measurements of desorption equilibrium and kinetics, and studies to develop and measure column performance are needed.

Demonstration of Ionomer Re-use After Desorption (Task 2)

A series of small column tests was designed to test how well ionomer can adsorb additional PFAS after desorption. **Table 15** presents the results of the test series. We can see in the table that incomplete desorption may have hindered subsequent PFOS adsorption, but that adsorption performance remained very good through the 5 cycles for the other three PFAS. While future work will aim to demonstrate reverse-flow desorption with concentration from large adsorption to small desorption volumes, and plain water rinse, this series of tests shows us that the desorb solution does not irreversibly degrade the ionomer, so that multiple re-uses after regeneration are possible.

Table 5 – Results of Repeated Adsorption and Desorption Tests with HG-1(Cl) Ionomer

	% Adsorbed from ~250 ppb each PFAS					% Desorbed by 20 mL aqueous solution			
	PFBA	PFBS	PFOA	PFOS		PFBA	PFBS	PFOA	PFOS
Cycle 1	100.0	100.0	99.9	93.2		120.2	98.2	97.8	82.3
Cycle 2	98.9	99.8	99.4	88.7		104.7	118.6	104.8	75.7
Cycle 3	99.6	99.3	95.7	44.3		106.4	90.5	104.2	92.2
Cycle 4	99.9	99.3	94.4	39.7		119.3	96.8	106.7	112.3
Cycle 5	100.0	99.9	98.7	68.7		107	95.9	105.9	88.2

In summary, ionomers were shown to be efficient, high-capacity PFAS adsorbents that can be regenerated by aqueous solutions and re-used. We discovered that neutral additives, our proprietary desorption agents, are effective at less than 1 wt% in water to effect desorption. Modeling work based on batch adsorption and desorption rate and equilibrium data, supported by a 5-cycle reuse test, indicate that ionomer may have the required properties for use in an all-aqueous column adsorption and regeneration system, producing a PFAS concentrate suitable for direct PFAS destruction using methods such as HALT.

Mineralization of Model PFAS by HALT (Task 3)

The extent of PFAS mineralization by HALT, determined based on fluoride yield, as a function of temperature for the 4 model PFAS are shown in **Figure 7**. All experiments were performed in 1M NaOH for 1 hour with an initial PFAS concentration of 0.1 mM each. Defluorination was limited at ≤300 ºC but increased markedly at 300 ºC and further to 80–90% at 360 °C for all four PFAS. ***The same defluorination efficiencies were obtained regardless of whether the four PFAS were tested individually or in combination***. This indicates no competition or inhibition occurred among the different PFAS being treated by HALT. Hence, ***the higher the combined PFAS mass is in a concentrate, the more cost-efficient the HALT process is.*** This is a major advantage of HALT.

We note that PFOA and PFBA were degraded within minutes even at 250 ºC. Therefore, the higher temperatures and longer treatment times were needed to degrade not the parent compounds but an unknown and highly fluorinated intermediate(s) that were more refractory than the parent PFAS.

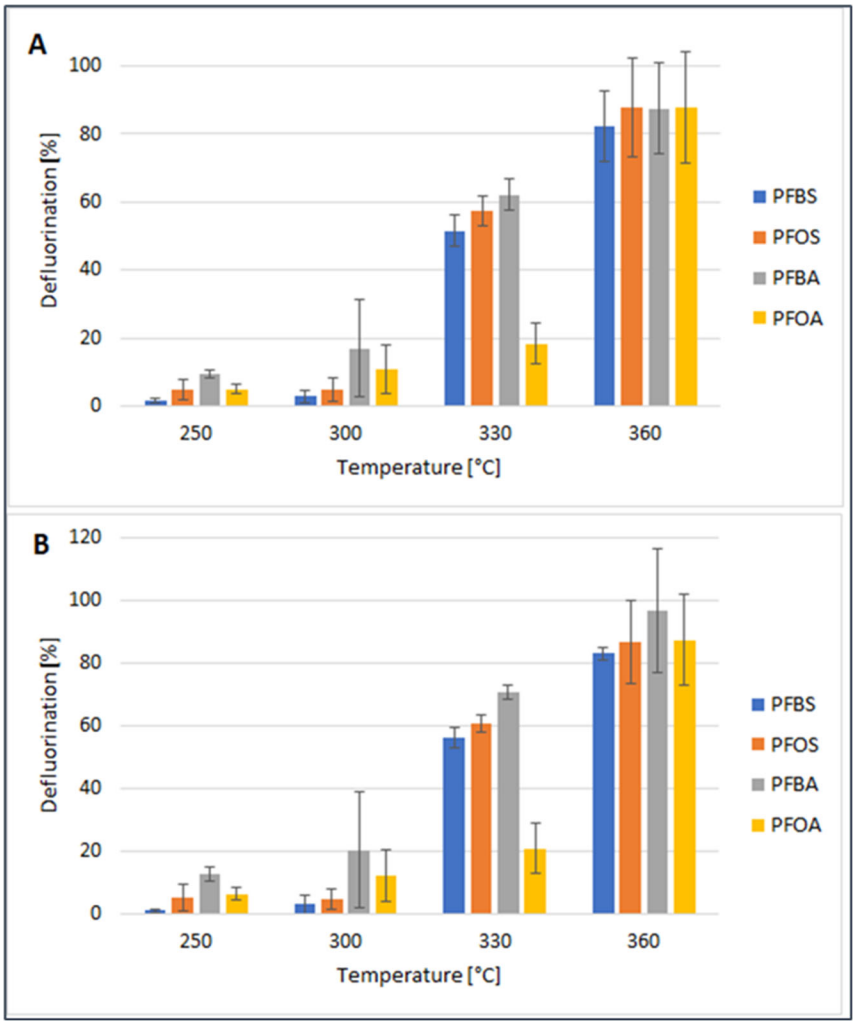

Figure 7 - Percent defluorination for four model PFAS following HALT treatment for 1 hour in 1 M NaOH. *Error bars represent 1 standard deviation based on 4 samples obtained from 2 separate experiments (and 6 samples from 3 experiments for PFOA).*

To assess the effect of the proprietary desorption promoters (PDP A and PDP B) on the performance of HALT, additional experiments were conducted in aqueous solutions that mimicked ionomer regenerants containing PDP A or PDP B and desorbed PFAS (0.1 mM, or *ca*. 21–50 ppm each). The fluoride yields from the degradation of PFAS mixture with and without PDP A or PDP B are shown in **Figure 8**. Consistent with our prior results (80–90%), the extent of defluorination for the four PFAS combined was 84.5±0.9% in the absence of PDP. The percent defluorination decreased to 77.4±1.1% and 71.4±3.6% in the presence of 0.2% PDP A and PDP B, respectively. The adverse effect of PDP on PFAS defluorination, while small (*ca*. 7% and 13%), is likely real, as it has been observed repeatedly in multiple replicate experiments. The reason for the lower fluoride yields is unknown but may involve protection/shielding of dissolved PFAS molecules by PDP A and PDP B from the attack by hydroxide ions. Although somewhat slowed in the presence of the desorption promoters, these results show HALT can still effectively mineralize PFAS in aqueous concentrates from ionomer regeneration, though a slightly higher temperature and/or a longer treatment time may be necessary to achieve the same degree of defluorination in the presence of either PDP.

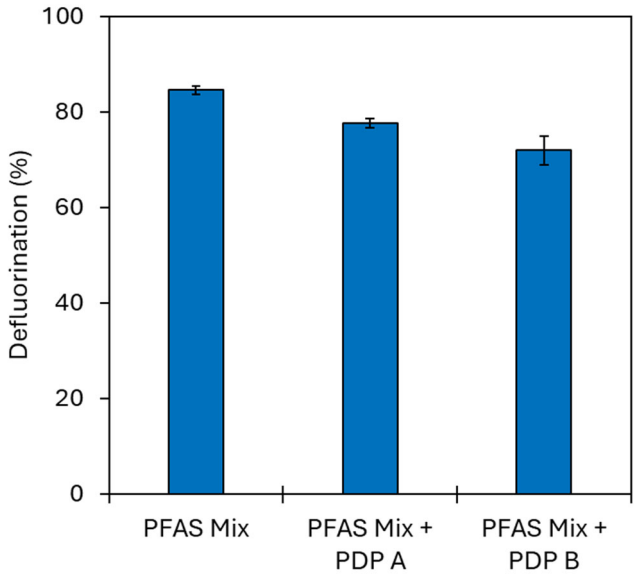

Figure 8 – Percent defluorination for a PFAS mixture (0.1 mM each of PFOA, PFBA, PFOS, and PFBS) following HALT treatment at 360 °C for 1 hour in 1 M NaOH. *Error bars represent one standard deviation based on triplicate measurements.*

Implications for Future Research and Benefits

Data developed in this project support the use of water-swellable ionomers for rapid and efficient PFAS sorption, solvent-free desorption and on-site regeneration, and production of aqueous PFAS concentrates for direct mineralization by HALT. Future research and development of this process is envisaged at both laboratory- and pilot-scale prior to field demonstration and deployment. Lab-scale studies are necessary to assess a broader range of PFAS and determine range-of-effectiveness in the presence of co-contaminants such as DOC, Fe, Mn, chloride, sulfate, (bi)carbonate, etc. Extended column sorption and regeneration studies are necessary to determine the concentration factors and re-use cycles. Semi-commercial scale synthesis of ionomer, via working with a toll manufacturer, would be an important next step for cost estimation of future pilot-scale studies and field demonstrations. We envision that stationary systems and mobile units based on the ionomer-HALT technology can be developed for the treatment of liquid IDW and PFAS-laden wastewaters and groundwaters.

Our swellable ionomers can offer faster and higher-capacity sorption of PFAS from contaminated waters – a potential treatment/remediation system that could meet the requirements of a circular economy, using the green chemistry principles to sorb, desorb, and mineralize PFAS. Our ionomers do not contain or use fluorinated chemicals, unlike some of the new sorbents developed for PFAS removal. Depending on the target application, ionomers can be custom prepared in the granular form for a packed bed, or in the colloidal form for injection into impacted porous media. The all-aqueous ionomer regenerant solution avoids the use of methanol, lowering costs and reducing secondary wastes. Unlike the other destructive methods, HALT does not require a surface, interface, UV photon, or reactive radicals to operate, is not limited by mass transfer, and does not generate toxic byproducts (e.g., perchlorate). The proposed ionomer-HALT technology may simplify and improve PFAS sorption, reduce treatment time and cost, and achieve high rates of mineralization with minimal environmental impact.

Objective

The Strategic Environmental Research and Development Program (SERDP) has identified under the 2022 Broad Agency Announcement research needs ERSON-22-C4 titled *Treatment of Per- and Polyfluoroalkyl Substance-Impacted Matrices*. The goal of this ***Limited Scope Project*** is to determine, whether a class of novel sorbents – swellable ionomers – outperforms conventional sorbents in removing a broad range of PFAS ***and*** can be regenerated and the PFAS fully mineralized in an integrated process without negative environmental impacts to maintain the highest value of all resources used from cradle to cradle as long as possible following the definition of Circular Economy (U.S. EPA, 2023). This addresses the ERSON objectives of developing cost-effective treatment for PFAS-impacted matrices such as groundwater, and of developing approaches that provide complete destruction of PFAS from spent media and regeneration of spent media with ancillary waste streams that are easily managed. Proving the combined concepts of adsorption, regeneration and destruction in laboratory testing should pave the way for further development of the sorbent for use in specific, practical applications.

Background

Hundreds of DoD sites in the U.S. are impacted by per- and poly-fluoroalkyl substances (PFAS) due to historic use of aqueous film-forming foams (AFFF) for fire suppression since the 1970's. PFAS-based formulations have proved to be the most effective, and recent and current formulations still use fluorinated surfactants. AFFF from extinguishing fires and firefighting training contaminates groundwater through runoff. For instance, 19 wells on the Delaware Air National Guard site in New Castle County, Delaware surrounding our Center have been found to be contaminated with PFOS and PFOA with one well having 34,000 ppt PFOS and 18,000 ppt PFOA (AECOM, 2016), (DNREC, 2015).

To treat PFAS-impacted waters, such as AFFF-polluted groundwater and aqueous investigation derived wastes, the standard methods usually involve sorption using granular activated carbon (GAC) or anion exchange resin (IX) as sorbent. These methods have several shortcomings. While GAC and IX are mature and field-proven technologies, they have slow adsorption rates and hence require long contact/operation times (McCleaf, et al., 2017), (Appleman, et al., 2014), (Ochoa-Herrera & Sierra-Alvarez, 2008), (Hansen, Borresen, Schlabach, & Cornelissen, 2010). In addition, GAC is not effective in removing branched and short-chain PFAS, (Ross, et al., 2018), (U.S. EPA, 2017) whereas IX are ineffective in treating PFAS solutions containing competing ions (Woodard, Berry, & Newman, 2017), (Zaggia, Conte, Falletti, Fant, & Chiorboli, 2016). Furthermore, used GAC needs to be transported off-site for thermal regeneration (Watanabe, Takata, Takemine, & Yamamoto, 2018), (Xiao, et al., 2020), which is inconvenient, time consuming, and expensive. Single-use IX need to be incinerated or landfilled as hazardous wastes, whereas reusable IX processes produce PFAS-laden brines and alcohol solutions, which complicate or prevent subsequent destruction of PFAS (Emery, Kempisty, Fain, & Mbonimpa, 2019). Although several novel sorbents, such as amine-functionalized materials, have been proposed and some show promise (Ateia, Alsbaiee, Karanfil, & Dichtel, 2019), (Ateia, et al., 2019), (McCleaf, et al., 2017), many of them are still in the research and development stage, and some would suffer the same problems listed above for GAC and IX.

Our Ionomers are solid water-insoluble polyelectrolyte polymers in granular form and consist of amine functional groups distributed along an organic polymer backbone. They do not have polymeric supports such as polystyrene or polyacrylic resins as is the case with IX. The entire

molecular mass of our ionomers – inside and on the surface – can interact with PFAS through hydrophobic and ionic interaction, offering potential for fast kinetics and high capacity for sorption. The hydrocarbon units of the ionomer offer non-ionic interactions (hydrogen bonding and Van-der-Waals) and the amine sites offer ionic interaction with the tail and head of the PFAS, respectively. Our ionomers are made in a single step from commercial monomers that do not contain fluorine or involve use of fluorinated chemicals. By choosing monomers of different sizes, degrees of branching, and type and content of charged functional groups, we can control the charge type and density, making them attractive for studying their performance to sorb short- vs. long-chain, and negatively vs. positively charged PFAS.

Preliminary experiments had shown that alkaline, aqueous solutions could release adsorbed PFAS from ionomers. Hydrothermal alkaline treatment (HALT) has been shown to degrade PFAS in aqueous and solid wastes (Wang, et al., 2022), and was selected for investigation as a means to destroy PFAS released from, and/or adsorbed on, our ionomers.

One key property of our ionomers makes them unique. They swell and shrink in water in response to pH change, which is expected to result in reversible uptake and release of sorbates such as PFAS.

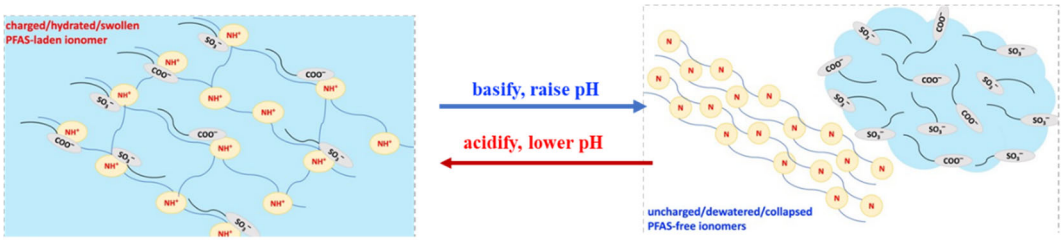

Our ionomers have been manufactured on a semi-commercial scale in existing chemical manufacturing plants for a different market. In association with that work, ionomer HG-1 was shown to be non-toxic (Appendix 2). Once proven effective and advantageous, upscaling and transition into large-scale application can proceed quickly without significant investment in R&D or manufacturing.

Task 1a – Relative Rates of Sorption

Adsorption and desorption studies (Tasks 1 and 2) were conducted at the STRIDE Center for PFAS Solutions laboratory. Materials, methods, results, and discussion for this portion of the project will be presented here, followed by the same headings for hydrothermal alkaline treatment studies on destruction of PFAS concentrate, which were conducted at the University of Delaware.

Materials and Methods

Sorbents used in these tests were as follows. Calgon Filtrasorb 400 GAC, Calgon CalRes 2301 macro-porous, strong base anion exchange resin, CalRes 2304 gel-type, strong base anion exchange resin, and two ionomers designated HG-1 and HG-5. Our ionomers are organic polyelectrolytes that consist of ionic functional groups distributed along an organic polymer backbone. HG-1 was synthesized in our laboratory from hexamethylene diamine and dibromodecane. HG-5 was synthesized from 600 molecular weight polyethyleneimine and dibromodecane. We describe the structural features which contribute to the faster rates and higher

capacity for sorption of PFAS in more detail below. Synthesis conditions and more information about our ionomers can be found in Appendix 2.

Targeted PFAS analyses were conducted using an Agilent Technologies Model 1290 Infinity II Liquid Chromatograph interfaced to an Agilent Model 6495C triple quadrupole mass spectrometer in our laboratory which is NELAP accredited for the EPA drinking water methods 537.1 and 533. Standard operating procedures adhering to the QA/QC requirements of the EPA Draft Method 1633 were applied.

Kinetic data were collected in batch, agitated adsorption tests. Conditions were selected to be similar to the lower-concentration kinetic measurements reported by Xiao, *et al.* in their report on PFAS adsorption by β-cyclodextrin polymer cross-linked with decafluorobiphenyl (DFB-CDP), (Xiao, et al., 2017). Tests were conducted at ambient temperature with vigorous agitation, which was interrupted at timed intervals to remove samples of the supernatant liquid for PFOA analysis by LC/MS/MS. Three such tests were conducted with each adsorbent.

Ionomer Characterization by NMR

We used solid state NMR (high field, magic angle spinning) to characterize ionomer HG-1 by studying the environment of its nitrogen atoms. Results confirmed that our ionomers are polymeric amines with alternating blocks of hydrocarbon units between amine sites. An example general structure is shown in

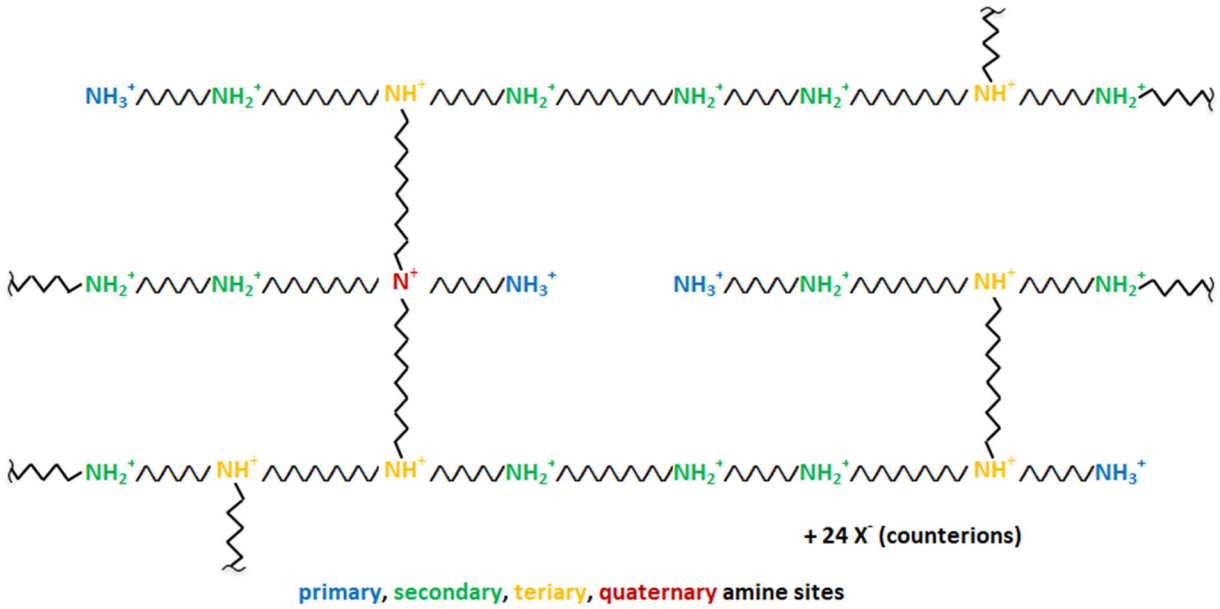

Figure 9. The ionomers consist of a three-dimensional network of which the figure is representative, but not definitive.

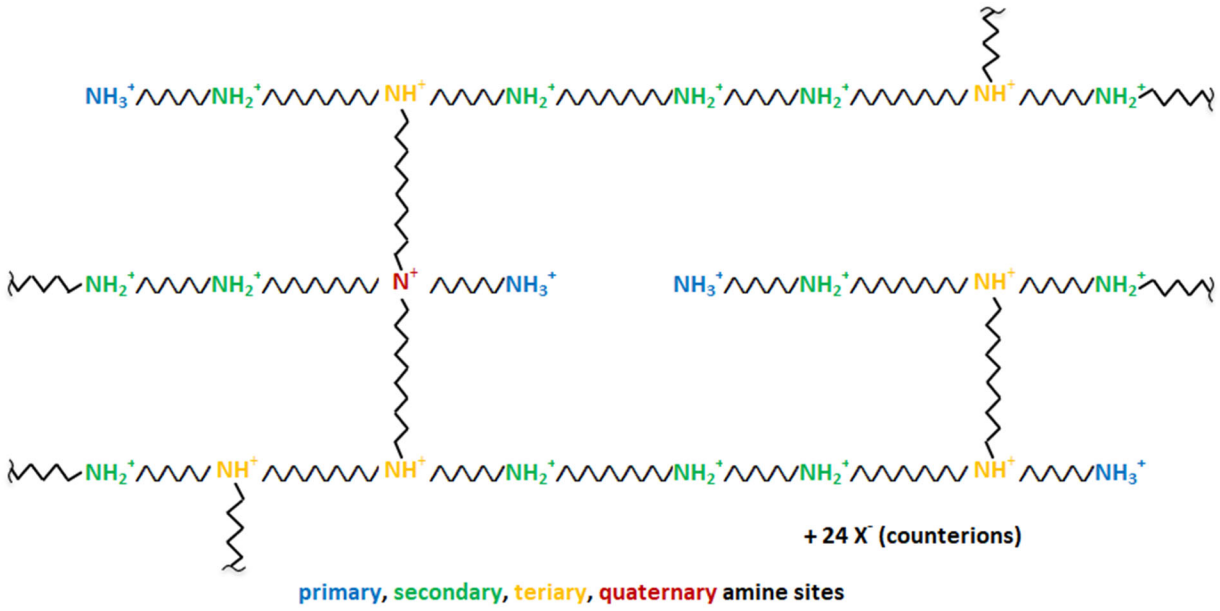

Figure 9 – Ionomer Skeletal Diagram Consistent with NMR Data

NMR spectra printed at 6, 12 and 24 hours showed 4 types of amine sites – primary, secondary, tertiary and permanently-ionized quaternary sites are present in the ionomer. Details are provided in Appendix 2. The ratios of types of nitrogen calculated from integration of the relevant signals are shown in **Table 6**.

Table 6 – Amine types in HG-1 identified by NMR. *Values in percentages.*

	6h	12h	24h	average
quaternary	1.5	1.0	1.4	1.3
tertiary	26.4	28.3	27.0	27.2
secondary	54.9	54.1	53.2	54.1
primary	17.1	16.6	18.3	17.3

Information from NMR explains the higher sorption capacity of HG-1 in comparison to other sorbents such as Anion Exchange Resins (AER). Three factors contribute to the higher capacity of HG-1 and our ionomers in general.

(i) Our ionomers do not have polymeric support such as polystyrene or polyacrylic resins as is the case with AERs. The entire molecular mass of our ionomers – inside and on the surface – can interact with PFAS through hydrophobic and ionic interaction. The hydrocarbon units of the ionomer offer non-ionic interactions (Hydrogen bonding and Van-der-Waals) and the amine sites offer ionic interaction with the tail and head of the PFAS respectively.

(ii) A preponderance of secondary amines: NMR shows that the majority of amines in HG-1 are secondary amines (54%) followed by tertiary amines (27%) and primary amines (17%). It is known that secondary amines are stronger bases than either tertiary or primary amines. Though

tertiary amines have highest nucleophilicity, they are more sterically hindered than secondary amines making them less accessible to acids.

(iii) Higher amine content than AER: The distribution of amine types together with knowledge of the two chain lengths connecting the nitrogen atoms, per

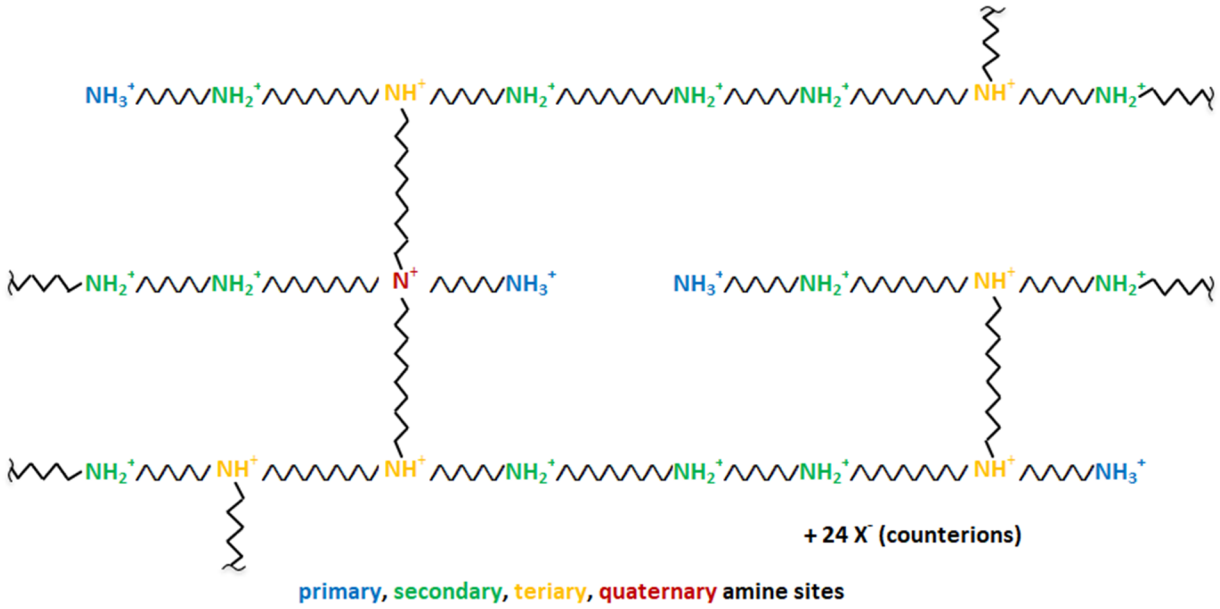

Figure 9, allows calculation of molar nitrogen content. From the NMR results, we calculate that our ionomer (HG-1) has around 8 milliequivalents (meq) per gram of free-base ionomer, compared with 2.5 to 4.5 meq/g found in the four IX's studied by Kassar, Graham and Boyer (Kassar, Graham, & Boyer, 2022).

Results and Discussion

Results of rate measurements in PFOA alone are presented first followed by results of testing in a mixture of four PFAS.

Adsorption Kinetics in Single-component PFOA Solutions

Data from PFOA adsorption kinetic tests appear in **Table 7** for ionomers HG-1 and HG-5. **Figure 10Figure 11** displays the data in the form of fraction PFOA removal from solution. Both plots show significant removal in the initial minutes, even at this low initial concentration and sorbent loading. It also appears that an equilibrium removal extent somewhat short of 100% may have been approached within an hour.

Table 7 – Kinetic Test Data (conditions described in text)

Time, min	0	1	2	5	10	20	60
Trial	HG-1, PFOA concentrations, µg/L						
1	0.689	0.277	0.246	0.142	0.093	0.108	0.08
2	0.723	0.318	0.274	0.232	0.201	0.146	0.085
3	0.762	0.326	0.199	0.173	0.269	0.044	0.017
	HG-5, PFOA concentrations, µg/L						
1	0.752	0.321	0.332	0.213	0.199	0.152	0.037
2	0.716	0.322	0.24	0.202	0.11	0.069	0.057
3	0.735	0.344	0.251	0.182	0.133	0.074	0.039

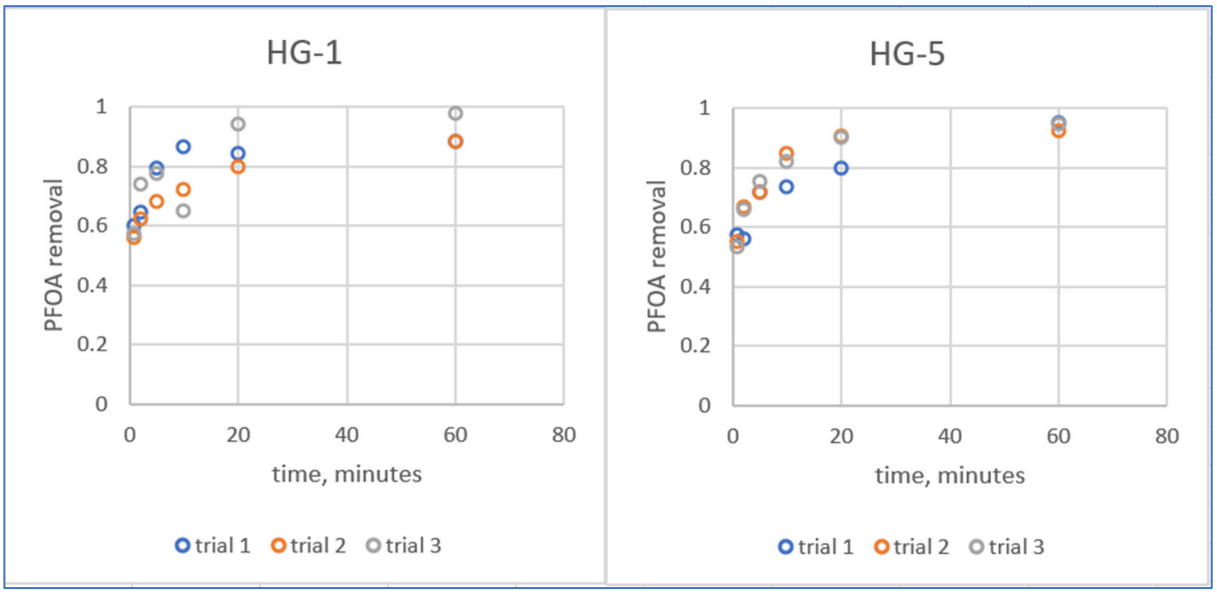

Figure 10 – PFOA Adsorption Kinetic Data as Fraction Removal.

Comparison PFOA adsorption kinetic tests were performed using GAC and IX adsorbents. We found that both the GAC (Calgon FiltraSorb 400) and the IX (Calgon CalRes 2301) adsorbed 1 µg/L PFOA too slowly for practical measurement at the 10 mg/L dosing used with HG-1 and HG-5. As a result, dosing for the comparison tests was increased to 100 mg/L. Initially, the IX adsorbed PFOA faster than the GAC but seemed to reach saturation with more PFOA remaining in solution. Even at the higher dosing, both materials removed PFOA from solution one to two orders of magnitude more slowly than HG-1 and HG-5, as can be seen in **Figure 11**. Supporting data for this and other figures that follow are tabulated in Appendix 1.

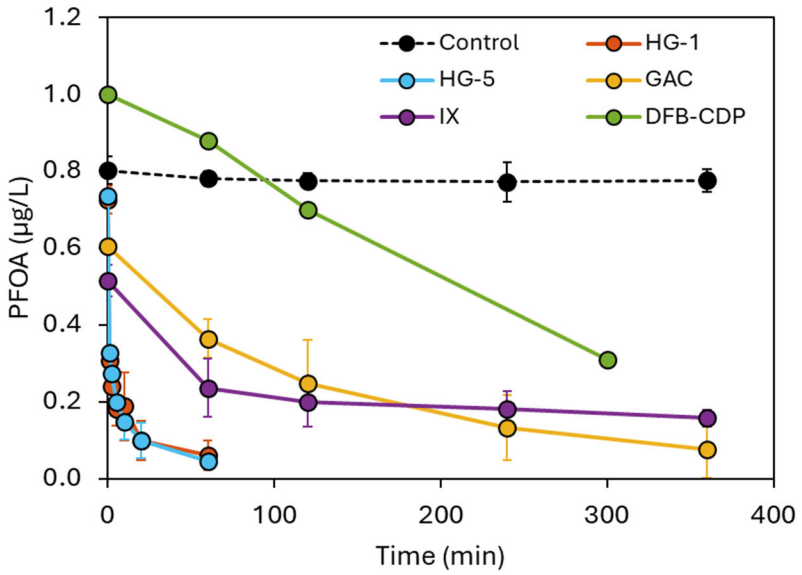

Figure 11 – PFOA adsorption kinetics for two novel ionomers (HG-1 and HG-5) and other sorbents. All sorbent loadings were 10 mg/L except for GAC and IX (100 mg/L). Data represent the average concentration ± one standard deviation of triplicate reactors. All data are from this study except for decafluorobiphenyl-cyclodextrin polymer [DFB-CDP] (Xiao, et al., 2017)

A pseudo-second order model, recommended in a highly-cited paper by Ho and McKay (Ho & McKay, 1999), has become a common means for analyzing data on adsorption kinetics. For example, Xiao *et al.* cite parameters for the model reported by eight different research groups for PFOA adsorption on various sorbents (supplement to (Xiao, et al., 2017)). The model derives from the following empirical rate equation.

$$\frac{dq}{dt} = k_{obs}(q_c - q_t)^2 \qquad (1)$$

where: q = quantity adsorbed per unit mass of sorbent
q_c = quantity adsorbed at equilibrium
t = time
k_{obs} = the pseudo-second order rate parameter

Separating variables and integrating from zero adsorption at time zero to q_t at time t gives the following equation for q as a function of time.

$$q_t = k_{obs}q_c^2 t/(1 + k_{obs}q_c t) \qquad (2)$$

While Ho and McKay suggest a linearization for data fitting, their method fails for some data sets, such as the low concentration data of Xiao et al., so we will use the more robust method of fitting the above equation directly to the data and finding the parameters q_c and k_{obs} by non-linear regression (readily accomplished with the Solver feature of Microsoft Excel spreadsheet software by minimizing the sum of squares of errors between model and data points).

The measured concentration data are converted to quantity adsorbed as follows.

$$q_t = (C_0 - C_t)/D \quad (3)$$

where: C_0 = the initial solution concentration of PFOA
D = sorbent dosing per unit volume of solution

Figure *12* shows the data as quantity adsorbed *vs.* time. The curves in **Figure *12*** trace the best-fit versions of Equation $q_t = k_{obs}q_C{}^2 t/(1 + k_{obs}q_c t)$ (2 using the parameters shown in the figure.

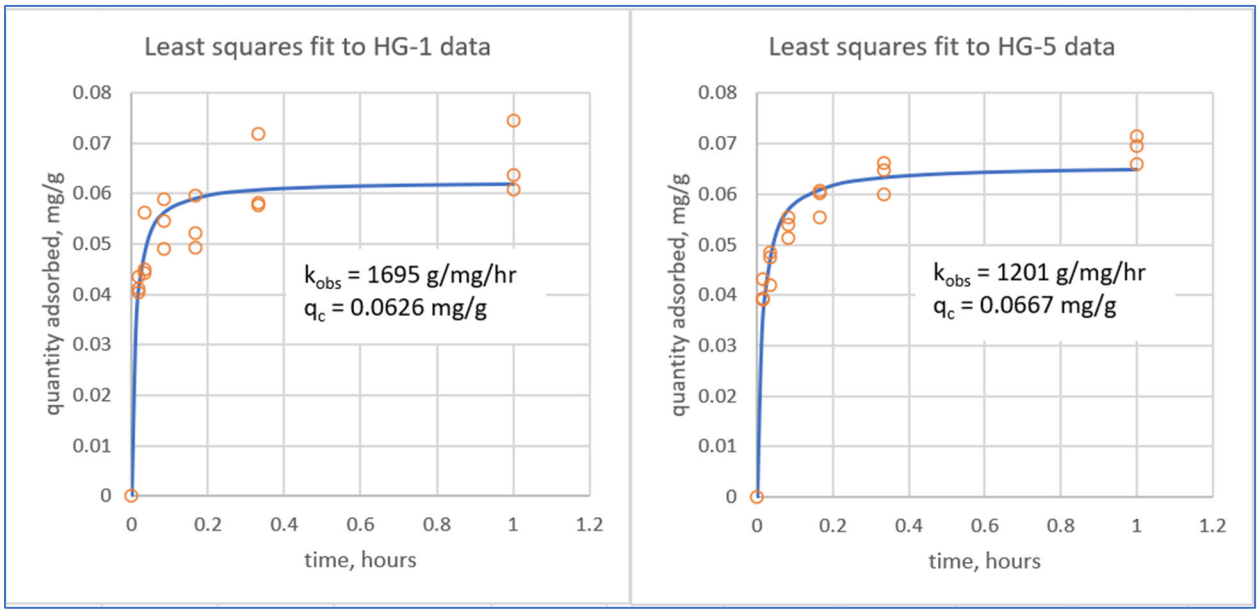

Figure 12 – Kinetic Data Fit to Pseudo-second Order Model.

Even in these kinetic experiments with vigorous agitation, adsorption rates are likely to be limited by a combination of mass transfer steps and reaction kinetics. The pseudo-second order model is not based on any particular mechanism. While the model provides a reasonable fit to the HG-1 and HG-5 data at one set of conditions, it has not been tested and is unlikely to accurately predict performance under other conditions. For that reason, we can currently make quantitative comparisons of adsorption rates only with sorbents with reported results in 1 µg/L PFOA with 10 mg/L dosing. **Table 8** lists the parameters determined from the tests reported here along with those reported by Xiao *et al.* for their DFB-CDP, another material (sieved coconut shell activated carbon, CCAC, S_{BET} = 1085 m^2 g^{-1}), that they tested under similar conditions, and for poly(ethylenimine)-functionalized cellulose microcrystals – PEI-f-CMC (Ateia, et al., 2018). Both HG-1 and HG-5 were found to adsorb PFOA faster than the comparison materials.

Table 8 – Pseudo-second Order Rate Parameter Comparison (conditions in text).

Material	k_{obs}, g/mg/hr
HG-1	1700
HG-5	1200
CCAC (Xiao, et al., 2017)	600
PEI-f-CMC (Ateia, et al., 2018)	12.8[1]
DFB-CDP (Xiao, et al., 2017)	2.9

Adsorption Kinetics of a 4-PFAS Mixture

A series of tests measured adsorption kinetics of ionomer HG-1 in mixtures of PFBA, PFBS, PFOA and PFOS and compared them with Filtrasorb 400 GAC, and CalRes 2304 IX. Dosing of each sorbent was nominally 100 mg/L. ***Figure 13****,* ***Figure 14****, and* ***Figure 15*** *show the rate of removal of the four PFAS (10 ppb each) by each of the three sorbents.* ***Figure 16*** *shows rates of removal by HG-1 from initial PFAS concentrations of 100 ppb each. First or second order reversible model fits are shown for one or two of the PFAS in each case to help with visualization. The models are described in*

Table 9. The 1st order reversible model fits the shorter-chain PFAS data while the 2nd order reversible model is a better fit to some of the longer chain data.

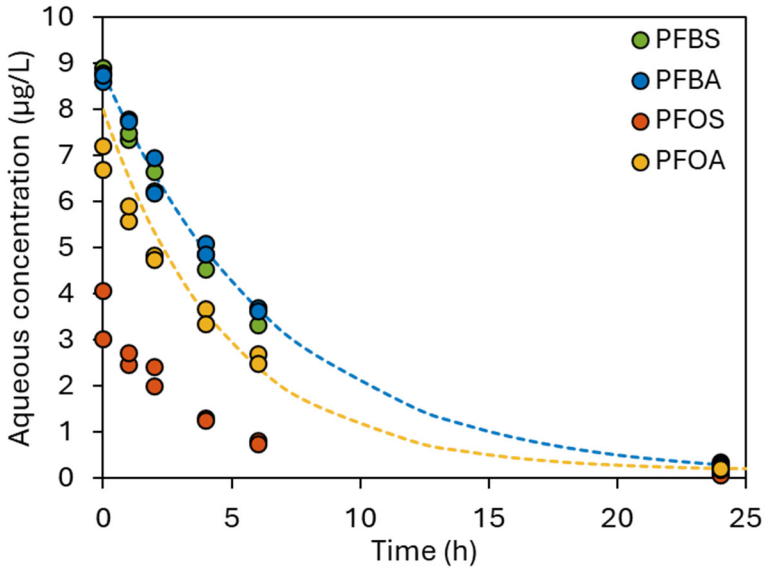

Figure 13 – Adsorption kinetics of a 4-PFAS mix onto GAC (Filtrasorb400). *The sorbent loading was 100mg/L. The dashed lines represent the 1st order reversible model fits to the data.*

[1] PEI-f-CMC was tested at 20 mg/L dosing in 1 µg/L PFOA.

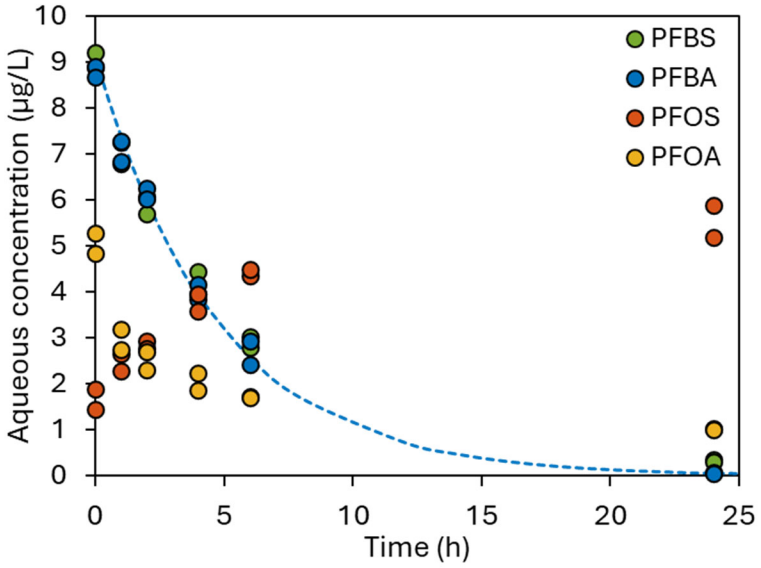

Figure 14 – Adsorption kinetics of a 4-PFAS mix onto IX (CalRes2304). *The sorbent loading was 100mg/L. The dashed lines represent the 1st order reversible model fits to the data.*

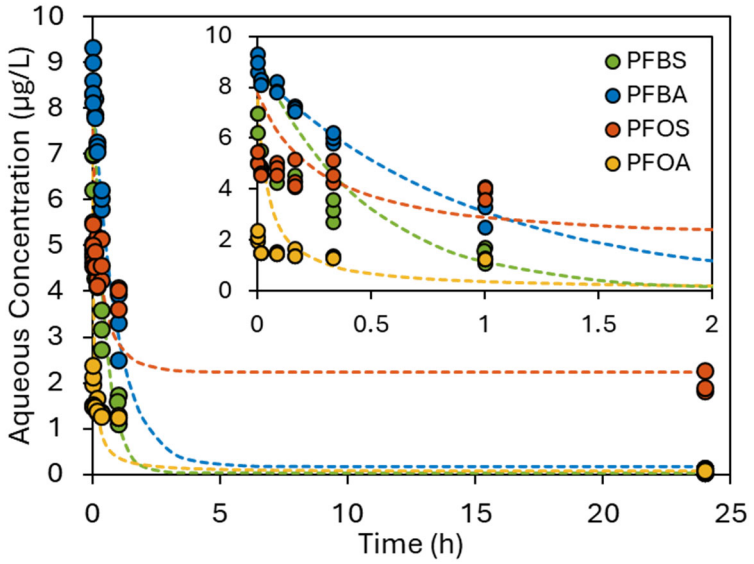

Figure 15 – Adsorption kinetics of a 4-PFAS mix onto ionomer (HG-1). *The sorbent loading was 100mg/L. The dashed lines represent the 1st and 2nd order reversible model fits to the data for short- and long- chain PFAS, respectively.*

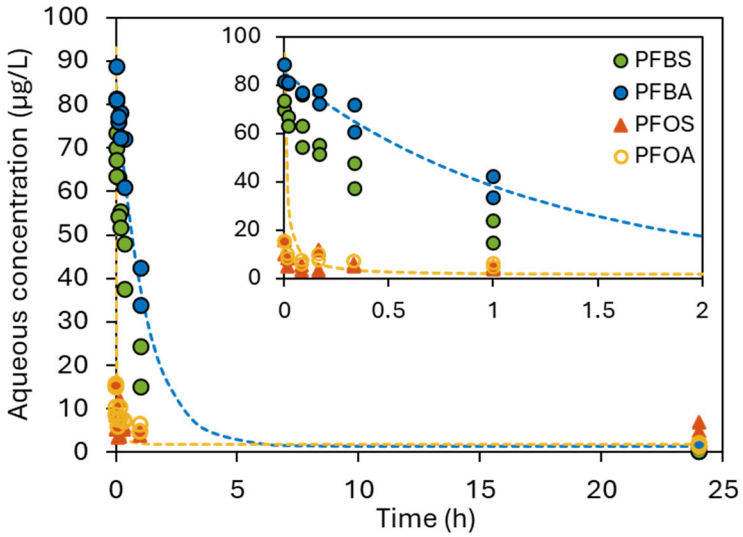

Figure 16 – Adsorption kinetics of a 4-PFAS mix onto ionomer (HG-1). *The sorbent loading was 100mg/L. Note that the PFAS concentrations are ~10x higher. The dashed lines represent the 1st and 2nd order reversible model fits to the data for short- and long- chain PFAS, respectively.*

Table 9 - Reaction Kinetic Adsorption Models

First order reversible model:		*Second order reversible model:*
$-\frac{dC}{dt} = D\frac{dq}{dt} = D(k_f C - k_r q)$	let:	$-\frac{dC}{dt} = D\frac{dq}{dt} = D(k_f C^2 - k_r qC)$
	C = sorbate [mg/L]	
where:	D = adsorbent [g/L]	where:
k_f = forward rate constant [L/hr/g]	q = adsorbent loading [mg/g]	k_f= forward rate constant [L^2/mg/hr/g]
k_r = reverse rate constant [1/hr]	$K_e = k_f/k_r$ [L/g]	k_r= reverse rate constant [L/mg/hr]
integrated and solved for C_t:	sorbate balance:	integrated and solved for C_t:
	$C_0 - C_t = D(q_t - q_0)$	
$C_t = C_0(1 + DK_e exp\left(-\left(D + \frac{1}{K_e}\right)k_f t\right)/(1 + DK_e)$		$C_t = C_0/(1 + K_e D(1 - exp(-(C_0/K_e)k_f t)))$

Comparing the figures, we see that HG-1 adsorption rate far exceeds that of GAC and IX for all four PFAS. **Figure 17** and **Figure 18** provide direct comparisons of PFBA removal rate

by HG-1 with GAC and IX, respectively. **Figure 19** compares PFOA removal rate by HG-1with GAC.

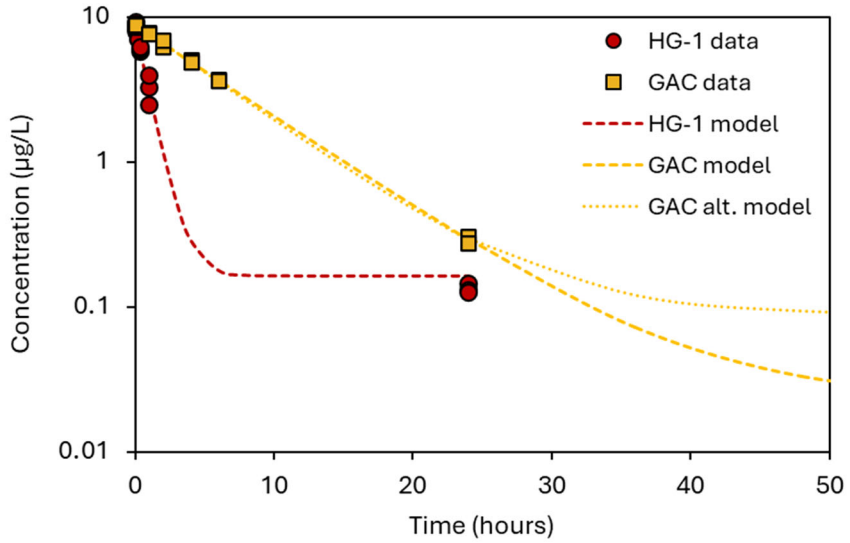

Figure 17 – PFBA Rate Comparison for GAC and Ionomer. *Lines show the 1st order reversible model fits. The alternate model curve reflects the uncertainty in projecting beyond the test period.*

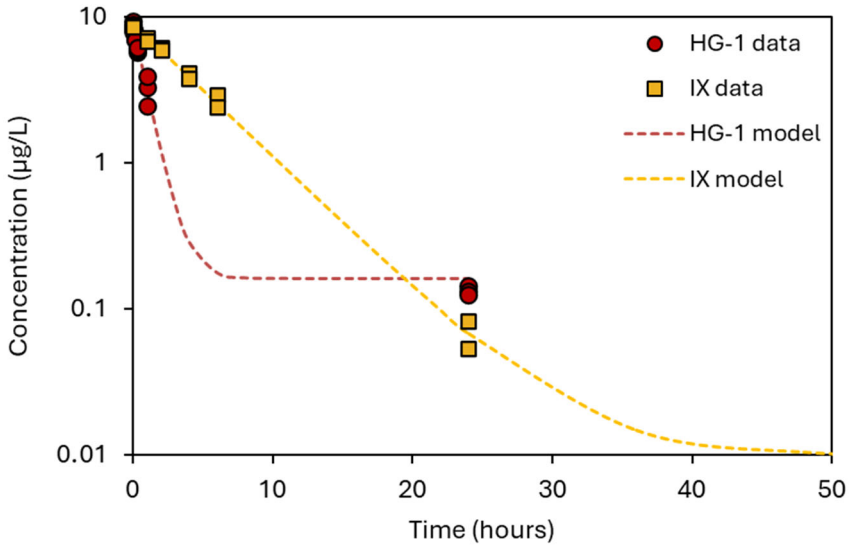

Figure 18 – PFBA Rate Comparison for IX and Ionomer. *Lines show the 1st order reversible model fits.*

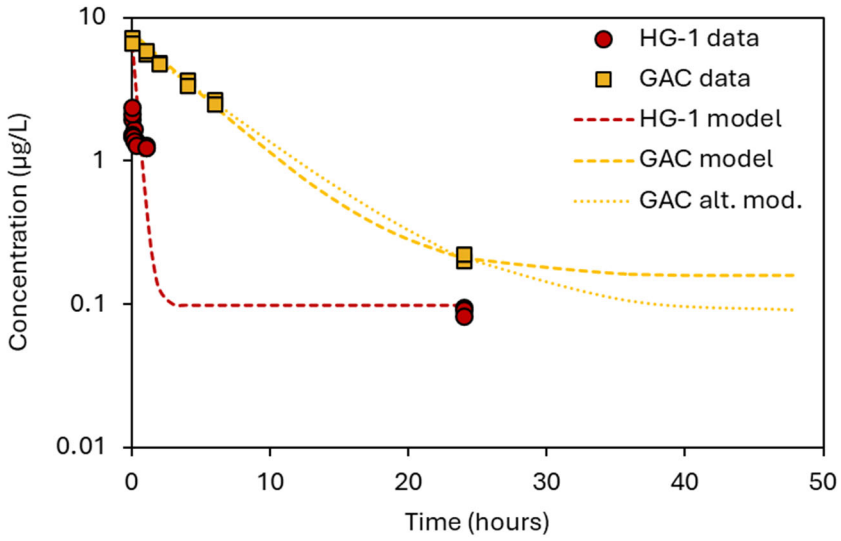

Figure 19 – PFOA Rate Comparison for GAC and Ionomer. *Lines show the 1st order reversible model fits. The alternate model curve reflects the uncertainty in projecting beyond the test period.*

First order reversible models (

Table 9), fit to the data plotted above, found rate constants as displayed in **Figure 20**. The figure shows how favorably measured HG-1 adsorption rates compare with the two commercial sorbents.

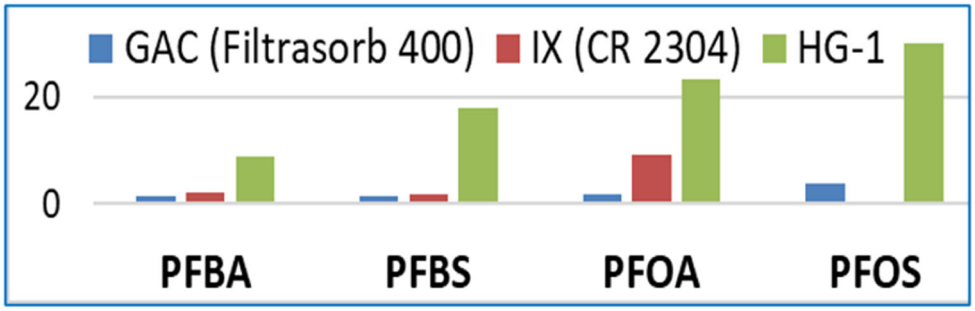

Figure 20 – First Order Reversible Rate Constant (L/g/hr) Compared

Task 1b – Sorption Capacity Studies

Materials and Methods

Sorbents used in these tests were as follows. Calgon Filtrasorb 400 GAC, Calgon CalRes 2304 gel-type, strong base anion exchange resin, and the ionomer designated HG-1, described previously. Isotherm data were collected in batch, agitated adsorption tests. PFAS concentrations and adsorbent dosing were chosen to span a wide range of final concentrations and bottles were agitated for 24 to 72 hours before liquid phase sampling and analysis by LC/MS/MS. The longer times were employed in some of the commercial sorbent comparison tests to allow for their slower adsorption kinetics.

Results and Discussion

Results of capacity measurements in PFOA alone are presented first followed by results of testing in a mixture of the four PFAS, and finally in an AFFF-impacted well water. Supporting data are tabulated in Appendix 1.

PFOA Adsorption Capacity Testing

In addition to the adsorption kinetics comparison, a PFOA adsorption isotherm for ionomer HG-1 was also determined and compared with published isotherm data. **Figure 21** illustrates the comparison. Over a broad concentration range, we measured adsorption capacity higher than all published reports we had located. Two sets of data show that HG-1 can sorb up to 18% its mass (175 mg/g) in PFOA, a capacity that is significantly greater than the comparison sorbents. In the figure, a Langmuir isotherm is plotted where quantity adsorbed equals $Q_{max}K_LC/(1 + K_LC)$. The values of Q_{max} and K_L for the line are 175 mg/g and 3.5 L/mg, respectively.

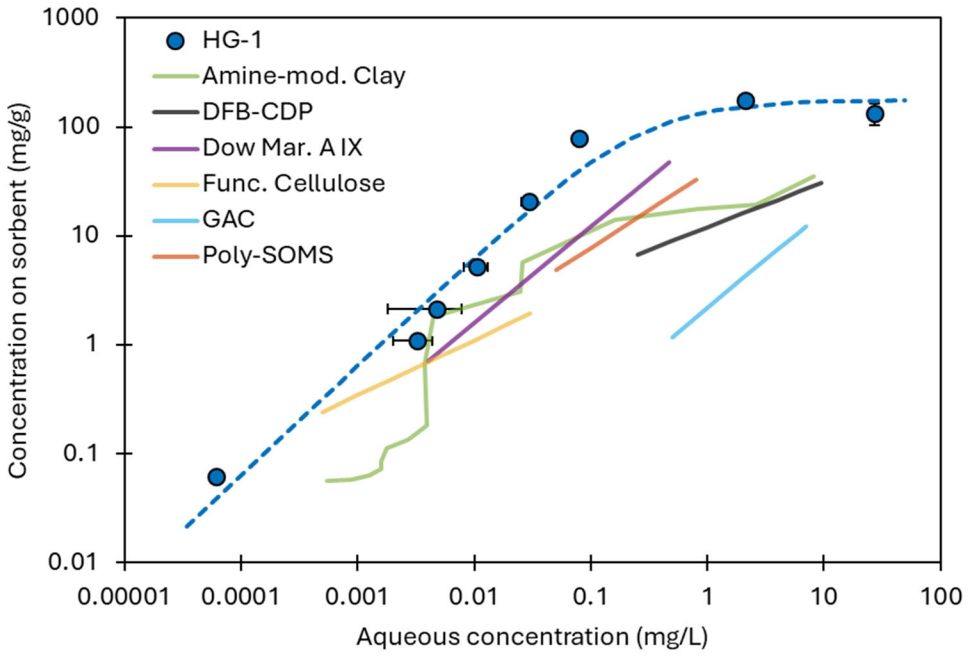

Figure 21 – **PFOA sorption isotherms for the ionomer HG-1 and other sorbents:** decafluorobiphenyl-cyclodextrin polymer [DFB-CDP] *(Xiao, et al., 2017)*, granular activated carbon [GAC] *(Zhang, et al., 2016)*, functionalized cellulose *(Ateia, et al., 2018)*, surfactant amine-modified clay *(Yan, Wang, & Liu, 2021)*, polymer-infused swellable organically modified silica [poly-SOMS] *(Stebel, et al., 2019)*, Dow Marathon anion exchange resin *(Chularueangaksorn, Tanaka, Fujii, & Kunacheva, 2014)*. Data are the average ± one standard deviation of triplicate (HG-1) experiments. The dashed line represents the Langmuir isotherm fit to the data.

Adsorption Capacity Testing in 4-PFAS Mixtures

Materials: In addition to the PFOA capacity testing, isotherms were also determined from batch, 48-hour adsorption tests in mixtures of PFBA, PFBS, PFOA and PFOS in water for ionomer and benchmark commercial sorbents. Sorbents used in these tests were as follows. Calgon Filtrasorb 400 GAC, Calgon CalRes 2304 gel-type, strong base anion exchange resin, and a chloride form of

HG-1 ionomer – HG-1(Cl). The latter is the same copolymer as the HG-1 used to produce previously-reported results, but with the bromide ion (that results from the bromide monomer) mostly removed, and replaced by chloride ion. HG-1(Cl) has similar fast adsorption kinetics, a higher swell factor, and more capacity than the un-exchanged ionomer, which we can designate as HG-1(Br). See the Appendix 2 for additional details.

Results of the 4 PFAS capacity measurements for the HG-1(Cl) ionomer are presented in **Figure 22**. The linear dependence of loading on concentration with a slope of 1 on a log-log scale for each PFAS is consistent with the low concentration end of a Langmuir isotherm or with a Freundlich isotherm where n = 1. Previously reported data on PFOA-alone adsorption by HG-1(Br) was well represented by a Langmuir isotherm, including the characteristic decrease in slope at high concentrations, beyond the range of the current data set for the PFAS mixture.

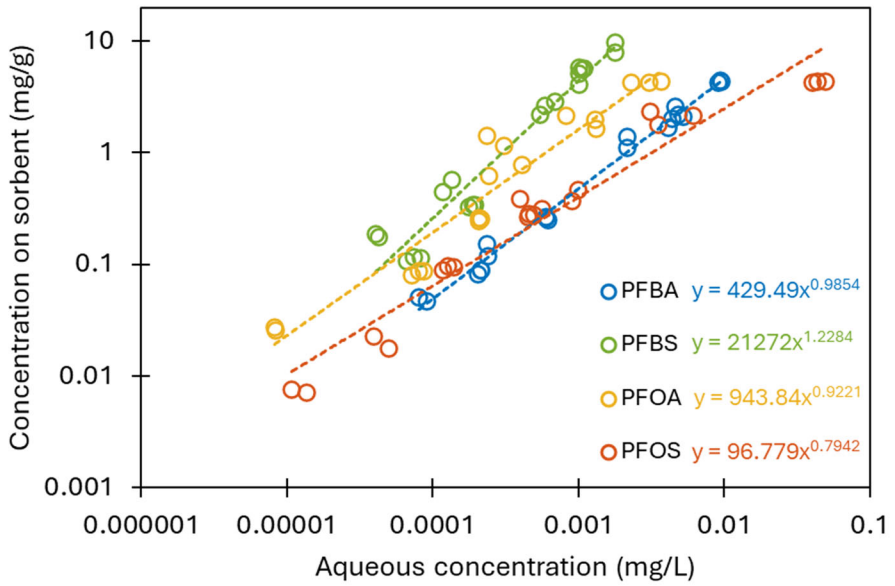

Figure 22 – Sorption isotherms of a 4-PFAS mix for HG-1. *The dashed lines and color-coded equations represent the Freundlich Isotherm Fits to the data.*

Figure 24 and **Figure 23** display the results from the capacity experiments with the tested IX and GAC, respectively. Although there was substantial scatter, there was no obvious trend between the data from bottles shaken for 48 hours and those shaken for 72 hours, so the results are combined for these plots. Dashed lines are included to help visualize the data trends, but, in most cases, meaningful equation parameters could not be determined.

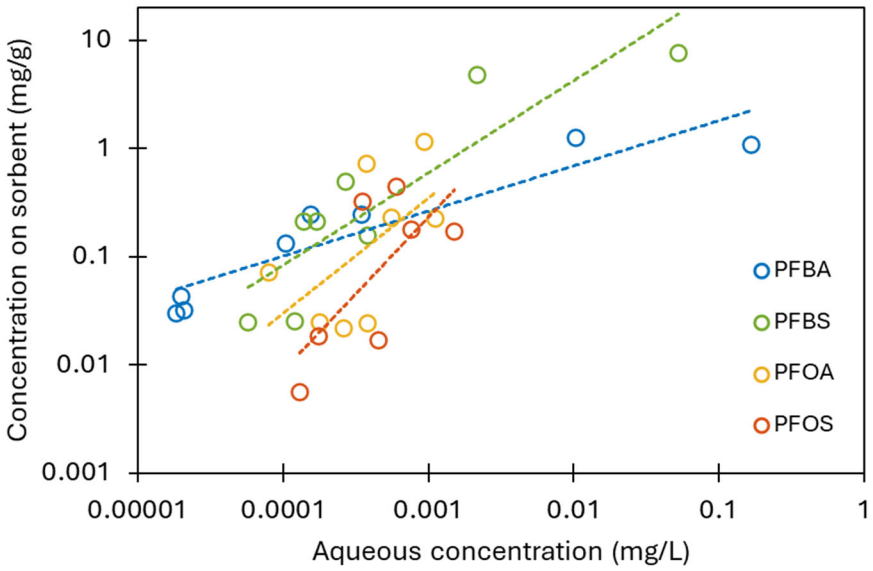

Figure 23 – Sorption isotherms of a 4-PFAS mix for GAC (F400). *The dashed represent the Freundlich Isotherm Fits to the data.*

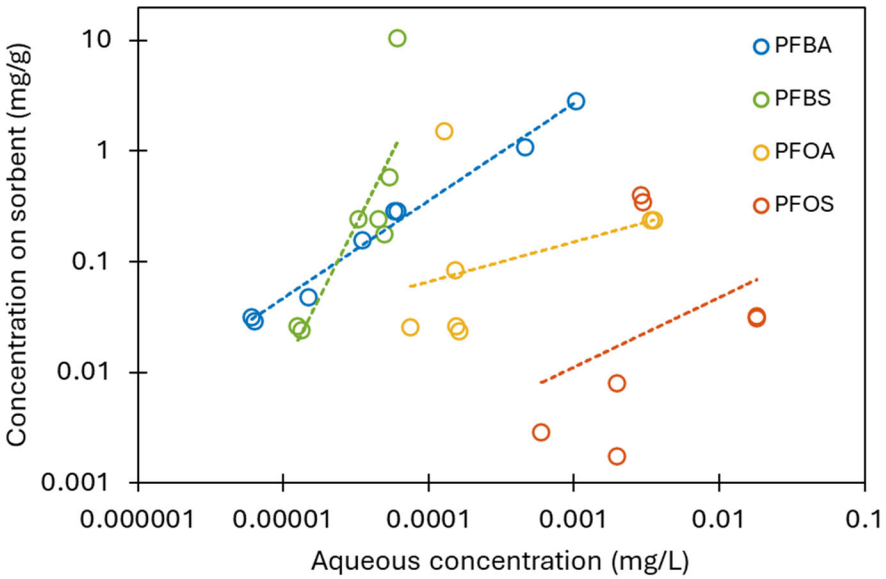

Figure 24 – Sorption isotherms of a 4-PFAS mix for IX (CalRes2304). *The dashed represent the Freundlich Isotherm Fits to the data.*

Although scatter would prevent meaningful extrapolation from the GAC and IX results, the data do allow interpolation to a single concentration of each concentration in the mixture for comparison with the HG-1 capacity results. **Table 10** compares the measured capacity HG-1(Cl) with those of the two benchmark sorbents at 10^{-3} mg/L (1 ppb). The table shows HG-1 capacity exceeding that of the tested GAC for each PFAS in the mixture and exceeding that of the benchmark IX for PFOA and PFOS. Limited data (plotted in Appendix 1) collected on a

macroporous AER, CR2301, could only be compared at lower concentrations, as indicated in the table.

Table 10 – Interpolated PFAS adsorption (mg/g) at the indicated aqueous concentrations.

	Comparison at 1 ppb in liquid			Comparison at the indicated concentration in liquid			
	GAC F400	**IX CR2304**	**HG-1(Cl)**		**PFAS (ppt)**	**IX CR 2301**	**HG-1(Cl)**
PFBA	0.26	2.59	0.48	PFBA	5	0.13	0.003
PFBS	0.60	>10	4.39	PFBS	5	0.08	0.007
PFOA	0.35	0.17	1.62	PFOA	10	0.04	0.02
PFOS	0.23	0.02	0.40	PFOS	100	0.04	0.06

* The calculated concentrations on the sorbents are interpolated from the corresponding isotherms.

PFAS Adsorption from AFFF-impacted Well Water

A series of tests explored adsorption of PFAS from an aqueous film-forming foam (AFFF) impacted well water by ionomer HG-1(Cl). Composition of the well water is provided in **Table 11**. Samples were equilibrated with various dosing of ionomer for 24 hours of bottle shaking. Results are provided in **Figure 25**.

Table 11 – AFFF-impacted Well Water PFAS and Co-contaminant Concentrations

PFAS	**ng/L**		**Contaminant**	**ppm**
PFBA	68.2		Chloride	46.6
PFPeA	119.8		Nitrate	3.69
PFBS	77.8		Sulfate	8.99
PFHxA	187.7		TDS	159
PFPeS	70.6		TOC	ND
PFHpA	66.2		Turbidity	0.13
5:3FTCA	1.2		Sodium	21.6
PFHxS	421.9		Iron	0.737
6:2FTS	160.7		Manganese	ND
PFOA	157.1			
PFHpS	31.3			
PFNA	9.9			
PFOS	1336.8			
8:2FTS	16.3			
PFDA	1.8			
PFOSA	3.0			

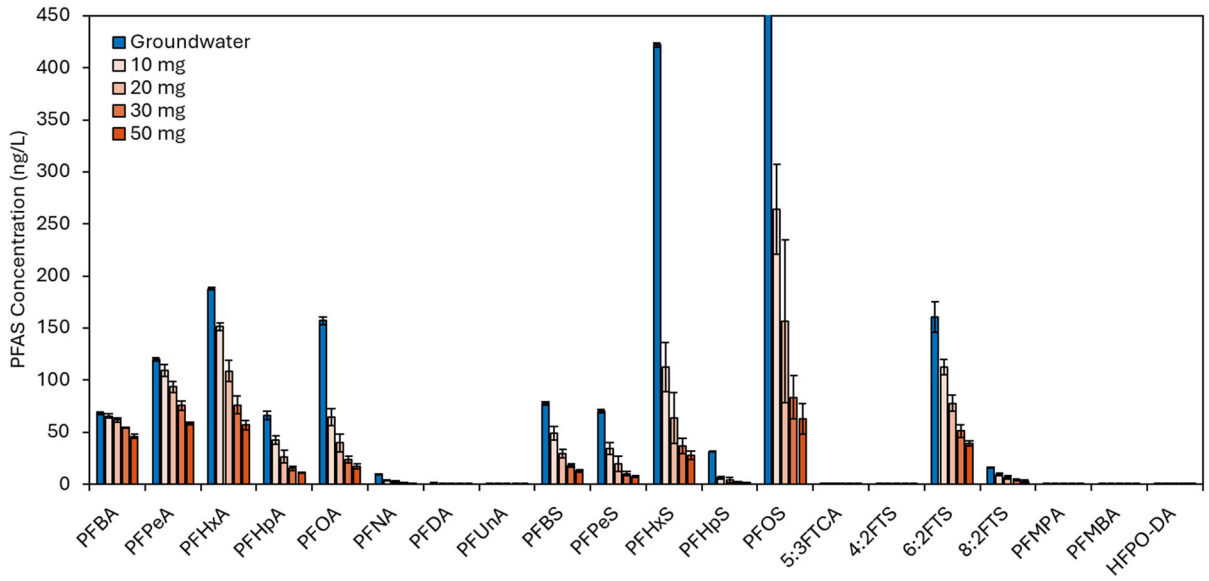

Figure 25 – PFAS removal from AFFF-impacted well water by HG-1(Cl) at variable sorbent loadings. *Reactors were equilibrated for 24 h. The total volume was 250 mL. The initial PFOS concentration was 1336.8 ± 31.9 ng/L. Data represent the average ± one standard deviation of triplicate reactors.*

The data can also be viewed as isotherms for the individual PFAS in this mixture of PFAS with its extant co-contaminants. **Figure 26**, which plots the data on logarithmic coordinates, shows that most of the PFAS fall along the same general trendline with a slope close to one. Data for the shorter-chain PFAS tend to fall below the others, and display zero or negative slopes, which could be a competitive adsorption effect. These less hydrophobic PFAS are probably more sensitive to displacement by anions in the well water. Comparing **Figure 26** with **Figure 22**, we see that, while capacity for all four PFAS is higher in the absence of co-contaminants, PFOS comes the closest to the same capacity in the well water as in the 4-PFAS solution. The order of capacities in the 4-PFAS solution was PFBS≈PFOA>PFBA≈PFOS, while in the well water data, it is PFOS>PFOA>PFBS>PFBA. It is worth noting that, as seen in **Figure 15** and particularly in **Figure 16**, the shorter-chain PFAS were more slowly adsorbed, so it is possible that their adsorption extents would improve with longer equilibration times.

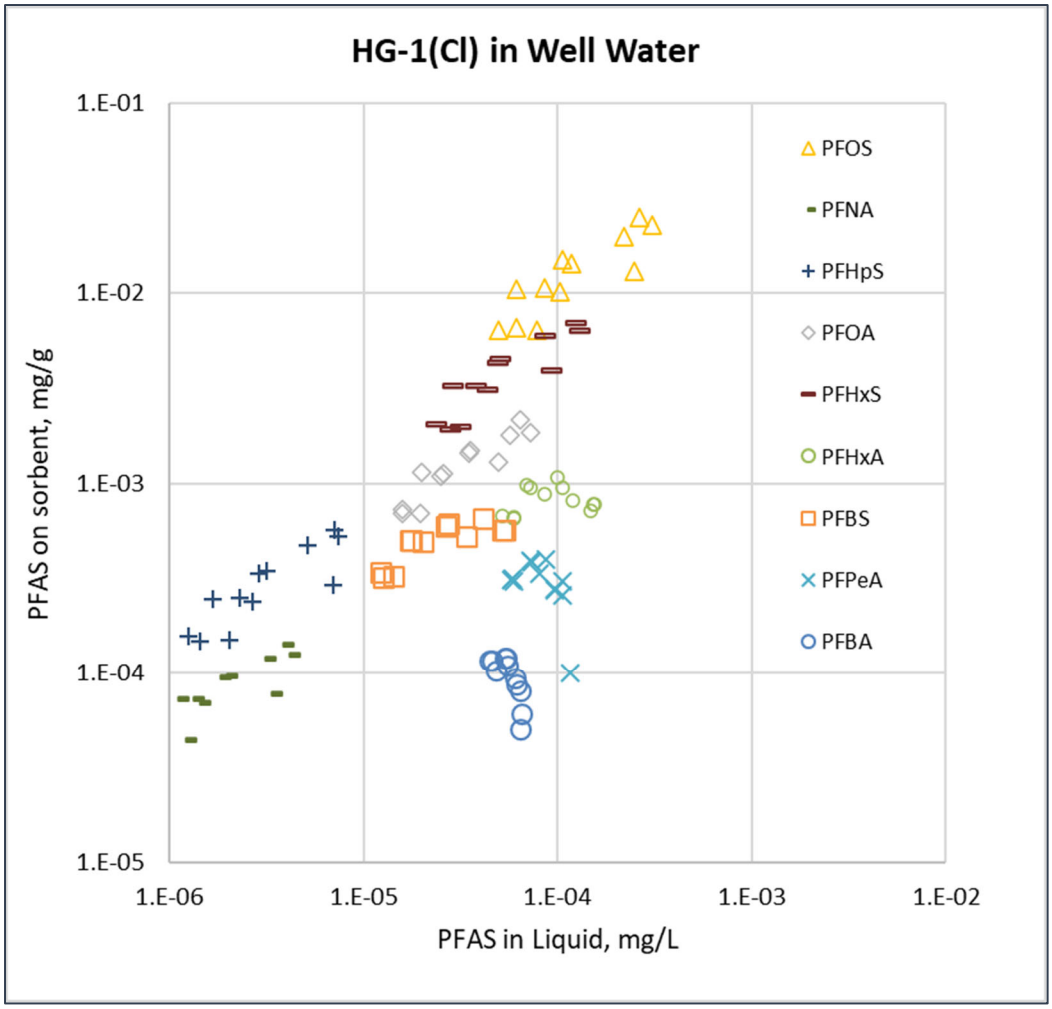

Figure 26 – Ionomer Isotherm Plot in AFFF-Impacted Water

In summary, our experiments found significantly faster adsorption kinetics for ionomer than for commercial GAC and IX materials in PFOA alone and in mixtures of the four PFAS. PFOA adsorption on ionomer was shown to follow a Langmuir-type isotherm with higher adsorption capacity than any comparable data we found in the literature. Our experiments showed ionomer adsorption capacity in the four PFAS exceeding that of GAC and exceeding a benchmark IX for PFOA and PFOS. Testing in AFFF-impacted well water showed all 16 detectable PFAS were adsorbed by ionomer with PFOS and PFOA adsorption less impacted by the co-contaminants than that of PFBS and PFBA.

Task 2 – Desorption Studies

Materials and Methods

The experiments used the HG-1(Cl) type of ionomer described above. Mixtures of PFBA, PFBS, PFOA, and PFOS were again used as model PFAS. Desorption testing started with 24-hour bottle adsorption tests. For most of the desorption tests, loaded sorbent was screened from the adsorption

solution and the screen transferred to a second bottle to which desorption solution (various compositions were tested) was added. The bottle was then agitated for 22 hours, interrupted for liquid phase sampling after 1 hour. Liquid samples of the initial and final adsorb solution, 1 hour, and 22 hour desorb solutions were all analyzed by LC/MS/MS. In one set of desorption tests, the 24-hour adsorption solution and sorbent were poured into a small column where the sorbent formed thin layer on top of a frit. Desorb solution was then passed slowly through the sorbent over a period of about an hour. In all cases, adsorbed amounts were determined from the adsorb solution volume and concentration change. Desorbed amounts were determined from the desorb solution volume and measured concentrations.

A set of repeated adsorption and desorption experiments provided a preliminary demonstration of ionomer re-use in a short column set-up. 30 mg of ionomer formed a 1 cm deep layer supported by a polyethylene frit in three identical 8 mm inside diameter columns. Flowrates of 0.5 cm/min were employed. The tests used downflow of 20 mL of a four PFAS mixture (approximately 250 ppb each) for each adsorption, and downflow of either 40 or 20 mL of aqueous desorb solution for the desorption steps, followed by a 20 mL rinse to remove desorb solution. For these tests, the rinse solution contained 0.02 N HCl and 0.5% NaCl.

Results and Discussion

Batch desorption results are presented first followed by flow through desorption results, then modeling to project full-scale column performance through adsorption and desorption cycles, and finally the demonstration of repeated ionomer re-use after desorption. Supporting data are tabulated in Appendix 1.

Batch Desorption Experiments

Four sets of batch adsorption-desorption experiments were conducted to begin developing technology to desorb PFAS from ionomer. Early results showed that aqueous alkaline solutions, which scouting results had shown effective at removing PFOA alone from at least one ionomer type, were not as effective at desorbing the PFAS mixture. In the first three sets of experiments, we also learned that the order of difficulty desorbing the four PFAS was PFOS>PFOA>PFBS>PFBA, that NaOH dissolved in methanol was an effective stripping agent for all four PFAS, and that desorption into an at least 10 times smaller volume than the starting solution was feasible. However, due to the negative environmental impacts and costs associated with methanol based PFAS desorbate solutions, we investigated all-aqueous reagents to desorb PFAS from our ionomers.

Our investigation of all-aqueous desorption reagents identified two proprietary desorption promoters (PDP A and PDP B) that can significantly enhance the effectiveness of aqueous solutions for desorbing the PFAS mixture. The fourth set of experiments is described, and the results presented in this report (**Table 12**).

The adsorption phase of these adsorption-desorption experiments used approximately 10 mg of sorbent in 20 mL of an aqueous PFAS mixture with nominal concentrations of 250 ppb each PFBA, PFBS, PFOA and PFOS in either a 125 mL or a 250 mL bottle. In the case of the 250 mL bottle, 230 mL of additional pure water diluted the starting solution. For the desorption phase, 20 mL of one of several candidate desorption solutions was used.

The adsorb phase of the adsorption-desorption experiments typically produced >98% adsorption of all four PFAS. The cases starting with the PFAS solution diluted to 250 mL and the same quantity of ionomer, produced 84 to 97% adsorption of the PFAS. **Table 12** presents the fraction desorbed of each PFAS based on the fraction adsorbed. Only the three indicated cases in the table started with dilution to 250 mL.

Table 12 – Batch Desorption Results

		PFBA	**PFBS**	**PFOA**	**PFOS**	
Desorb solution*	Exp# and Sorbent type used	**Percent of PFAS desorbed based on PFAS sorbed**				**Eq. time**
0.5M NaOH in MeOH	1a) HG-1(Cl) (250mL->20mL)	78.2	78.3	73.2	75.2	1hr
		89.7	91.4	95.3	95.0	22hrs
	1b) HG-1(Cl) (20mL->20mL)	87.7	93.4	93.8	98.8	1hr
		78.4	80.4	80.0	81.2	22hrs
	1c) GAC (Filtrasorb 400)	79.5	88.6	80.2	61.2	1hr
		83.5	83.8	80.8	56.2	22hrs
	1d) IX (CR2304)	68.7	30.9	73.2	54.2	1hr
		70.8	32.7	75.3	48.8	22hrs
0.5M NaOH in EtOH	2) HG-1(Cl)	87.2	96.4	95.8	102	1hr
		84.8	87.5	87.3	93.5	22hrs
0.2% PDP A	3a) HG-1(Cl)	74.3	37.6	14.3	48.3	1hr
		82.9	82.2	33.4	41.0	22hrs
	3b) GAC (Filtrasorb 400)	4.80	1.24	2.09	2.61	1hr
		29.5	16.9	27.3	16.6	22hrs
	3c) IX (CR2304)	28.8	5.43	10.3	58.2	1hr
		74.5	22.6	11.0	41.1	22hrs
0.2% PDP A + 0.5% NaCl	4a) HG-1(Cl)	84.5	108	73.6	51.1	1hr
		86.2	90.0	77.7	73.3	22hrs
	4b) HG-1(Cl) (250mL->20mL)	80.9	73.0	48.8	23.7	1hr
		91.7	97.4	79.6	59.3	24hrs
0.2% PDP A + HCl	5a) HG-1(Cl)	75.1	69.2	27.1	71.0	1hr
		77.2	65.1	35.1	64.3	22hrs
	5b) HG-1(Cl) (250mL->20mL)	81.6	47.6	16.5	13.3	1hr
		102	101	83.3	62.5	24hrs
0.2% PDP B	6) HG-1(Cl)	86.3	87.8	73.3	28.4	1hr
		90.6	93.0	84.0	29.5	22hrs
2M NaCl	7) HG-1(Cl)	77.7	45.7	6.26	0.0853	1hr
		88.3	39.2	6.61	2.85	22hrs
*aqueous unless specified otherwise						

These results show that desorption into relatively concentrated solutions is possible. Even the 20 mL to 20 mL tests represent two orders of magnitude increase in concentration from the PFAS in the depleted water equilibrated with the PFAS-loaded sorbent to the desorb solution equilibrated with the un-loaded sorbent. With the 250 mL adsorb to 20 mL desorb cases (1a, 4b, 5b), another order of magnitude concentration was demonstrated. While alkaline alcohol solutions were effective (1, 2), the proprietary desorption promoters(3,4,5,6), particularly PDP A with added NaCl (4), were more promising because they allowed desorption into more practical aqueous solutions. The 1-hour samples allow the observation that kinetics may be a factor in aqueous desorption. Finally, **Table 12** includes comparison desorption experiments with the tested GAC and IX (1c, 1d, 3b, 3c) which show that PFAS are more readily desorbed from HG-1(Cl). The alkaline MeOH solutions which were effective at desorbing all four PFAS from ionomer, desorbed significantly less of the sulfonates from IX and less of PFOS from GAC. Further, PDP A in aqueous solution was less effective on both comparison materials.

Flow-through desorption experiments

As part of the transition from bottle-shaking, batch tests to small column testing, a set of experiments was conducted featuring bottle adsorption followed by flow-through desorption. The adsorption phase was as described previously: 10 mg of sorbent in 20 mL of a nominally 0.25 mg/L total PFAS aqueous solution comprising PFBA, PFBS, PFOA and PFOS. After 24 hours of shaking, the water and sorbent were transferred to a small column containing a bed of glass beads, where the water was collected from the bottom of the column for adsorption efficiency sampling, and the sorbent was retained as a thin layer on the glass beads for the desorption tests. This method avoided possible particle attrition during the desorption phase, allowing the effect of particle size to be included as an experimental variable. Two size cuts of HG-1(Cl), from sieving freshly-produced ionomer, were tested as well as a sample of the un-sized material used for previously-reported experiments. Desorption was conducted in two phases. First 20 mL of water with 0.5% PDP A and 0.5% NaCl (no methanol) was passed through the column over the course of about an hour, then 20 mL of methanol with 2% NH_4OH was applied. Effluent from each desorption phase was collected for analysis by LC-MS-MS. We hypothesized that the methanol solution would remove most of the PFAS not removed by the aqueous solution, allowing a check on mass balance.

Results of the experiment are presented in **Table 13**. Adsorption efficiency was like previous batch experiments, and showed a possible effect of particle size for the heavier PFAS. For three of the PFAS, aqueous desorption efficiency in the flow-through mode was similar or higher than previous batch desorption results, while for PFOS, desorption was somewhat less efficient compared with previously-reported 24-hour batch desorption experiments. This would indicate that desorption kinetics are slower for PFOS than for the other three PFAS tested, consistent with earlier observations comparing 1- and 22-hour batch desorption times. The methanol desorption phase successfully recovered most or all the remaining PFAS, including PFOS. The un-normalized totals provide a measure of mass balance closure, which was generally within experimental error.

Table 13 - Results of Batch Adsorb/Flow-through Desorb Tests

Sample		PFBA	PFBS	PFOA	PFOS
Name	Comment	ng/mL	ng/mL	ng/mL	ng/mL
4 PFAS starting mixture	Stock Solution	60.8	92.1	54.1	60.2
		percent adsorbed			
HG-1(Cl), >425µm	24hr bottle adsorption	96.4%	99.3%	97.7%	82.1%
HG-1(Cl), 180-425µm		98.2%	99.4%	99.0%	96.4%
HG-1(Cl), unsized		97.9%	99.5%	99.5%	97.8%
		percent desorbed			
HG-1(Cl), >425µm	0.5% PDP A and 0.5% NaCl all-aqueous flow-through desorption	91%	74%	75%	44%
HG-1(Cl), 180-425µm		99%	98%	78%	44%
HG-1(Cl), unsized		96%	88%	90%	46%
		additional percentage desorbed			
HG-1(Cl), >425µm	subsequent 2% NH_4OH + MeOH flow-through desorption for mass balance	1%	2%	18%	56%
HG-1(Cl), 180-425µm		1%	1%	7%	39%
HG-1(Cl), unsized		1%	1%	10%	48%
		total percent desorbed			
HG-1(Cl), >425µm	total of aqueous and methanol desorption percentages	92%	76%	93%	100%
HG-1(Cl), 180-425µm		100%	99%	85%	83%
HG-1(Cl), unsized		97%	89%	100%	94%
		un-normalized totals			
HG-1(Cl), >425µm	measured desorption amounts for each species were normalized such that no desorption total exceeds 100%	103.1%	75.8%	111.4%	112.0%
HG-1(Cl), 180-425µm		111.6%	99.3%	101.9%	93.2%
HG-1(Cl), unsized		108.3%	89.3%	120.2%	105.0%

Projecting Column Adsorption and Desorption Performance from Batch Data

The following analysis was conducted to determine whether the desorption performance found in the preliminary, batch desorption data reported above could be sufficient to realize a column adsorption system with aqueous regeneration into a concentrated solution for destruction. **Figure 27** includes batch adsorption isotherm data reported earlier. The figure also includes batch, aqueous desorption data from the set of tests reported above. PFAS content (loading, q, mg/g) remaining on the sorbent after desorption is calculated as follows.

$$q = (Va * (Cf - Ca) - Vd * Cd)/m \quad (4)$$

where: Va = volume of adsorption solution, L

Vd = volume of desorption solution, L

Cf = initial PFAS concentration in adsorption solution, mg/L

Ca = PFAS concentration after adsorption, mg/L

Cd = final PFAS concentration in desorb solution, mg/L

m = mass of sorbent, g

The plot is based on the idea that after a day of batch desorption, the sorbent reaches a new equilibrium with the desorption solution which can be represented as a desorption isotherm. We have found that HG-1(Cl) adsorption isotherms have slopes close to one on this type of plot. Based on our understanding of how PDP functions, we expect a desorption isotherm with a similar slope. We are currently running tests to check this assumption. In the plot, we can see that at the same sorbent loading, switching to the aqueous desorption solution can provide more than three orders of magnitude increase in equilibrium PFAS concentrations.

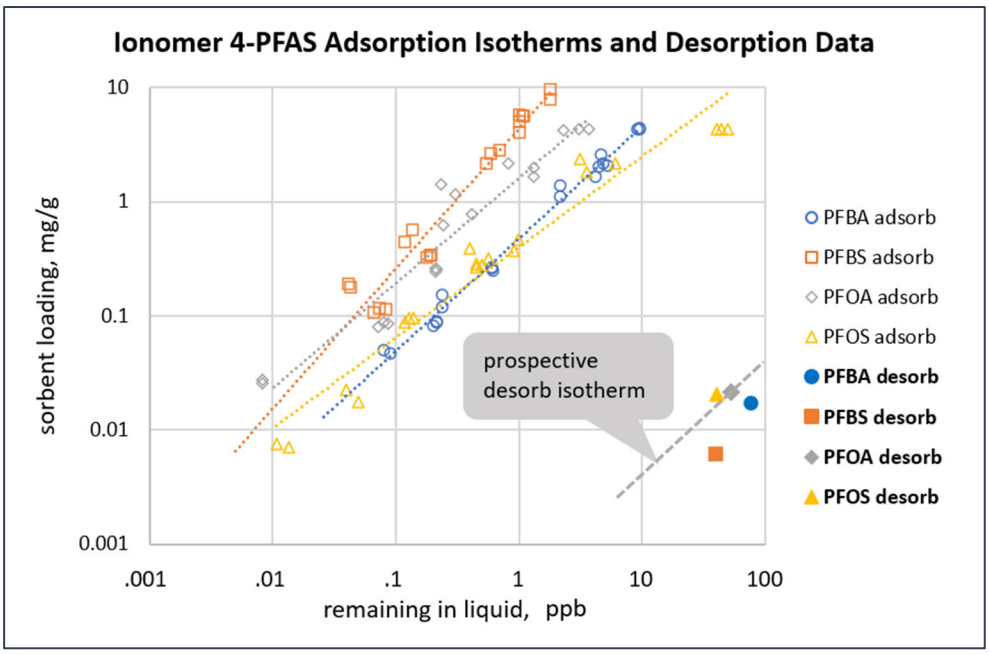

Figure 27 - HG-1(Cl) adsorption isotherms in combined PFAS and data from desorption into water with 0.2% PDP A and 0.5% NaCl

The data and analysis of **Figure 27** provide equilibrium information that we can combine with kinetic information in an appropriate model to project performance of an adsorption column. The linear driving force (ldf) approximation has proven useful for modeling column performance (LeVan, Carta, & Yon, 1997) and uses a kinetic parameter that we can evaluate from batch data. The approximation defines an overall mass transfer coefficient between a sorbent particle surface composition that would be saturated with the local liquid concentration and the bulk average particle loading. For batch adsorption and desorption, the following equations apply.

$$dC / dt = - b \cdot dq / dt = - k_O \cdot b \cdot (qs - q) \quad (5)$$

$$q = q_0 + (C_0 - C) / b \quad (6)$$

$$qs = K_F \cdot C^{(1/n)} \quad (7)$$

where: C = sorbate liquid concentration (mg/L)
C_0 = initial liquid concentration (mg/L)
t = time (minutes)
b = sorbent bulk density, or dosing, in liquid (g/L)
q = loading of sorbate on sorbent (mg/g)
qs = loading at saturation (mg/g)
q_0 = initial sorbent loading (mg/g)
k_O = overall mass transfer coefficient (/minute)
K_F = Freundlich isotherm constant $(mg/g/(mg/L)^{(1/n)})$
n = Freundlich exponential factor (-)

The three equations can be combined and solved by numerical integration, in the general case. For the case where n = 1, known as the constant separation factor case, they can be solved analytically. For adsorption, when $q_0 = 0$, the solution is

$$C / C_0 = (1 + b \cdot K_F \cdot \exp(- (b \cdot K_F + 1) \cdot k_O \cdot t)) / (b \cdot K_F + 1). \quad (8)$$

This equation is the same as the first order reversible equation for the same problem, presented in

Table 9, when Ke replaces K_F and kf replaces $K_F \cdot k_O$. For the desorption case, where $C_0 = 0$, the solution is

$$C = b \cdot q_0 \cdot (1 - \exp(- (b \cdot K_F + 1) \cdot k_O \cdot t)) / (b \cdot K_F + 1). \quad (9)$$

These equations can be compared with measured concentration data from batch adsorption and desorption experiments to find values for k_O. Because k_O is an overall coefficient that combines parallel liquid and solid diffusion pathways, we can expect its value to differ between adsorption and desorption, when the relationship between liquid and solid concentrations changes. **Figure 28** shows the comparison of Equation $C = b \cdot q_0 \cdot (1 - \exp(- (b \cdot K_F + 1) \cdot k_O \cdot t)) / (b \cdot K_F + 1)$. (*9*) with the 1-hour and 22-hour batch desorption data previously reported. The steady state concentration levels differ between the PFAS mainly because of differing initial concentrations during the adsorb phase. Although limited, the data allow rough estimations of k_O values.

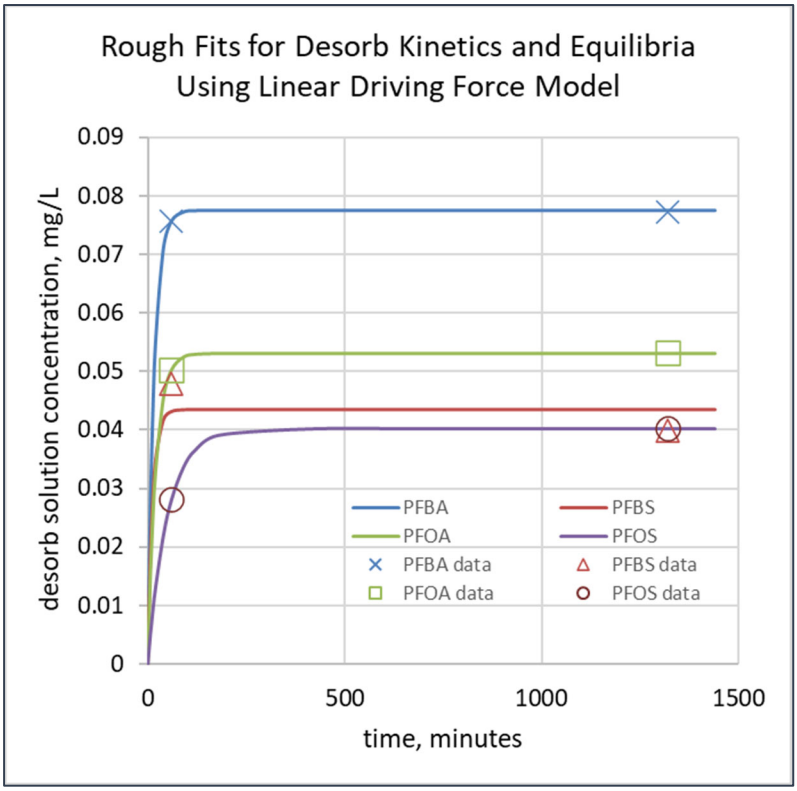

Figure 28 – Equation (9) compared with data for PFAS desorption from HG-1(Cl)

Next, we apply the ldf approximation in partial differential equations that represent variation of fluid and sorbent contents of contaminant with time and depth in an adsorption column,

$$\partial C / \partial x = - (k_O \cdot b / u) \cdot (qs - q) = - (k_O \cdot b / u) \cdot (K_F \cdot C^{(1/n)} - q) \qquad (10)$$

$$\partial q / \partial t = k_O \cdot (qs - q) = k_O \cdot (K_F \cdot C^{(1/n)} - q) \qquad (11)$$

where: x = distance in the direction of liquid flow through the column (cm)

u = superficial velocity of liquid in the column (cm/min)

and other symbols are as defined for the batch treatment. A spreadsheet had been constructed that numerically integrates the linked differential equations $\partial C / \partial x = - (kO \cdot b / u) \cdot (qs - q) = - (kO \cdot b / u) \cdot (KF \cdot C^{(1/n)} - q)$ (*10*) and $\partial q / \partial t = k_O \cdot (qs - q) = k_O \cdot (K_F \cdot C^{(1/n)} - q)$ (11) to find liquid concentration and sorbent loading profiles as a function of time and position in an adsorption column that obeys equations $dC / dt = - b \cdot dq / dt = - kO \cdot b \cdot (qs - q)$ (*5*) and $qs = K_F \cdot C^{(1/n)}$ (7). For the current analysis, the spreadsheet was expanded to simulate a column operated in a cycle, alternating between adsorption and counter-current regeneration. The distribution of sorbent loading with PFAS through the column after each regeneration is used at the start of the next adsorption cycle and the calculation can quickly find a steady-state condition. Current results

should be considered only a preliminary assessment of possible performance because only batch data have been used to evaluate parameters, limited batch data were available to evaluate the desorption parameters, rate measurements used small samples of unknown size distribution, and because the model is based on the ldf approximation.

Table 14 lists parameters found from batch data together with column design parameters selected for the case to be presented, PFOA adsorption and regeneration. A 1.2-meter bed depth would be easily accommodated in typical water treatment adsorption columns and velocities from 9 to 45 cm/min are within the 1-12 gpm/ft^2 surface loading rate range recommended for IX columns (U.S. EPA Office of Water, 2023). Adsorption would typically be in downflow. The lower up flow desorption velocity should prevent fluidization of bed particles but is high enough to assure good liquid distribution. The 60 g/L bulk density results from the ionomer's water-swelling characteristic. Despite this low density, the 2.7-minute empty bed contact time represents high volumetric productivity for PFAS removal, compared with current water treatment practice.

Table 14 - Parameters Used for Column Performance Projection

Parameter	Units	PFOA adsorption	PFOA desorption
K_F	$(mg/g)/(mg/L)^{(1/n)}$	2,030	0.40
n	none	1	1
k_O	/min	1.92E-4	3.80E-2
b	g/L	60	60
Cf (feed concentration)	mg/L	5E-5 (50 ppt)	0
u	cm/min	45	9 (reverse direction)
sorbent bed depth	cm	120	120
cycle time	days	150	0.25 (6 hours)

Figure 29 displays the calculated adsorption breakthrough curve based on the adsorption and desorption cycles of **Table 14**. Calculated concentration half-way through the 120 cm column is also displayed.

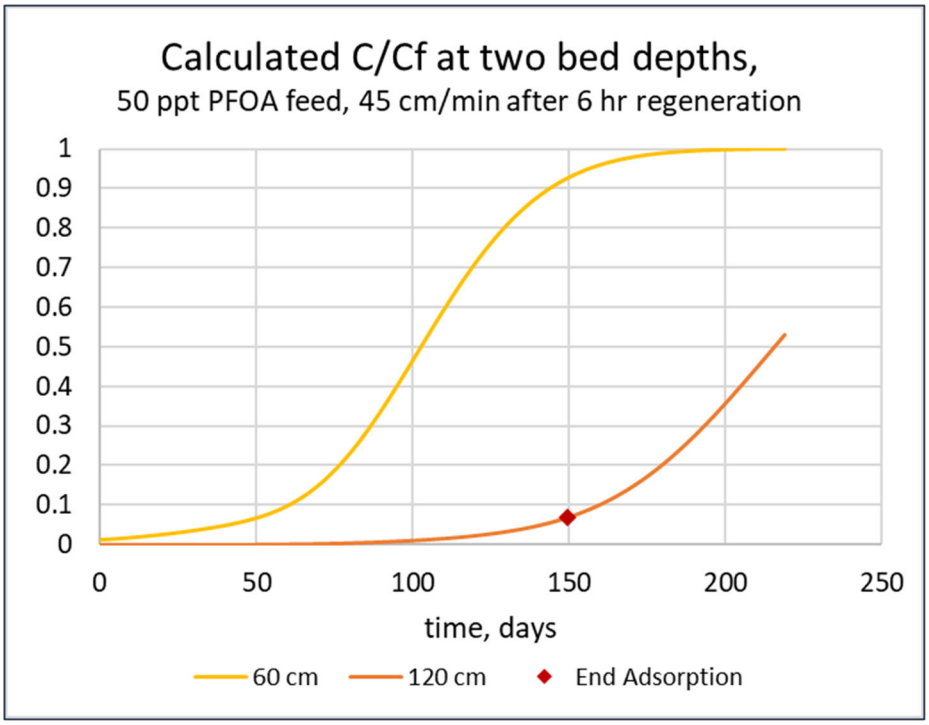

Figure 29 – Modeled PFOA Breakthrough Curve

Figure 30 displays the calculated desorption product concentration factor over the 6-hour regeneration cycle. From the 50 ppt PFOA feed, the calculation indicates that regeneration can produce a 150 ppb PFOA concentrate with volume reduction by a factor of 3,000.

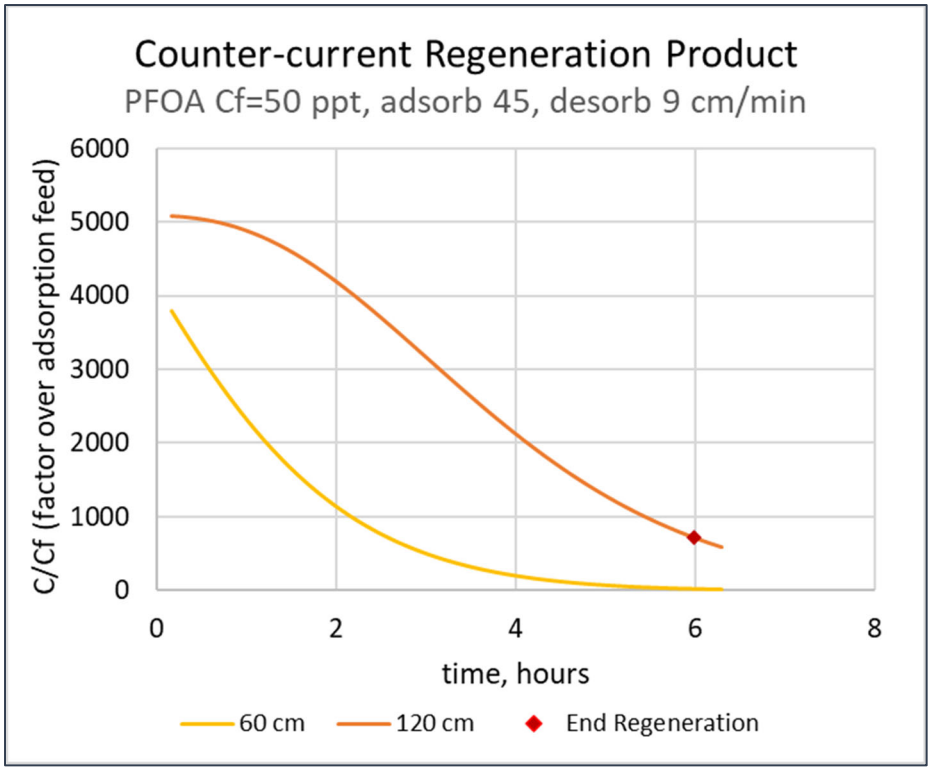

Figure 30 – Modeled Regeneration Product PFOA Concentration

Figure 31 displays the calculated bed loading profiles after adsorption and counter-current regeneration.

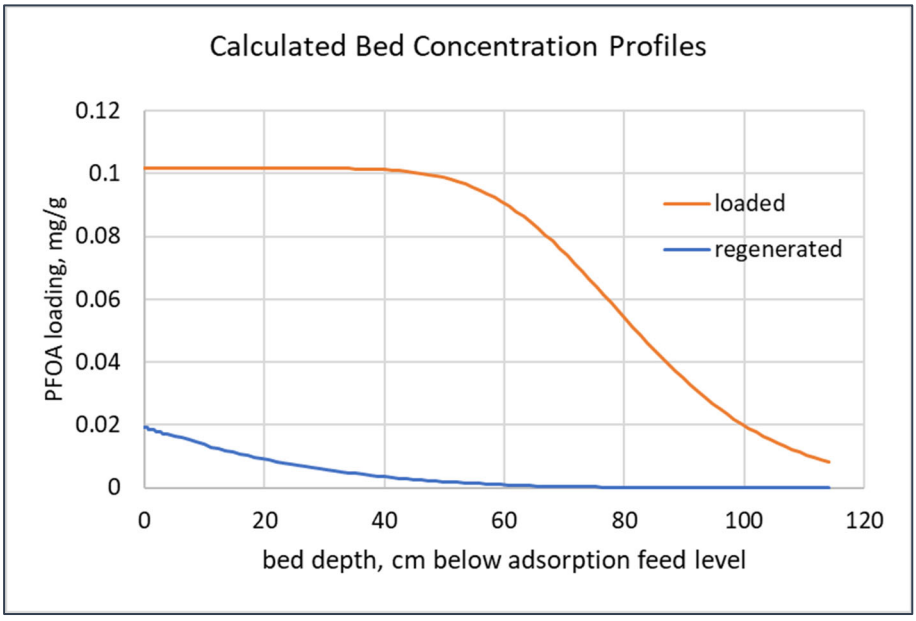

Figure 31 – Modeled PFOA Bed Loading Profile After Adsorption and Regeneration

In addition to the adsorption feed and desorption solution-fed regeneration, each cycle would also require a purge step to remove desorb solution from the bed before the next adsorption feed. Treated water (adsorption product) could feed that step. Assuming three empty bed volumes

would be sufficient for that purpose, the purge step reduces the expected concentration factor from 3000 to 2700 times the adsorption feed PFAS concentration.

The desorption isotherm used in the above modeling was based on data at a single concentration and an assumed slope, as illustrated in **Figure 27**. In an attempt to confirm the desorption isotherm, additional batch adsorption and desorption experiments were conducted using different ratios of adsorb solution volume to desorb solution volume, resulting in equilibration at several additional concentrations. The results show considerable scatter, due, apparently, to the fact that each post-desorption sorbent PFAS loading value is determined from two differences between three measured liquid concentrations multiplied by the corresponding solution volumes, per equation (4). Any random error in the three concentration values is amplified in calculating that PFAS loading value. **Figure 32** shows that although the data are insufficient to fully define desorption isotherms, they are consistent with the isotherm lines chosen for the modeling already presented.

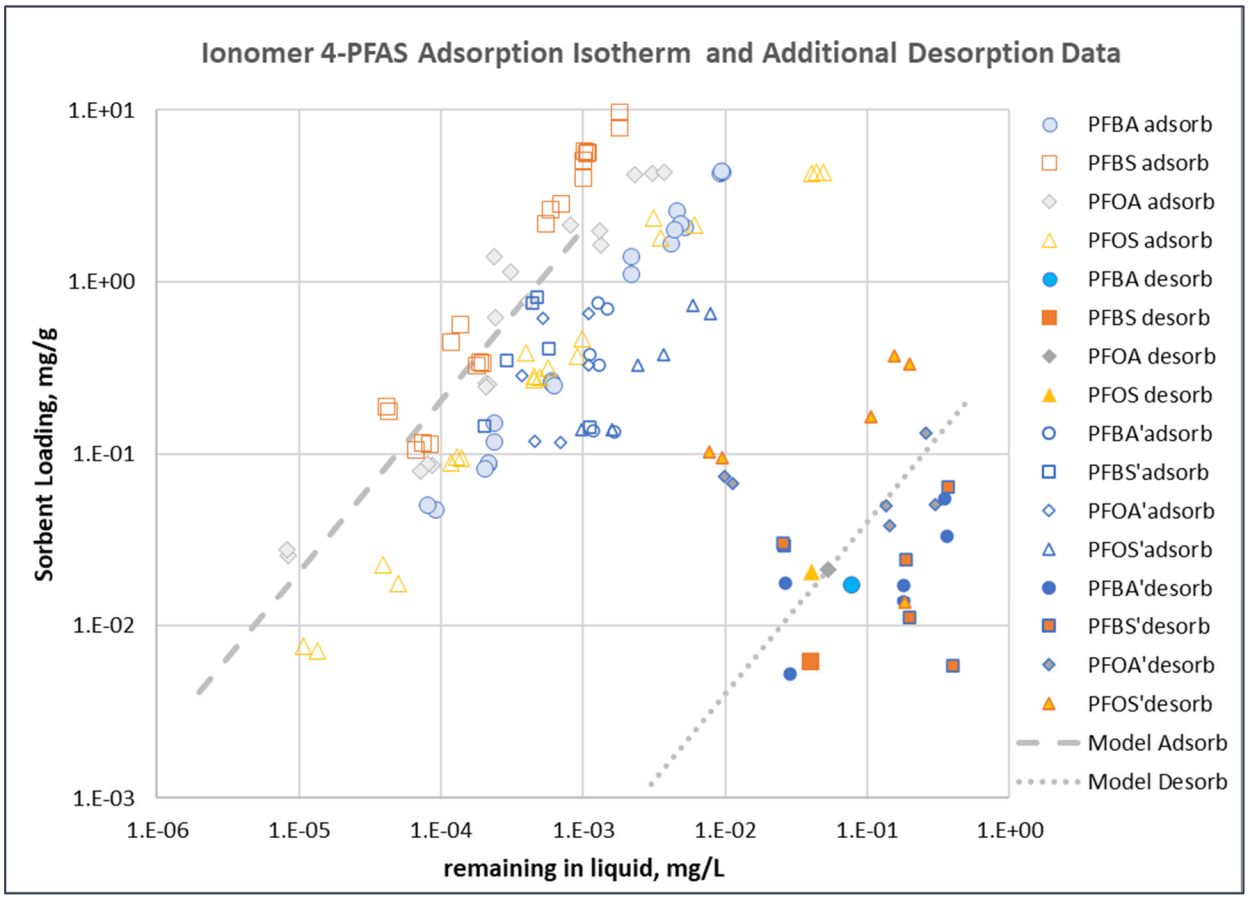

Figure 32 – Adsorption-Desorption Equilibrium Data Compared with PFOA Model Isotherms. *PFAS' in the legend indicates a separate data set.*

In summary, two-stage desorption was shown capable of fully removing adsorbed PFAS. Modeling work, however, indicates that a second, non-aqueous stage of desorption should not be necessary. The presented analysis shows that adsorption and aqueous desorption performance measured in batch experiments appears sufficient to project a flow system comprising a regenerable adsorption column, operable in a cycle, efficiently removing PFAS and producing

concentrate for destruction. More precise measurements of desorption equilibrium and kinetics are needed as well as studies to develop and measure sorbent column performance.

Demonstration of Ionomer Re-use After Desorption

A series of small column tests was designed to test how well ionomer can adsorb additional PFAS after desorption. The first two of five repeated adsorption and desorption cycles used 20 mL of a 4-PFAS mixture for adsorption and two doses of 20 mL each of aqueous desorb solution for the desorption, followed by 20 mL of 0.02 N HCl plus 0.5% NaCl to rinse out the desorb solution. As analytical results showed that the second desorb solution dose was removing only 0 to 4% of the adsorbed PFAS, it was eliminated from the third through fifth cycle. We suspect that in real-world application, a relatively small volume of treated water, without additives, may serve for the rinse step, as our proprietary desorption promoters do not contribute alkalinity.

Table 15 and **Figure 33** present the results of the test series. We can see in the table that incomplete desorption may have hindered subsequent PFOS adsorption, but that adsorption performance remained very good through the 5 cycles for the other three PFAS. While future work will aim to demonstrate reverse-flow desorption with concentration from large adsorption to small desorption volumes, and plain water rinse, this series of tests shows us that the desorb solution does not irreversibly degrade the ionomer, so that multiple re-uses after regeneration are possible.

Table 15 – Results of Repeated Adsorption and Desorption Tests with HG-1(Cl) Ionomer.
Values are the average of triplicate experiments.

% Adsorbed from ~250 ppb each PFAS*						% Desorbed by 20 mL aqueous solution			
	PFBA	PFBS	PFOA	PFOS		PFBA	PFBS	PFOA	PFOS
Cycle 1	100.0	100.0	99.9	93.2		120.2	98.2	97.8	82.3
Cycle 2	98.9	99.8	99.4	88.7		104.7	118.6	104.8	75.7
Cycle 3	99.6	99.3	95.7	44.3		106.4	90.5	104.2	92.2
Cycle 4	99.9	99.3	94.4	39.7		119.3	96.8	106.7	112.3
Cycle 5	100.0	99.9	98.7	68.7		107	95.9	105.9	88.2

* PFAS in the feed used for the first two cycles was found to be lower than intended. PFBA, PFBS, PFOA, and PFOS feed concentrations were 90, 74, 65, and 68 ppb, respectively, then increased to 250, 392, 248, and 252 ppb, respectively, in the feed used for the 3rd through 5th cycles.

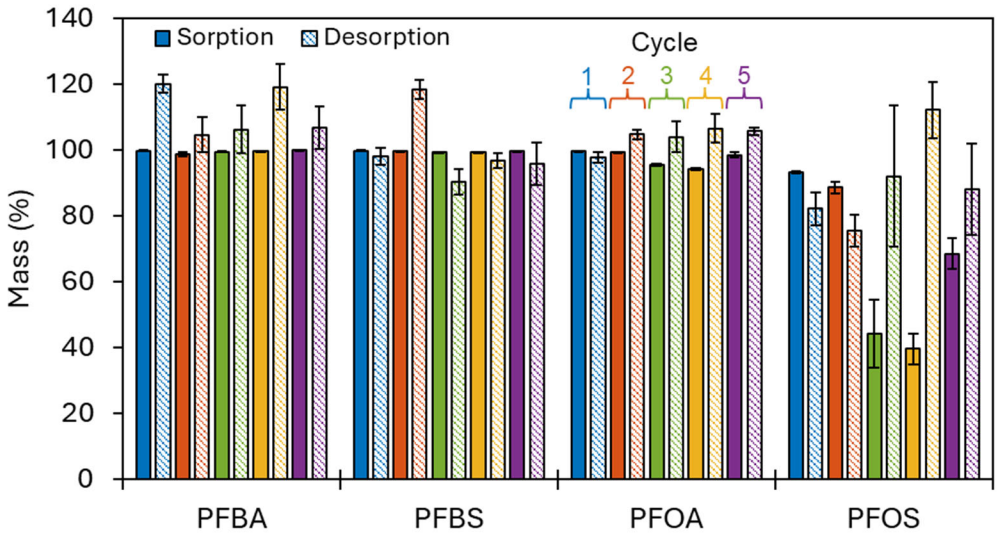

Figure 33 – Sorption/desorption of four PFAS in laboratory water (~250 ppb each) by novel ionomer HG-1 over five regeneration cycles. *Values are the average ± one standard deviation of triplicate experiments.*

In summary, we found that the initially-targeted aqueous alkaline desorption method was not sufficiently effective at regenerating sorbent after loading with the four PFAS mixture. Subsequently, we discovered that neutral additives, our proprietary desorption agents, are more effective and can be used at less than 1 wt% in water to effect desorption. Modeling work based on batch adsorption and desorption rate and equilibrium data, supported by a 5-cycle reuse test, indicates that ionomer may have the required properties for use in an all-aqueous column adsorption and regeneration system producing a PFAS concentrate suitable for economical PFAS destruction by methods such as hydrothermal alkaline treatment.

Task 3 – Hydrothermal Alkaline Treatment of Model PFAS (University of Delaware)

Materials and Methods

Hydrothermal degradation experiments were performed using a Parr 4790 pressure reactor with a capacity of 0.1 liter and a maximum allowable working pressure (MAWP) rating of 5,000 psi a 500 °C. Experiments were carried out at these four temperatures: 250, 300, 330 and 360 °C. Approximately 50 mL of aqueous solution containing 1 M NaOH and a single model PFAS at 0.1 mM was used for each experiment. The exact volume of the solution used was slightly below the maximum volume allowable, as calculated based on the unit volumes of liquid water and steam from the steam table for the maximum temperature in each experiment (e.g., the unit volumes of water and saturated steam are 1.893 and 6.945 mL/g, respectively, at 360 °C). In a second series of experiments, defluorination of a mixture of PFBA, PFBS, PFOA and PFOS was similarly tested.

The lowest temperature investigated was 250 °C as preliminary tests showed that negligible defluorination occurred at 200 °C for the model PFAS. The treatment time was fixed at 1 h for each temperature. Due to the limited total solution volume, the large sample size (5 mL) needed for fluoride measurement, and the significant dead volume in the sampling tube, we decided to test only two temperatures in each experiment; i.e., either 250 and 330 °C or 300 and 360 °C. After loading of PFAS sample, the reactor was sealed, heated to the first target temperature, and held at that temperature for 1 h. At this point, two samples were taken via the sampling valve. The reactor was then heated to the second target temperature and held at that temperature for 1 h. Two additional samples were collected directly from the reactor after cooling. A total of four samples were obtained at two different temperatures from each experiment. Samples were stored in 15-mL polypropylene centrifuge vials prior to fluoride measurement.

Fluoride concentrations in all samples were determined using ion selective electrodes (ISE). For data quality assurance, two fluoride ISE from two different vendors were used: Hannah Instruments HI4110 and Orion^{TM} fluoride electrode 9609BNWP from ThermoFisher. Each ISE was connected to an Orion Star^{TM} benchtop meter and a calibration curve was obtained for each ISE using the same calibration standards containing 0.02, 0.1, 0.5, 1.0 and 2.0 mM NaF. All calibration standards were prepared in 1.0 M NaOH.

As suggested by the vendors, 5 mL of TISAB III was added to each sample and calibration standard, even though TISAB had little impact on the pH and ionic strength due to the high NaOH concentration. To achieve the recommended pH of between 5 and 8, acetic acid (0.3 mL) was added to each sample and calibration standard.

Results and Discussion

The calibration curves for the Hannah and ThermoFisher ISE are shown in **Figure 34**. The R^2 values for both calibration curves are >0.99, although the ThermoFisher ISE shows a higher sensitivity to changing fluoride concentration (i.e., 15% steeper slope, –57.961 vs. –50.059 mV/log[F^-]). In both vendor manuals the default slope at room temperature is –56 ± 4 units, which is closer to that observed for the ThermoFisher ISE. In addition, the time required for a stable electrode response was also shorter for the ThermoFisher ISE. For these reasons we may use the ThermoFisher ISE for fluoride quantification (and use the Hannah ISE only for data confirmation).

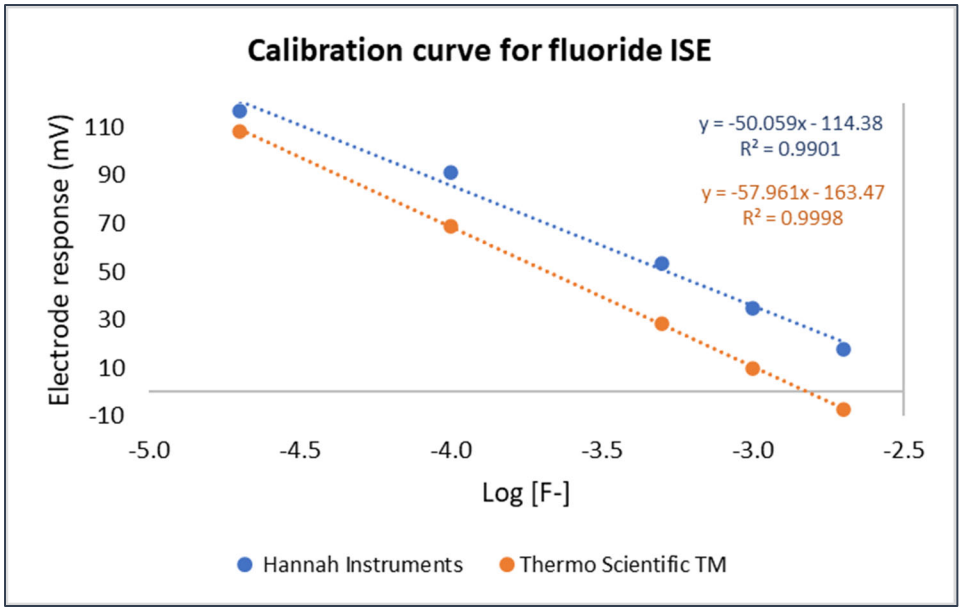

Figure 34 - Calibration curves for two fluoride ion selective electrodes (ISE). *Fluoride concentrations are in M (mol/L). All calibration standards were prepared with NaF in 1 M NaOH.*

The fluoride yields as a function of temperature for the 4 model PFAS are shown in **Figure 35**. Defluorination increased with temperature, was limited at ≤300 °C, but increased to 80–90% at 360 °C for all compounds. Note that, as we reported previously, PFOA and PFBA were degraded within minutes even at 250 °C; therefore, the higher temperatures and longer treatment times are necessary to degrade not the parent compounds but an unknown and highly fluorinated intermediate(s) that are more refractory than the parent compounds.

Pinkard et al. (Pinkard, Austin, Purohit, Li, & Novosselov, 2022) suggested that carboxylates (e.g., PFBA and PFOA) were decomposed more completely at 350 °C and 1 M NaOH than the sulfonates (e.g., PFBS and PFOS). If this is the case, the similar fluoride yields we obtained for all four PFAS at 360 °C may be due to the fact that PFBS and PFOS contain two more fluorine atoms than their carboxylate counterparts. Our results are comparable to that of Strathmann et al. (Strathmann, Wu, Hao, Choi, & Higgins, 2019), who reported that PFOS was about 80% defluorinated after 90 min of reaction in 1 M NaOH at 350 °C. The 10–20% fluorine mass balance gap in **Figure 35** suggests that organo-fluorides were produced; e.g., trifluoro-acetate and perfluoro-proprionate. We will analyze HALT-treated samples in the future for these and other potential degradation products to close the fluorine mass balance gap.

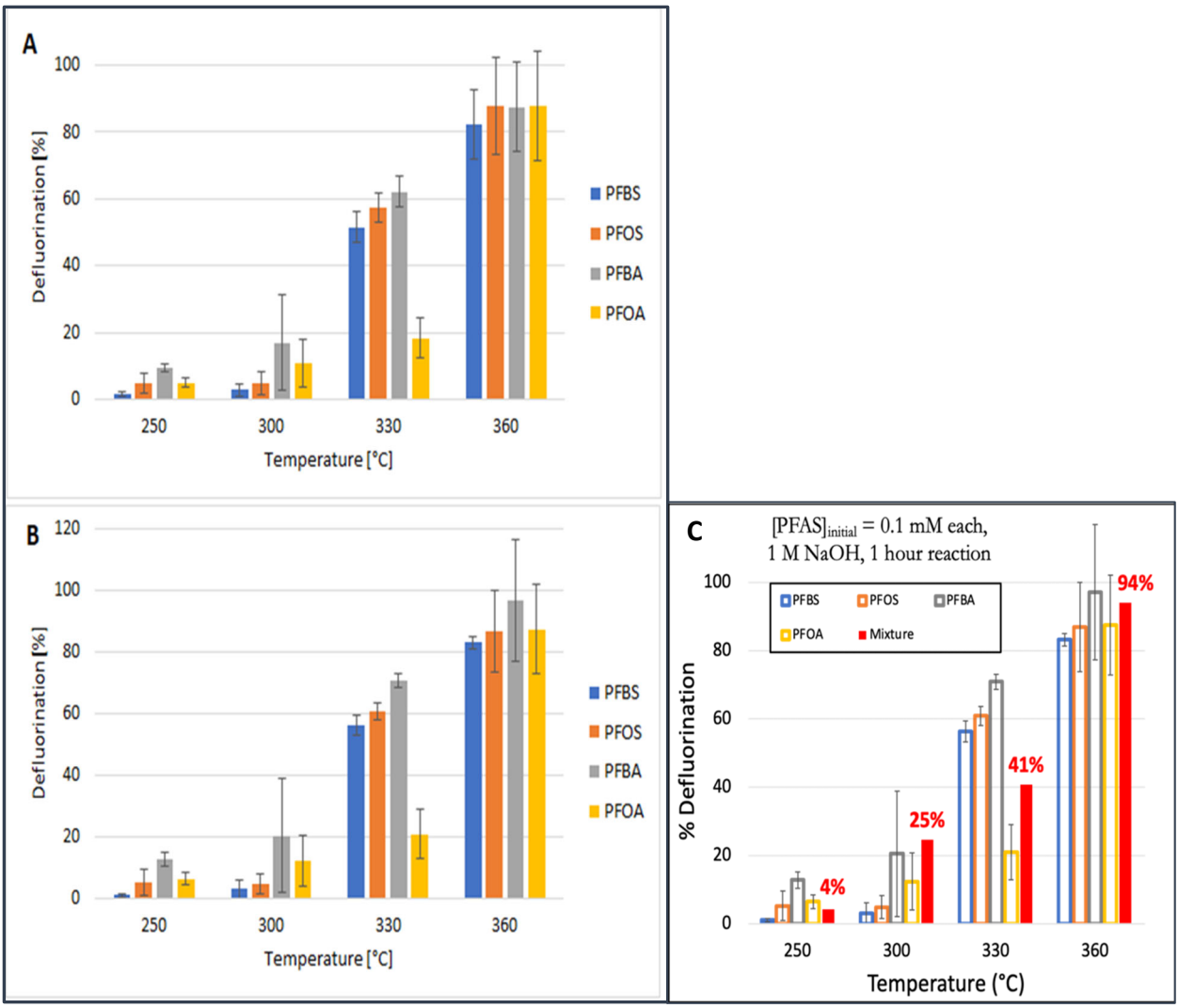

Figure 35 - Percent defluorination for four model PFAS following HALT treatment for 1 hour in 1 M NaOH. *Data obtained using the Hannah ISE* ***(A)*** *and the ThermoFisher ISE* ***(B)*** *are consistent, and comparable with data for a mixture of the four PFAS* ***(C)****. Error bars represent 1 standard deviation based on 4 samples obtained from 2 separate experiments (and 6 samples from 3 experiments for PFOA).*

In summary, our results are consistent with previous reports and support the hypothesis that HALT can be a compatible technology for PFAS destruction in alkaline concentrates from ionomer regeneration. The efficacy of PFAS desorption/ionomer regeneration using 1.0 M NaOH will be further evaluated.

Investigation of intermediates formed during HALT

Perfluoroheptanoyl Fluoride (PFHpF) as a Potential Intermediate Product of PFOA

Though PFOA was rapidly degraded within minutes in 1.0 M NaOH at 200, 225, and 250 °C, the fluoride yield was minimal even at 250 °C and complete fluoride recovery from PFOA was not obtained until 350 °C. This suggests that 1) no highly fluorinated volatile products of PFOA were formed or lost during experiments and 2) an unidentified and highly fluorinated intermediate(s) of

PFOA was formed that was more refractory than PFOA and would degrade and released fluoride only at 300–350 °C (**Figure 36**).

Based on the reaction mechanism proposed by Strathmann et al., Figure 4.6.1, (Strathmann, Higgins, & Deeb, September, 2020), the only possible intermediate (that is sufficiently stable and contains a large number of fluorine atoms) in the proposed pathway was perfluoroheptanoyl fluoride (PFHpF). We purchased PFHpF and used it as a starting material for hydrothermal degradation experiments. However, PFHpF was found to hydrolyze instantly in deionized water at room temperature, and a stoichiometric amount of fluoride was released (green dash line in **Figure 36**). This indicates that PFHpF would hydrolyze in water to PFHpA even under ambient conditions (see scheme below) and cannot be the persistent, highly fluorinated intermediate. These results suggest treatment criteria for PFOA and other PFAS should be based on fluoride recovery rather than disappearance of parent compounds.

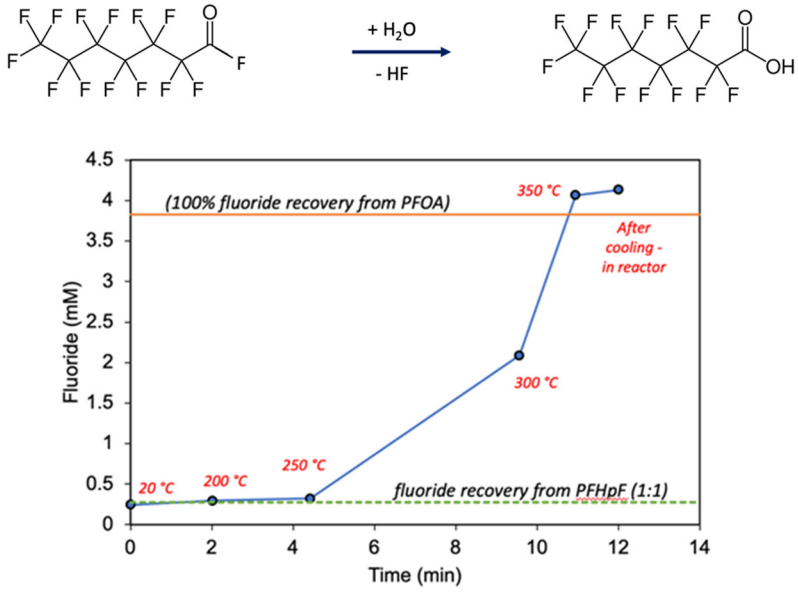

Figure 36 - Fluoride yields from hydrothermal alkaline hydrolysis of PFOA in 1.0 M NaOH and from room temperature hydrolysis of PFHpF in deionized water.

Activation Energy for Hydrothermal Alkaline Hydrolysis of PFOA and PFBA

Additional kinetic experiments were conducted to investigate the effect of temperature on the rates of PFOA and PFBA degradation. All experiments were carried out using a 100-mL high-temperature/high-pressure stainless steel reactor (Parr Instrument, Moline, IL) in an environmental engineering laboratory at the University of Delaware. The reactor was equipped with a heater and temperature controller that permits reactions under sub- or super-critical conditions. A predetermined amount (based on the molar volumes of liquid and gaseous water from the phase diagram) of PFBA or PFOA aqueous solution (40–50 mg/L) was placed in the reactor and NaOH was added to give an initial concentration of 1 M. The reactor was sealed and then placed inside a ceramic heating unit. Reaction began (i.e., time zero) when reactor temperature reached the set value (which took 20–30 min). Liquid samples were withdrawn at different reaction times through

a built-in sampling port for PFOA/PFBA and fluoride quantification. Experiments were repeated for different temperatures under otherwise identical conditions.

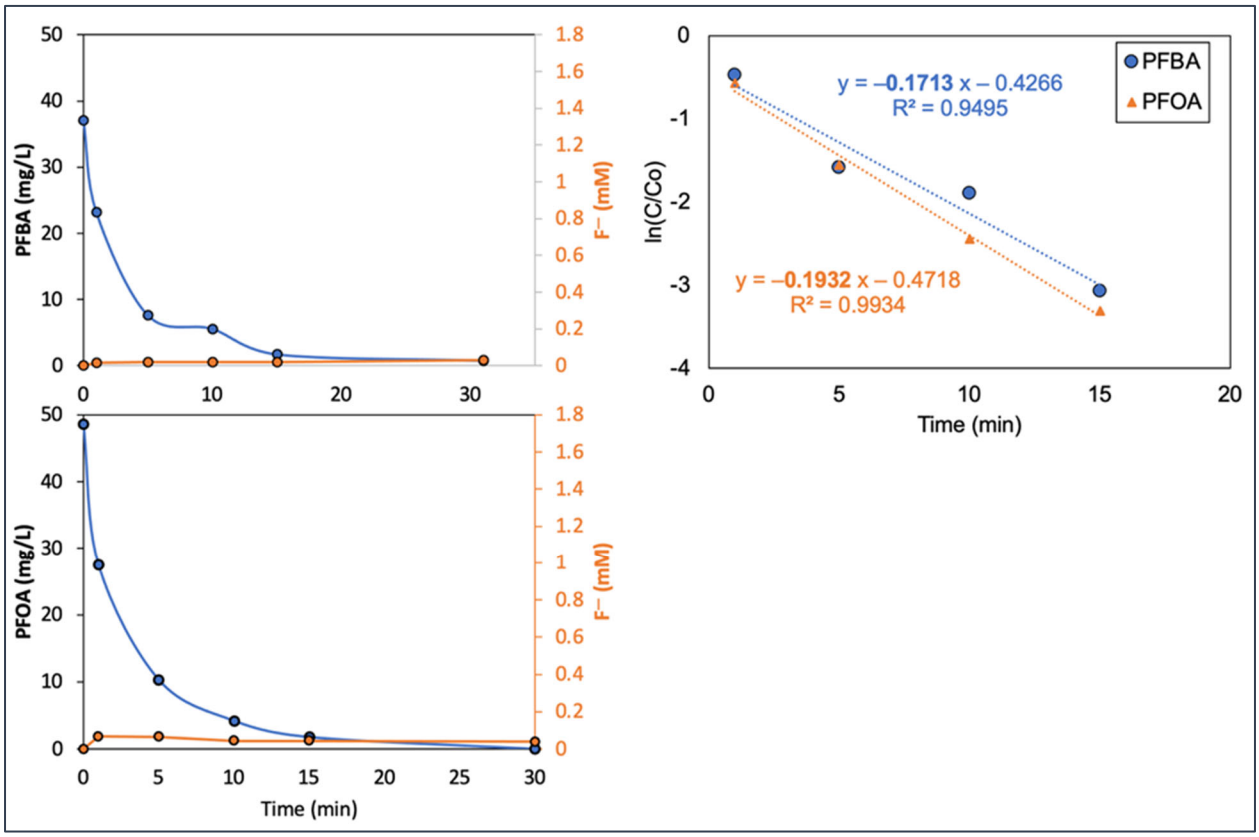

Figure 37 - PFBA and PFOA degradation and fluoride yields during hydrothermal alkaline hydrolysis in 1 M NaOH at 200 °C.

PFBA and PFOA were both degraded in minutes in a pseudo-first-order manner. The data for 200 °C are shown in **Figure 37**. The fitted rate constants are similar for PFBA and PFOA (0.17 min^{-1} and 0.19 min^{-1}, respectively), suggesting the degradation occurred at the head (carboxylate) group and was not (or only weakly) dependent on the chain length. As discussed above, minimal fluoride was released at 200 °C for both compounds, suggesting formation of stable, highly fluorinated intermediates.

Experiments were repeated at many additional temperatures for PFBA and PFOA. However, because the reaction rate was highly dependent on temperature, and because only a small number of samples (4–5) can be collected from the reactor, only a few experiments successfully produced reliable first-order rate constants. The fitted first-order rate constants were then divided by the NaOH concentration to give the corresponding second-order rate constants. Using the data for PFBA (**Figure 38**), the activation energy for the alkaline hydrolysis of PFBA can be estimated from the Arrhenius equation: Ea = R x slope = 8.3143E-3 x 20067 ≈ 167 kJ/mol (or 39.9 kcal/mol). A mechanism integrating this hydrolysis activation energy with defluorination kinetics remains to be developed.

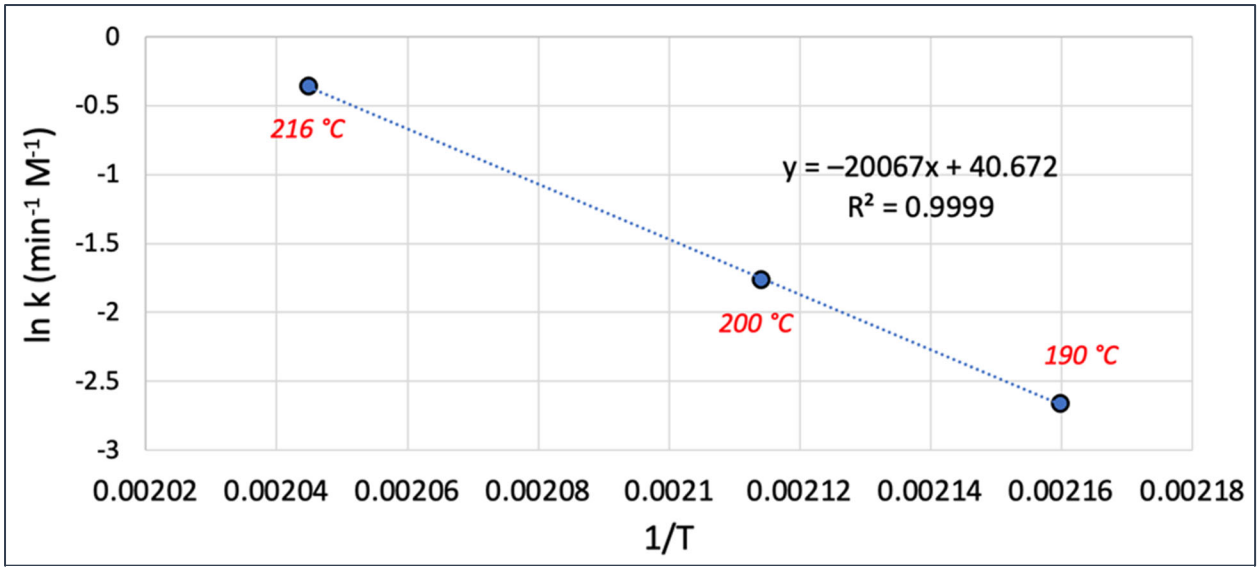

Figure 38 - Arrhenius plot for PFBA degradation at three temperatures. The activation energy derived from the slope is 167 kJ/mol.

Hydrothermal Alkaline Treatment (HALT) of 4 Model PFAS in desorbate from the ionomer

Hydrothermal alkaline treatment (HALT) has been shown to mineralize PFAS in aqueous and solid matrices at high efficiencies (Strathmann, Hao, Choi, Deeb, & Higgins, 2022). Previously, we showed that HALT could defluorinate the four model PFAS – PFOA, PFBA, PFOS, and PFBS – both individually and in combination (0.1 mM each) at high efficiencies. To determine whether HALT can effectively defluorinate PFAS mixture in ionomer regenerants, we performed additional HALT experiments in aqueous solutions that mimicked the ionomer regenerants.

The effect of two reagents called Proprietary Desorption Promoters (PDP) which are under development by the Center for PFAS Solutions on the defluorination efficiency, and the extent of their degradation during HALT were investigated.

All experiments were performed using a Parr 4790 pressure reactor with a capacity of 0.1 liter, under conditions similar to those described earlier. Briefly, experiments were carried out at 360 °C for 1 h in 50 mL of aqueous solution containing 1 M NaOH and 0.1 mM each of PFOA, PFBA, PFOS, and PFBS. The solution volume (50 mL) was chosen based on the unit volume of liquid water (1.893 mL/g) at 360 °C. Two PDP formulations (PDP A and PDP B) were added individually to the PFAS solution at various % (w/w).

At the end of each experiment, three aqueous samples were collected directly from the reactor after the reactor was cooled to ambient temperature. Fluoride concentrations were measured using an OrionTM fluoride ion selective electrode 9609BNWP (ThermoFisher) connected to an Orion StarTM benchtop meter. A calibration curve was obtained using calibration standards that contained 0.003, 0.03, 0.3, 3, and 6 mM NaF, 1 M NaOH, and either PDP A or PDP B. To achieve the vendor recommended pH range of 5 to 8, 0.3 mL of acetic acid was added to each sample and calibration standard.

Ammonia concentration was determined using the Hach Nitrogen-Ammonia reagent based on the salicylate method and quantified based on absorbance at 655 nm measured using a Vernier UV-vis spectrophotometer.

The fluoride yields for the degradation of PFAS mixture with and without PDP A or PDP B are shown in **Figure 39**. Consistent with our prior results (80–90%), the extent of defluorination for the four PFAS combined was 84.5±0.9% in the absence of PDP. The percentage of defluorination decreased to 77.4±1.1% and 71.4±3.6% in the presence of 0.2% PDP A and PDP B, respectively. The adverse effect of PDP on PFAS defluorination, while small (ca. 7% and 13%), is likely real, as it has been observed repeatedly in multiple experiments. The reason for the lower fluoride yields is unknown but may involve protection/shielding of PFAS molecules by PDP A and PDP B from the attack by hydroxide ions. Regardless of the cause, this result suggests that a slightly higher temperature or longer treatment time may be necessary to achieve the same extent of PFAS defluorination in the presence of either PDP.

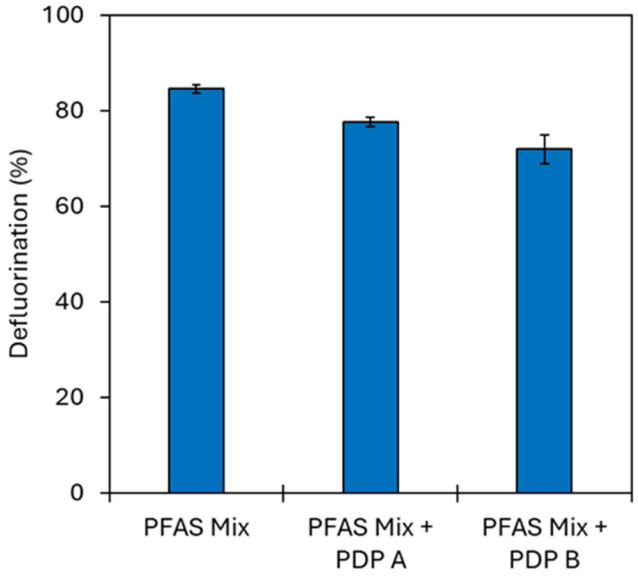

Figure 39 - Percent defluorination for a PFAS mixture (0.1 mM each of PFOA, PFBA, PFOS, and PFBS) following HALT treatment at 360 °C for 1 hour in 1 M NaOH. *Error bars represent one standard deviation based on triplicate measurements.*

We expected ammonia to be an end-product of PDP A hydrolysis if the reagent is degraded during HALT. After 1-hour treatment at 360 °C and pH 14, ammonia formation in the PDP A solution was negligible, statistically no different from the control (without HALT treatment). Following 3-hour treatment under the same conditions, the amount of ammonia formed was 2.7±1.7% of the total nitrogen mass in the PDP A. The result may appear to indicate that PDP A was essentially intact following 1 hour of HALT reaction; however, partial degradation in advance of ammonia release is possible.

Conclusions and Implications

Data developed in this project support using water-swellable ionomers in high-efficiency, on-site, all-aqueous, adsorption, regeneration, and destruction of PFAS. The studied ionomer was found to compare favorably in both adsorption kinetics and capacity with commercial sorbents. Further, a novel aqueous, methanol-free, desorption solution composition was identified which regenerates

the ionomer for reuse while producing a concentrate that, in a column implementation, may approach 3,000 times the concentration of the adsorption feed. This concentration factor has yet to be proven beyond batch equilibration testing. Such a desorbed concentrate was shown to be amenable to complete PFAS destruction and mineralization by hydrothermal alkaline treatment, and should also be treatable by other destruction technologies, producing an aqueous waste stream that is not expected to pose disposal difficulties. These results provide a basis for further development with good prospects for achieving the goal of an economical treatment process that can remove and destroy the PFAS in aqueous media without producing an ancillary waste stream that would require off-site management.

Future research is envisaged at both laboratory scale and semi-commercial scale for field demonstration:

Laboratory scale studies to determine range-of-effectiveness in the presence of co-contaminants, TOC, Mn, Nitrates, etc. are required. Extended column sorption and regeneration studies are required to prove the concentration factors and re-use for which some optimization of ionomer physical properties such as particle size, strength and swell-control may be required. These would be achievable through small ionomer recipe adjustments on a lab scale. Synthesizing other ionomer grades on a lab scale for studying sorption of a wider range of PFAS, telomers, ethers will expand their usefulness.

Semi-commercial scale synthesis of the ionomer would allow field demonstration for above and or below ground treatment. A better understanding of the cost of manufacturing water-swellable ionomers would aid in evaluating their feasibility for specific applications. Working with a toll manufacturer to produce ton quantities of ionomer would be an effective next step to improve our understanding of costs for larger-scale manufacture while also supplying material for field and other testing that requires larger volumes of sorbent. This could include testing an integrated adsorption-regeneration-destruction system that could be transported to operate at AFFF-impacted sites.

The novel desorption solution formulations developed in this work may be applicable beyond regenerating water-swellable ionomer. Certain anion exchange resins of so-called ‘weak base’ composition, currently used in applications such as water softening, may be used for PFAS removal with regeneration by a novel desorption solution, and integrated with a destruction process. This concept could be tested relatively rapidly and could then advance quickly toward real-world application.

Benefits. Our swellable ionomers offer the prospects for a PFAS remediation system that meets the requirements of a circular economy and uses green chemistry principles to sorb, desorb and mineralize PFAS. Our Ionomers do not contain or use fluorinated chemicals, unlike several of the new sorbents being developed for PFAS removal. Hence, there is no risk of releasing fluorinated chemicals during production or use or after disposal. The all-aqueous desorption reagent avoids use of methanol which is not allowed on drinking water sites. The sorption, all-aqueous desorption and regeneration of the ionomers followed by direct HALT treatment of the regenerants to degrade and mineralize PFAS simplifies the treatment train and reduces treatment time, environmental impact, costs, and complexity.

Literature Cited

AECOM. (2016). *Poly- and Perfluoralkkyl Substance Groundwater Sampling Report - Event #1. Installation Restoration Program Site 9 Delaware Air National Guard Base, New Castle, Delaware.* Dallas, TX: AECOM.

Appleman, T. D., Higgins, C. P., Quinones, O., Vanderford, B. J., Kolstad, C., Zeigler-Holady, J. C., & Dickenson, E. R. (2014). Treatment of poly- and perfluoroalkyl substances in U.S. full-scale water treatment systems. *Water Research, 15*(51), 246-255.

Ateia, M., Alsbaiee, A., Karanfil, T., & Dichtel, W. (2019). Efficient PFAS Removal by AmineFunctionalized Sorbents: Critical Review of the Current Literature. *Environ. Sci. Technol. Lett., 6*, 688-695.

Ateia, M., Arifuzzaman, M., Pellizzeri, S., Attia, M. F., Tharayil, N., Anker, J. N., & Karanfil, T. (2019). Cationic polymer for selective removal of GenX and short-chain PFAS from surface waters and wastewaters at ng/L levels. *Water Research, 163*, 11487.

Ateia, M., Attia, M. F., Maroli, A., Tharayil, N., Alexis, F., Whitehead, D. C., & Karanfil, T. (2018). Rapid Removal of Poly- and Perfluorinated Alkyl Substances by Poly(ethylenimine)-Functionalized Cellulose Microcrystals at Environmentally Relevant Conditions. *Environmental Science and Technology Letters, 5*, 764-769.

Chularueangaksorn, P., Tanaka, S., Fujii, S., & Kunacheva, C. (2014). Adsorption of perfluorooctanoic acid (PFOA) onto anion exchange resin, non-ion exchange resin, and granular-activated carbon by batch and column. *Desalination and Water Treatment, 52*, 6542-6548.

Coleman-Kammula, S. M., Figuly, G. D., Powley, C. R., & Massouda, D. F. (2022). *United States Patent No. Application 2022/0088570 A1.*

DNREC. (2015). *Preliminary Assessment of Zero (0) E. Basin Road Site PFOS & PFOA Impacted Public Wells in New Castle, Delaware.* Dover, DE: State of Delaware.

Emery, I., Kempisty, D., Fain, B., & Mbonimpa, E. (2019). Evaluation of Treatment Options for Well Water Contaminated with Perfluorinated Alkyl Substances Using Life Cycle Assessment. *J. Life Cycle Assess., 24*(1), 117-128.

Flowers, R. C., & Singer, P. C. (2013). Anion Exchange Resins as a Source of Nitrosamines and Nitrosamine Precursors. *Environ. Sci. Technol.*, 7365-7372.

Hainer, J. W., Hunninghake, D. B., Benedek, I. H., Broyles, F. E., Garner, D. M., Jenkins, R. M., . . . Gillies, P. J. (1997). DMP 504, a novel hydrogel bile acid sequestrant: III. Safety, tolerability, and cholesterol-lowering in healthy hypercholesteroiemic subjects. *Drug Development Research, 41*(2), 76-84.

Hansen, M. C., Borresen, M. H., Schlabach, M., & Cornelissen, G. (2010). Sorption of perfluorinated compounds from contaminated water to activated carbon. *J. Soils Sediments, 10*(2), 179-185.

Ho, Y. S., & McKay, G. (1999). Pseudo-second order model for sorption processes. *Process Biochemistry, 34*, 451-465.

Kassar, C., Graham, C., & Boyer, T. H. (2022). Removal of perfluoroalkyl acids and common drinking water contaminants by weak-base anion exchange resins: Impacts of solution pH and resin properties. *Water Research X, 17*, 1-15.

LeVan, M. D., Carta, G., & Yon, C. M. (1997). Adsorption and Ion Exchange. In R. H. Perry, D. W. Green, & J. O. Maloney, *Perry's Chemical Engineers' Handbook, 7th Edition* (pp. 16-1 to 16-66). New York, NY: McGraw-Hill Company.

McCleaf, P., Englund, S., Ostlund, A., Lindegren, K., Wiberg, K., & Ahrens, L. (2017). Removal efficiency of multiple poly- and perfluoroalkyl substances (PFASs) in drinking water using granular activated carbon and anion exchange column tests. *Water Research, 120*, 77-87.

Ochoa-Herrera, V., & Sierra-Alvarez, R. (2008). Removal of perfluorinated surfactantsby sorption onto granular activated carbon, zeolite and sludge. *Chemosphere, 72*(10), 1588-1593.

Pinkard, B., Austin, C., Purohit, A., Li, J., & Novosselov, I. V. (2022). Destruction of PFAS in AFFF-impacted fire training pit water with a continuous hydrothermal alkaline treatment reactor. *Chemosphere, 314*. doi:10.1016/j.chemosphere.2022.137681

Ross, I., McDonough, J., Miles, J., Stroch, P., Kochunarayanan, P. T., Kalve, E., . . . Dasgupta, S. S. (2018). A review of emerging technologies for remediation of PFASs. *Remediation, 28*, 101-126.

Stebel, E. K., Pike, K. A., Nguyen, H., Hartmann, H. A., Klonowski, M. J., Lawrence, M. G., . . . Edmiston, P. L. (2019). Adsorption of short-chain to long-chain perfluoroalkyl substances using swellable organically modified silica. *Environmental Science: Water Research Technology, 5*, 1854-1866.

Strathmann, T. J., Hao, S., Choi, Y. J., Deeb, R. A., & Higgins, C. P. (2022). Application of Hydrothermal Alkaline Treatment for Destruction of Per- and Polyfluoroalkyl Substances in Contaminated Groundwater and Soil. *Environmental Science & Technology, 56*(10), 6647-6657. doi:10.1021/acs.est.2c00654

Strathmann, T. J., Higgins, C., & Deeb, R. (September, 2020). *Hydrothermal Technologies for On-Site Destruction of Site Investigation Wastes Contaminated with Per- and Polyfluoroalkyl Substances (PFAS).* SERDP Project ER18-1501 Final Report.

Strathmann, T. J., Wu, B., Hao, S., Choi, Y., & Higgins, C. P. (2019). Rapid Destruction and Defluorination of Perfluorooctanesulfonate by Alkaline Hydrothermal Reaction. *Environmental Science & Technology Letters, 6*(10), 630-636. doi:10.1021/acs.estlett.9b00506

U.S. EPA. (2017). *Treatment of Perfluorinated Alkyl Substances in Wash Water Using Granular Activated Carbon and Mixed-Media.* Washington, DC: EPA.

U.S. EPA. (2023, November 6). *What is a Circular Economy*. Retrieved from Circular Economy: https://www.epa.gov/circulareconomy/what-circular-economy

U.S. EPA Office of Water. (2023). *Work Breakdown Structure-Based Cost Model for Ion Exchange Treatment of Per- and Polyfluoroalkyl Substances (PFAS) in Drinking Water.* Washington, DC: U.S. EPA. Retrieved from https://www.epa.gov/system/files/documents/2023-04/WBS-IXPFAS-Documentation-March-2023 - 508 Completed.pdf

Wang, J., Lin, Z., He, X., Song, M., Westerhoff, P., Doudrick, K., & Hanigan, D. (2022). Critical Review of Thermal Decomposition of Per- and Polyfluoroalkyl Substances: Mechanisms and Implications for Thermal Treatment Processes. *Environmental Science & Technology, 56*(9), 5355-5370. doi:10.1021/acs.est.2c2251

Watanabe, N., Takata, M., Takemine, S., & Yamamoto, K. (2018). Thermal Mineralization Behavior of PFOA, PFHxA, and PFOS during Reactivation of Granular Activated Carbon (GAC) in Nitrogen Atmosphere. *Environ. Sci. Pollut. Res. Int., 25*(8), 7200-7205.

Woodard, S., Berry, J., & Newman, B. (2017). Ion exchange resin for PFAS removal and pilot test comparison to GAC. *Remediation, 27*, 19-27.

Xiao, F., Sasi, P. C., Yao, B., Kubatova, A., Golovko, S. A., Golovko, M. Y., & Soli, D. (2020). Thermal Stability and Decomposition of Perfluoroalkyl Substances on Spent Granular Activated Carbon. *Environ. Sci. Technol. Lett., 7*(5), 343-350.

Xiao, L., Ling, Y., Alsbaiee, A., Li, C., Helbling, D. E., & Dichtel, W. R. (2017). β-Cyclodextrin Polymer Network Sequesters Perfluorooctanoic Acid at Environmentally Relevant Concentrations. *Journal of the American Chemical Society, 139*, 7689-7692.

Yan, B., Wang, J., & Liu, J. (2021). STXM-XANES and computational investigations of adsorption of per- and polyfluoroalkyl substances on modified clay. *Water Research, 201*, 1-10.

Zaggia, A., Conte, L., Falletti, L., Fant, M., & Chiorboli, A. (2016). Use of strong anion exchange resins for the removal of perfluoroalkylated substances from contaminated drinking water in batch and continuous pilot plants. *Water Research, 91*, 137-146.

Zhang, D., Luo, Q., Gao, B., Chiang, D., Woodward, D., & Huang, Q. (2016). Sorption of Perfluorooctanoic Acid, Perfluorooctane Sulfonate and Perfluoroheptanoic Acid 2 on Granular Activated Carbon. *Chemosphere, 144*, 2336-2342.

Appendix 1 – Supporting Data

The following tables provide data in numerical form that are plotted in figures throughout the report. In some cases, the provided data are the values reported out of chemical analysis, and in others the data were determined from such experimental values by simple calculations or using formulas presented in the report.

Table 16 - PFOA Adsorption Kinetic Data for Figures 1 and 11

Time, minutes	PFOA, µg/L			Average
HG-1, 10 mg/L				
0	0.689	0.723	0.762	0.725
1	0.277	0.318	0.326	0.307
2	0.246	0.274	0.199	0.240
5	0.142	0.232	0.173	0.182
10	0.093	0.201	0.269	0.188
20	0.108	0.146	0.044	0.100
60	0.080	0.085	0.017	0.061
HG-5, 10 mg/L				
0	0.752	0.716	0.735	0.735
1	0.321	0.322	0.344	0.329
2	0.332	0.240	0.251	0.274
5	0.213	0.202	0.182	0.199
10	0.199	0.110	0.133	0.147
20	0.152	0.069	0.074	0.098
60	0.037	0.057	0.039	0.045
GAC F400, 100 mg/L				
0	0.627	0.602	0.585	0.605
60	0.418	0.318	0.357	0.364
120	0.350	0.127	0.267	0.248
240	0.2213	0.0503	0.1251	0.132
360	0.149	0.000	0.079	0.076
1440	0.000	0.000	0.000	0.000
IX, CR2301 AER, 100 mg/L				
0	0.472	0.554	0.516	0.514
60	0.158	0.308	0.240	0.235
120	0.129	0.256	0.210	0.198
240	0.1286	0.2212	0.1906	0.180
360	0.135	0.178	0.160	0.158
1440	0.094	0.158	0.116	0.123
Decafluorobiphenyl-cyclodextrin polymer, (Xiao et. al. 2017), 10 mg/L				
0				1.000
60	(data read from plot in paper)			0.880
120				0.700
300				0.310

Table 17 – PFOA Adsorption Kinetics Data for Figure 12

Time, minutes	Calculated PFOA loading, mg/g		
HG-1, 10 mg/L			
0	0.0000	0.0000	0.0000
1	0.0413	0.0404	0.0436
2	0.0443	0.0449	0.0563
5	0.0548	0.0491	0.0589
10	0.0596	0.0522	0.0493
20	0.0581	0.0576	0.0718
60	0.0609	0.0638	0.0745
HG-5, 10 mg/L			
0	0.0000	0.0000	0.0000
1	0.0432	0.0394	0.0392
2	0.0420	0.0476	0.0484
5	0.0540	0.0514	0.0553
10	0.0554	0.0606	0.0602
20	0.0601	0.0647	0.0661
60	0.0715	0.0659	0.0696

Table 18 - Four PFAS Adsorption Kinetic Data for Figures 2a and 15

Time, hours	PFBA, ppb	PFBS, ppb	PFOA, ppb	PFOS, ppb
HG-1, Trial 1, 105 m/L				
0.000	9.33	6.98	1.97	5.05
0.017	8.32	5.51	1.50	4.75
0.083	8.22	4.60	1.56	5.07
0.167	7.26	4.31	1.67	5.21
0.333	5.80	2.74	1.37	5.14
1.000	2.49	1.11	1.25	4.08
24.000	0.14	0.03	0.10	1.83
HG-1, Trial 2, 121 mg/L				
0.000	8.61	7.00	2.13	5.02
0.017	8.33	4.83	1.53	4.63
0.083	7.87	4.28	1.47	4.86
0.167	7.17	4.10	1.37	4.29
0.333	6.04	3.17	1.35	4.25
1.000	3.30	1.59	1.29	4.04
24.000	0.13	0.04	0.09	2.28
HG-1, Trial 3, 125 mg/L				
0.000	9.00	6.22	2.39	5.47
0.017	8.12	4.91	1.49	4.55
0.083	7.80	4.85	1.48	4.54
0.167	7.05	4.56	1.38	4.12
0.333	6.22	3.59	1.28	4.57
1.000	3.95	1.73	1.24	3.61
24.000	0.13	0.04	0.08	1.89

Table 19 - Four PFAS Adsorption Kinetic Data for Figures 2b and 16

Time, hours	PFBA, ppb	PFBS, ppb	PFOA, ppb	PFOS, ppb
HG-1, Trial 1, 120 mg/L				
0.000	88.74	69.94	15.09	10.11
0.017	80.81	67.21	8.49	5.38
0.083	76.14	63.20	6.02	3.41
0.167	78.05	55.51	7.66	3.71
0.333	72.06	48.01	7.13	5.41
1.000	42.56	24.34	6.43	5.09
24.000	1.39	0.39	2.06	6.88
HG-1, Trial 2, 124 mg/L				
0.000	81.44	73.60	15.81	16.06
0.017	81.10	63.48	10.38	8.52
0.083	77.19	54.39	7.62	5.65
0.167	72.44	51.77	10.33	11.91
0.333	60.93	37.57	7.43	6.06
1.000	33.82	15.19	4.89	3.91
24.000	1.48	0.35	1.44	4.83

Table 20 – Four PFAS Adsorption Kinetic Data for Figures 2c and 13

Time, hours	PFBA, ppb	PFBS, ppb	PFOA, ppb	PFOS, ppb
GAC F400, Trial 1, 133 mg/L				
0	8.60	8.92	7.22	4.09
1	7.81	7.36	5.60	2.48
2	6.20	6.23	4.84	2.42
4	5.10	4.87	3.69	1.30
6	3.70	3.67	2.70	0.82
24	0.31	0.35	0.20	0.14
GAC F400, Trial 2, 117 mg/L				
0	8.76	8.81	6.70	3.04
1	7.75	7.49	5.92	2.72
2	6.95	6.67	4.74	2.00
4	4.87	4.54	3.36	1.26
6	3.63	3.33	2.50	0.76
24	0.28	0.31	0.22	0.09

Table 21 - Four PFAS Adsorption Kinetic Data for Tables 2d and 14

Time, hours	PFBA, ppb	PFBS, ppb	PFOA, ppb	PFOS, ppb
IX CR2304, Trial 1, 111 mg/L				
0	8.91	9.21	5.28	1.89
1	7.27	7.27	3.19	2.67
2	6.25	6.07	2.70	2.94
4	4.17	4.45	2.23	3.95
6	2.93	3.02	1.72	4.35
24	0.08	0.37	1.04	5.20
IX CR2304, Trial 2, 127 mg/L				
0	8.67	8.89	4.85	1.46
1	6.83	6.79	2.74	2.28
2	6.02	5.69	2.31	2.77
4	3.85	3.96	1.86	3.59
6	2.43	2.80	1.70	4.50
24	0.05	0.31	1.01	5.89

Table 22 - Adsorption Kinetic Rate Parameters for Figures 3 and 20

	1st order reversible rate parameters, L/g/hr			
	PFBA	PFBS	PFOA	PFOS
GAC (Filtrasorb 400)	1.3	1.4	1.9	3.6
IX (CR 2304)	2.0	1.7	9.1	**
HG-1	8.8	17.9	23.5	30.1

** Our rate data for PFOS on CR2304 do not allow a reasonable rate equation fit.

Table 23 - HG-1 Equilibrium Data for Figures 4 and 21

	C, mg/L	q, mg/g
from kinetics	6.05E-05	6.25E-02
isotherm experiments	*Trial 1*	
	1.87E-03	1.10E+00
	6.96E-03	2.12E+00
	7.84E-03	5.22E+00
	3.41E-02	2.05E+01
	7.43E-02	7.82E+01
	2.22E+00	1.76E+02
	2.41E+01	1.65E+02
	Trial 2	
	3.68E-03	1.08E+00
	6.07E-03	2.13E+00
	1.11E-02	5.18E+00
	2.92E-02	2.05E+01
	8.62E-02	7.81E+01
	1.96E+00	1.79E+02
	2.99E+01	1.07E+02
	Trial 3	
	4.06E-03	1.08E+00
	1.41E-03	2.18E+00
	1.28E-02	5.17E+00
	2.59E-02	2.06E+01
	7.69E-02	7.82E+01
	2.14E+00	1.77E+02
	2.77E+01	1.29E+02

Table 24 - Published PFOA Isotherm Data for Comparison, Figures 4 and 21

$q = K_F C^{1/n}$ isotherm form fit to published data				
			concentration range	
Material Abbreviation*	K_F mg/g/(mg/L)$^{1/n}$	n	from mg/L	to mg/L
DFB-CDP	12	2.4	0.25	9.4
GAC	2.2	1.1	0.5	7
func. cell.	11	2.0	0.0005	0.03
amine/clay	5.8	1.6	0.0005	0.004
amine/clay	18	3.6	0.2	8
poly-SOMS	38	1.4	0.05	0.8
Dow Mar. A IX	93	1.1	0.004	0.47

For the unusual amine/clay data set, the following data were read directly from a plot in the cited paper.

C, mg/L	q, mg/g
5.40E-04	5.60E-02
8.70E-04	5.80E-02
1.25E-03	6.40E-02
1.58E-03	7.20E-02
1.60E-03	8.60E-02
1.77E-03	1.12E-01
2.72E-03	1.35E-01
3.90E-03	1.82E-01
3.80E-03	6.80E-01
4.50E-03	1.80E+00
2.50E-02	3.10E+00
2.60E-02	5.75E+00
1.60E-01	1.40E+01
8.30E-01	1.77E+01
2.60E+00	1.93E+01
8.08E+00	3.50E+01

* DFB-CDP: decafluorobiphenyl-cyclodextrin polymer (Xiao, et al., 2017), GAC: granular activated carbon (Zhang, et al., 2016), functionalized cellulose (Ateia, et al., 2018), surfactant amine-modified clay (Yan, Wang, & Liu, 2021), poly-SOMS: polymer-infused swellable organically modified silica (Stebel, et al., 2019), Dow Marathon anion exchange resin (Chularueangaksorn, Tanaka, Fujii, & Kunacheva, 2014)

Table 25 - Adsorption and Desorption Equilibrium Data for 4 PFAS on HG-1(Cl)

Sorbent Loading, mg/g				Equilibrium Liquid, mg/L			
PFBA	PFBS	PFOA	PFOS	PFBA	PFBS	PFOA	PFOS
Adsorption Experiments in De-Ionized Water (Figures 5, 6, 22, 27, 32,39)							
4.71E-02	1.77E-01	2.58E-02	7.07E-03	9.11E-05	4.27E-05	8.33E-06	1.36E-05
1.19E-01	4.44E-01	**	1.77E-02	2.38E-04	1.17E-04	**	4.99E-05
1.11E+00	4.04E+00	6.18E-01	3.72E-01	2.16E-03	1.01E-03	2.42E-04	9.03E-04
2.09E+00	7.87E+00	1.15E+00	3.16E-01	5.21E-03	1.80E-03	3.08E-04	5.67E-04
5.05E-02	1.89E-01	2.76E-02	7.58E-03	8.04E-05	4.10E-05	8.19E-06	1.08E-05
1.51E-01	5.67E-01	**	2.27E-02	2.37E-04	1.36E-04	**	3.92E-05
1.40E+00	5.08E+00	7.76E-01	4.67E-01	2.17E-03	1.01E-03	4.13E-04	9.89E-04
2.58E+00	9.67E+00	1.41E+00	3.89E-01	4.60E-03	1.79E-03	2.35E-04	3.95E-04
8.79E-02	1.15E-01	8.63E-02	9.50E-02	2.15E-04	8.34E-05	8.71E-05	1.39E-04
2.64E-01	3.44E-01	2.59E-01	2.85E-01	6.01E-04	1.89E-04	2.09E-04	4.55E-04
1.67E+00	2.18E+00	1.64E+00	1.80E+00	4.14E-03	5.43E-04	1.32E-03	3.52E-03
4.28E+00	5.59E+00	4.21E+00	4.29E+00	9.14E-03	1.06E-03	2.29E-03	4.06E-02
8.88E-02	1.16E-01	8.72E-02	9.61E-02	2.15E-04	7.38E-05	8.01E-05	1.28E-04
2.59E-01	3.38E-01	2.54E-01	2.79E-01	6.01E-04	1.94E-04	2.14E-04	4.95E-04
2.18E+00	2.85E+00	2.15E+00	2.36E+00	4.81E-03	6.96E-04	8.20E-04	3.13E-03
4.36E+00	5.70E+00	4.29E+00	4.34E+00	9.60E-03	1.09E-03	3.08E-03	4.34E-02
8.15E-02	1.06E-01	8.00E-02	8.82E-02	2.03E-04	6.62E-05	7.20E-05	1.18E-04
2.49E-01	3.25E-01	2.45E-01	2.69E-01	6.19E-04	1.78E-04	2.08E-04	4.50E-04
2.03E+00	2.64E+00	1.99E+00	2.16E+00	4.42E-03	5.86E-04	1.31E-03	6.10E-03
4.41E+00	5.76E+00	4.32E+00	4.33E+00	9.45E-03	1.02E-03	3.72E-03	4.91E-02
Adsorption Experiments in De-ionized Water (Figures 6, 32)							
3.81E-01	4.07E-01	3.29E-01	3.77E-01	1.12E-03	5.74E-04	1.09E-03	3.70E-03
7.60E-01	8.15E-01	6.59E-01	7.32E-01	1.27E-03	4.70E-04	1.10E-03	5.92E-03
1.36E-01	1.46E-01	1.19E-01	1.38E-01	1.18E-03	2.03E-04	4.54E-04	1.61E-03
3.27E-01	3.52E-01	2.87E-01	3.30E-01	1.29E-03	2.89E-04	3.73E-04	2.44E-03
7.01E-01	7.54E-01	6.15E-01	6.59E-01	1.47E-03	4.38E-04	5.16E-04	7.89E-03
1.34E-01	1.43E-01	1.17E-01	1.38E-01	1.66E-03	1.10E-03	6.89E-04	9.80E-04
Desorption into Aqueous Solution of 0.2% PDP A and 0.5% NaCl (Figures 6, 27, 32)							
1.73E-02	6.19E-03	2.13E-02	2.06E-02	7.73E-02	3.98E-02	5.31E-02	4.03E-02
Desorption into Aqueous Solution of 0.5% PDP A and 0.5% NaCl (Figures 6, 32)							
1.71E-02	1.11E-02	3.84E-02	1.64E-01	1.80E-01	1.96E-01	1.44E-01	1.05E-01
3.32E-02	5.88E-03	5.05E-02	3.36E-01	3.60E-01	4.01E-01	3.01E-01	1.96E-01
1.77E-02	2.92E-02	7.46E-02	9.56E-02	2.62E-02	2.59E-02	9.77E-03	9.49E-03
1.37E-02	2.43E-02	4.99E-02	1.36E-02	1.80E-01	1.88E-01	1.36E-01	1.82E-01
5.48E-02	6.47E-02	1.32E-01	3.73E-01	3.46E-01	3.69E-01	2.58E-01	1.53E-01
5.22E-03	3.01E-02	6.73E-02	1.04E-01	2.88E-02	2.53E-02	1.12E-02	7.73E-03

A limited set of data was collected on 48-hour equilibrium adsorption of a 4 PFAS mixture by the macroporous anion exchange resin CalRes 2301. **Figure 40** shows how the comparison with HG-1(Cl) performance presented in **Table 10** was accomplished. Because we had only four data points for each PFAS on CR2301, extrapolation would have been uncertain and the data did not allow interpolation to 1 ppb, as was done with the benchmark GAC and IX sorbents. The four plus marks in the figure indicate CR2301 adsorption of each PFAS interpolated to lower comparison concentrations of 5, 5, 10, and 100 ppt for PFBA, PFBS, PFOA, and PFOS, respectively. These values are compared in the table with interpolated, or slightly projected in the cases of PFBA and PFBS, performance of HG-1(Cl) along the best-fit dotted lines.

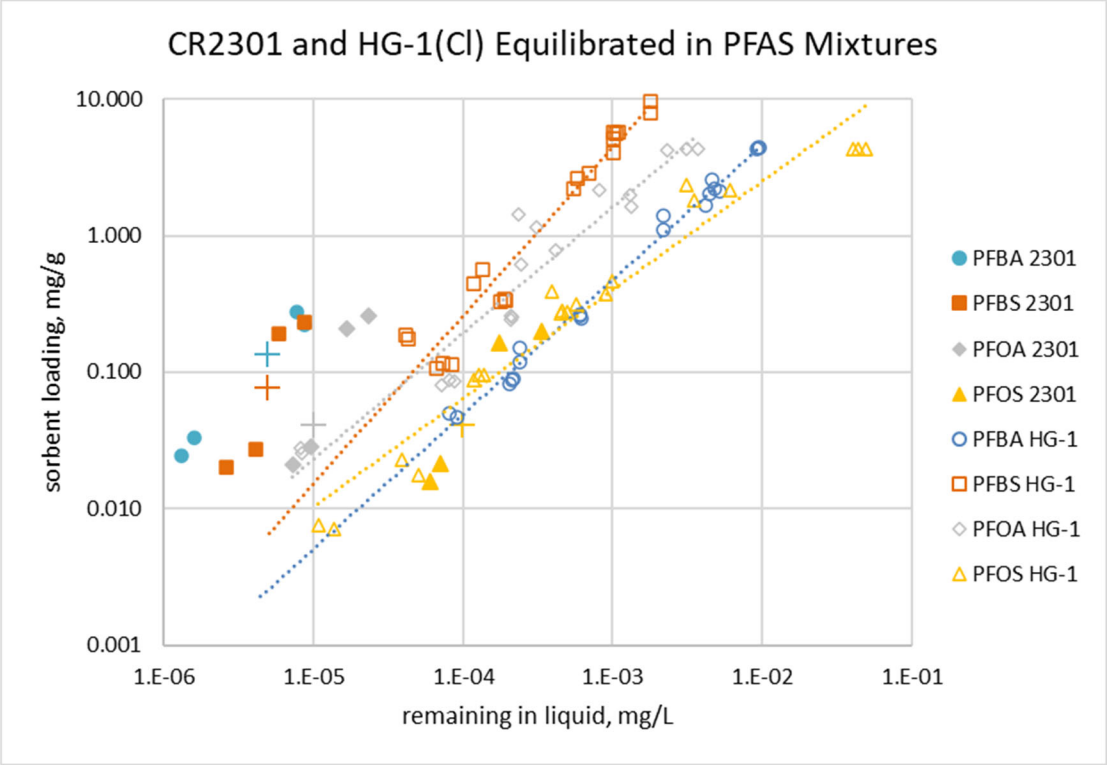

Figure 40 - Comparison of CR2301 Adsorption Data with HG-1(Cl) Isotherms

Best fit lines (not shown) to the CR2301 data have steeper slopes than the HG-1 lines for all four PFAS. The CR2301 slopes are all greater than one. This indicates concave, or type III, isotherms which predict breakthrough curves that broaden as they move through the column (LeVan, Carta, & Yon, 1997), such that low concentrations of the adsorbates may appear well before the full breakthrough curve. Making comparisons in the ppt range, closer to the levels that may be set as maximum acceptable column outlet concentrations, is therefore appropriate.

Table 26 - PFAS in AFFF-Impacted Well Water After 24 h Adsorption by HG-1(Cl)

mg sorbent	*0 mg*	*10 mg*	*10 mg*	*10 mg*	*20 mg*	*20 mg*	*20 mg*
PFBA	68.8	65.4	68.1	63.7	60.2	64.0	61.0
PFMPA	0.491	0.464	0.563	0.509	0.469	0.465	0.423
PFPeA	119	106	116	105	96.2	96.9	87.6
PFBS	76.7	52.2	53.5	41.5	26.7	33.8	27.4
PFMBA	0.484	0.510	0.520	0.470	0.408	0.465	0.373
4-2FTS	0.380	0.428	0.642	0.482	0.532	0.482	0.432
PFHxA	187	152	155	148	107	120	99.6
PFPeS	69.4	37.0	38.5	27.8	15.6	28.6	16.0
HFPO-DA	0.897	0.829	0.875	0.801	0.661	0.797	0.732
PFHpA	68.9	44.7	44.4	37.4	23.3	33.4	23.2
5-3 FTCA	1.24	1.31	0.998	0.757	0.945	0.880	0.785
PFHxS	423	130	123	85.3	48.8	91.8	50.0
6-2FTS	171	117	116	105	71.0	86.5	76.3
PFOA	160	72.8	64.4	56.6	34.7	49.8	35.4
PFHpS	31.2	7.38	7.06	5.12	2.90	6.97	3.18
PFNA	9.92	4.17	3.84	3.13	1.82	3.37	1.99
PFOS	1309	307	265	221	117	247	106
8-2FTS	16.6	10.5	9.56	8.38	6.06	8.36	5.67
PFDA	1.95	0.841	0.804	0.681	0.404	0.662	0.348
PFOSA	3.00	1.58	1.44	1.14	0.710	1.28	0.628
PFUnA	0.325	0.234	0.192	0.177	0.118	0.125	0.0767
mg sorbent	*0 mg*	*30 mg*	*30 mg*	*30 mg*	*50 mg*	*50 mg*	*50 mg*
PFBA	67.6	54.2	54.9	53.6	45.7	48.0	44.6
PFMPA	0.488	0.396	0.407	0.379	0.332	0.335	0.288
PFPeA	121	80.6	72.9	73.2	58.6	59.9	57.3
PFBS	78.9	20.1	17.6	17.3	12.2	14.2	12.6
PFMBA	0.442	0.365	0.326	0.334	0.251	0.278	0.233
4-2FTS	0.476	0.519			0.360		
PFHxA	189	85.9	72.9	69.4	59.0	59.8	52.0
PFPeS	71.8	12.0	10.3	8.18	6.53	7.84	7.37
HFPO-DA	0.940	0.502	0.654	0.535	0.490	0.579	0.481
PFHpA	63.5	17.4	15.8	13.0	11.2	11.7	11.1
5-3 FTCA	1.25	0.685	0.699	0.556	0.510	0.698	0.648
PFHxS	421	37.8	43.3	28.7	23.5	31.6	27.8
6-2FTS	150	57.7	48.6	47.0	39.2	41.6	36.8
PFOA	154	25.6	25.2	19.8	15.8	19.7	15.8
PFHpS	31.5	2.30	2.70	1.68	1.26	2.04	1.44
PFNA	9.85	1.34	1.43	1.11	0.831	1.21	0.832
PFOS	1364	85.7	103	61.7	61.2	78.4	49.4
8-2FTS	16.0	4.07	5.21	3.65	2.76	3.93	2.25
PFDA	1.72	0.311	0.320	0.245	0.206	0.325	0.193
PFOSA	3.00	0.620	0.519	0.478	0.394	0.445	0.295
PFUnA	0.307	0.0535	0.101	0.0704	0.0539	0.0552	0.0394

Table 26 provides the data underlying **Figure 25** and **Figure 26**.

Appendix 2 – Ionomer Structure, Synthesis and Properties

Our Ionomers are pharmaceutically acceptable crosslinked water insoluble polyamine polyelectrolyte ammonium salts (ionomers) that were developed as cholesterol lowering agents. A group of scientists at the Center for PFAS Solutions hypothesized that such ionomers would have the required structural features to sorb PFAS. It was also recognized that by choosing the monomers and the process conditions the following properties can be incorporated: (i) provision of a molecular environment in the polyamines that balances lipophilic and hydrophilic forces to attract amphiphilic PFAS molecules; (ii) ability to tune the chain length of lipophilic blocks to match the chain length of the PFAS molecules; and (iii) ability to desorb and reuse them.

Structure

The structure of the ionomer labelled HG-1 given below serves as an example of the versatility provided by the ionomers. The figure is representative, but not definitive of the ionomer's full, three-dimensional network structure. In HG-1 the amine sites are distanced by 6 and 10 carbons. In the polymer labelled HG-5 the amine sites are distanced by 2 and 10 carbons. Design logic was that HG-5 would sorb short chain PFAS because of the smaller "cage" size.

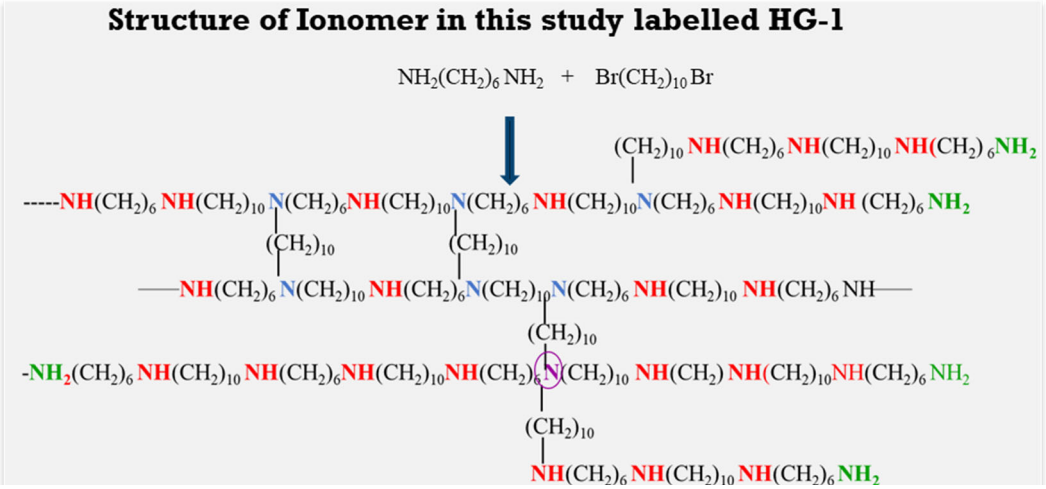

Figure 41 - Representative Ionomer Structure

One of the key properties used to screen these ionomers is swell in water. We measured swell as the mass of water sorbed by a given mass of polymer (e.g. g of water/g of polymer). HG-5 was found to have excessive swell (swell factor 50). It was difficult to process and dry for use. Other combinations of monomers were synthesized and screened for PFOA sorption rates. HG-1 was selected for optimum yield, ease of synthesis and swell.

Patent application US2022/0088570A (Coleman-Kammula et. al., 2022) describes several ionomer grades synthesized and tested. HG-1 was the investigation focus during this limited scope project, but this body of knowledge serves to support further work that can optimize costs, adsorption, and desorption performance.

Synthesis

The following procedure was used to produce HG-1. Into a flask equipped with an overhead stirrer, reflux condenser, and nitrogen port were added 120 ml each of methanol and dimethyl formamide, 38.7 grams of hexamethylene diamine, and 100 grams of dibromodecane. The resulting homogeneous solution was stirred rapidly at reflux. After an hour the solution became viscous. Stirring was halted, and the flask held at 25-40 °C for a minimum of 18 h to allow cross-linking. The resulting product was broken with a spatula, then chopped in a blender in the presence of aqueous ammonium hydroxide, washed with water and then methanol, acidified with aqueous hydrochloric acid, and washed with water and finally ethanol, until a neutral filtrate was detected. Treatment with base at pH ~10 neutralizes the ionic ammonium groups to free amines, and the polymer de-swells. Highly pure polymer is obtained by alternate swelling and deswelling with aqueous base and acid along with washing with polar organics (e.g. methanol or ethanol). The product was then dried in a vacuum oven with a nitrogen purge at 60 °C, and the resulting hard product was cryogenically ground. Repeated swell by acidification with aqueous hydrochloric acid followed by de-swell with ammonium hydroxide removes the bromide and replaces it with chloride. This product is designated as HG-1(Cl).

HG-1(Br) has the same composition as HG-1 and is made as per the method described above. After stirring was halted and the flask held at 25-40 °C for a minimum of 18 hr to allow cross-linking, the resulting product was broken with a spatula, then chopped in a blender in the presence of aqueous ammonium hydroxide, washed with water and then with methanol. The product was dried and ground. Elemental analysis (CHNX) shows it contains up to 5% Bromine.

The following procedure was used to produce HG-5. Into a flask equipped with an overhead stirrer, reflux condenser, and nitrogen port were added 50 ml each of methanol and dimethyl formamide, 50 grams of polyethyleneimine (molecular weight 600), and 25 grams of dibromodecane. The resulting homogeneous solution was stirred rapidly at reflux. After an hour the solution became viscous. Stirring was halted, and the flask held at 25-40 °C for a minimum of 18 h to allow cross-linking. The resulting product was processed following the same procedure as for HG-1.

Physical and chemical properties of HG-1

The cross-linked nature of the final polymeric product does not allow dissolution or melt processing; therefore, all characterization of the polymer must be carried out either in the dry solid state or the swollen gel state.

^{13}C NMR spectra of HG-1: We had high-field solid-state (150 MHz) NMR run on the ionomer at the university of Delaware. Spectra printed at 6 and 24 hours are shown below.

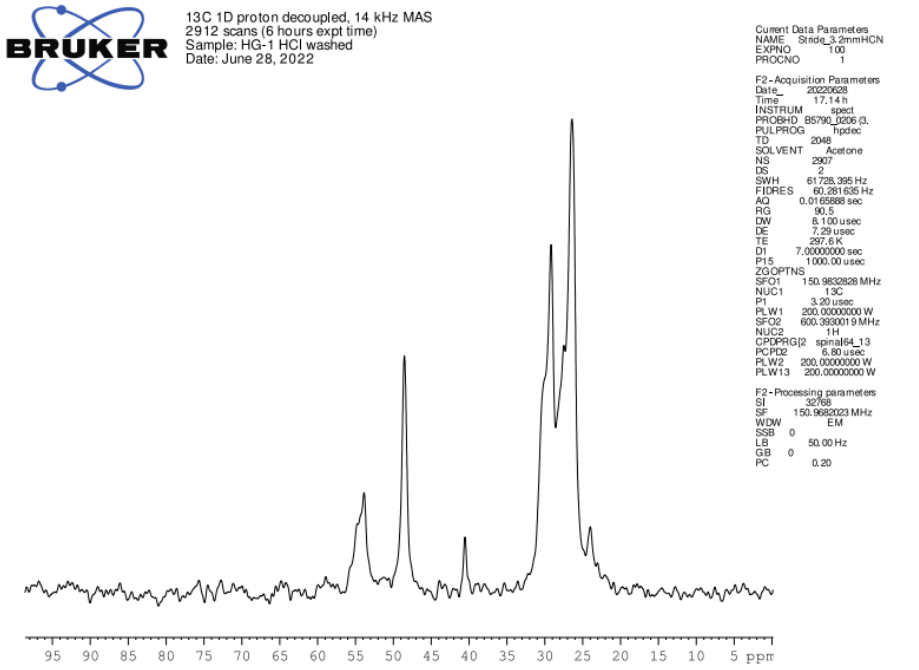

Figure 42 - NMR Spectrum of HG-1 (6 hr)

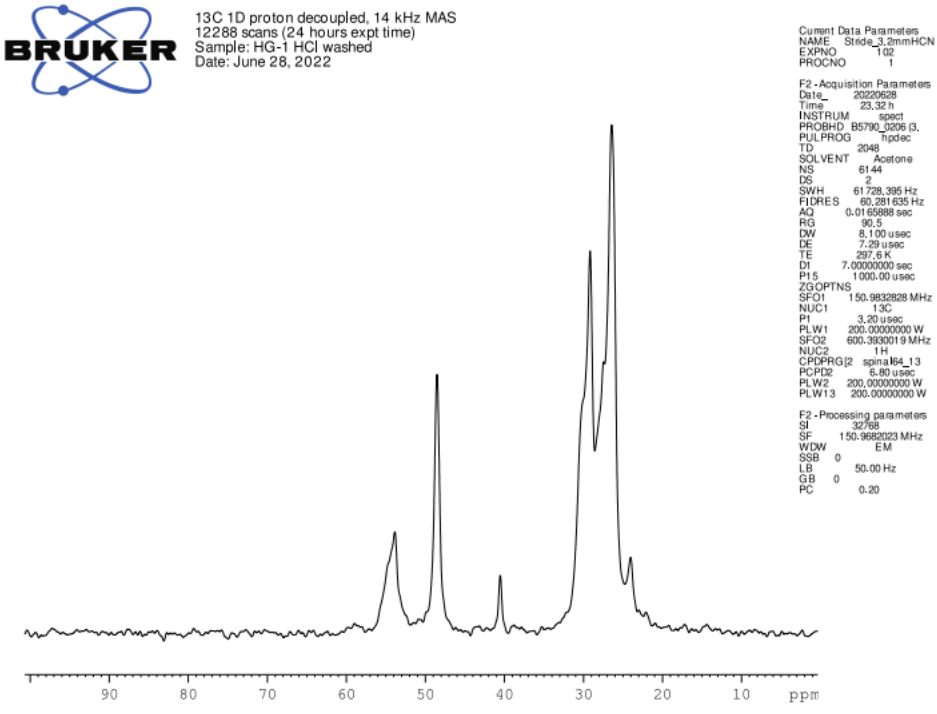

Figure 43 - NMR Spectrum of HG-1 (24 hr)

Table 27 - HG-1 NMR Data

6 hours scan time

Object	Integral [abs]	Integral [rel]	ν(F1) [ppm]	Integrated Region		
Integral 1	45702262.85	1.9341	50.125	64.545	35.705	full region
Integral 2	1333300.13	0.0564	59.0389	61.598	56.480	quaternary
Integral 3	17052330.6	0.7217	54.994	58.153	51.835	tertiary
Integral 4	23629142.15	1	48.3647	51.860	44.869	secondary
Integral 5	3673328.14	0.1555	40.4496	43.071	37.828	primary

12 hours scan time

Object	Integral [abs]	Integral [rel]	ν(F1) [ppm]	Integrated Region		
Integral 1	93418844.04	1.8969	50.1325	64.562	35.703	full region
Integral 2	1781868.27	0.0362	59.045	61.609	56.481	quaternary
Integral 3	38719164.01	0.7862	54.4948	58.146	50.844	tertiary
Integral 4	49247046.02	1	48.8708	51.864	45.878	secondary
Integral 5	7553245.93	0.1534	40.455	43.086	37.824	primary

24 hours scan time

Object	Integral [abs]	Integral [rel]	ν(F1) [ppm]	Integrated Region		
Integral 1	194466023.7	1.9439	50.1299	64.553	35.706	full region
Integral 2	5361787.01	0.0536	59.0404	61.605	56.476	quaternary
Integral 3	76228008.66	0.762	54.489	58.143	50.835	tertiary
Integral 4	100037912.2	1	48.367	51.861	44.873	secondary
Integral 5	17250915.64	0.1724	40.4501	43.078	37.822	primary

The ratios of types of nitrogen calculated from integration of the relevant signals gave the following numbers:

Table 28 - Amine Types (%) from NMR Data

	6h	12h	24h	Average
Quaternary	1.5	1.0	1.4	1.3
Tertiary	26.4	28.3	27.0	27.2
Secondary	54.9	54.1	53.2	54.1
Primary	17.1	16.6	18.3	17.3

Toxicity of HG-1

STRIDE did not conduct toxicity tests but one of the STRIDE team members was part of the group that developed these products**.** HG-1 had the code DMP 504. It was taken into clinical trials in humans. A paper published in the journal Drug Development Research (Hainer, et al., 1997) speaks to the safety of the material and its efficacy, from which we quote.

"This multiple-dose study of DMP 504, a hydrogel bile acid sequestrant, employed a randomized, double-blind, sequential-cohort design with placebo (blinded) and open-label cholestyramine (CS) controls. Ninety-three healthy primary hypercholesterolemic subjects (serum LDL cholesterol 130 to 200 mg/dL; triglycerides ≤280 mg/dL) maintaining a stable diet (NCEP Step One) for 3 weeks received either DMP 504 or placebo DMP 504 in capsules, or CS powder for suspension (16 g/d). The DMP 504 dose (0.9, 1.8, 2.7, 3.6, 5.4, 7.2 g/d) escalated with sequential enrollment of cohorts (DMP 504 n = 10, placebo n = 2, and CS n = 3 for Cohorts I–V; DMP 504 n = 8, placebo n = 2 for Cohort VI). An additional cohort (VII) included DMP 504 3.6 g/d, n = 9, and placebo, n = 2.

. . . There was no dose-limiting toxicity with DMP 504. One subject (DMP 504 2.7 g/d) withdrew because of gastrointestinal disturbance."

Breakdown products before and after use and impact on water chemistry:

Before use: During the finishing step of HG-1, is subject to repeated washes of base and acid. Treatment with base at pH ∼10 neutralizes the ionic ammonium groups to free amines, and the polymer de-swells. Highly pure polymer is obtained by alternate swelling and deswelling with aqueous base and acid along with washing with polar organics (e.g. methanol or ethanol) as described above. The two monomers, dibromodecane being soluble in methanol is removed during this wash and hexamethylene diamine, being water soluble, is also removed.

Breakdown products during use and impact on water quality: There was a question about formation of nitrosamines from amine-containing sorbents during the August 2023 SERDP meeting.

Nitrosamines are a family of chemical carcinogens including, among others, n-nitrosodimethylamine (NDMA), n-nitrosodiethylamine (NDEA), n-nitrosodi-n-propylamine (NDPA) and n-nitrosodi-n-butylamine (NDBA). Use of anion exchange resins has been linked to

the presence of nitrosamines in treated drinking water. In bench-scale batch and column experiments, anion exchange resins from a large, representative group were investigated by others (Flowers & Singer, 2013). Several resins were found to release high levels (up to >2000 ng/L, orders of magnitude above drinking water regulatory levels) of nitrosamines upon initial rinsing with lab-grade water, with levels subsiding within 50-100 bed volumes of rinsing. Resins released similarly high levels of nitrosamine precursors, with spikes in precursor release triggered by regeneration of resins with sodium chloride or by interruptions in flow resulting in prolonged contact times. Free chlorine or preformed monochloramine in feed water were shown to lead to the production of nitrosamines.

Anion exchange resins are synthesized using trimethylamine (TMA), triethylamine (TEA), tri-n-propylamine (TPA) or tri-n-butylamine (TBA) and they can react with chloramines to form NDMA, NDEA, NDPA and NDBA, respectively. The authors proposed a pathway to NDMA for formation from pendant dimethylamino groups bound to polystyrene divinyl benzene ion exchange resins. This is shown in the figure below. Anion exchange resins consist of polymers such as polystyrene with pendant amine groups.

The mechanism in the figure below shows cleavage of dimethyl amine pendant groups and release of NDMA (Flowers & Singer, 2013).

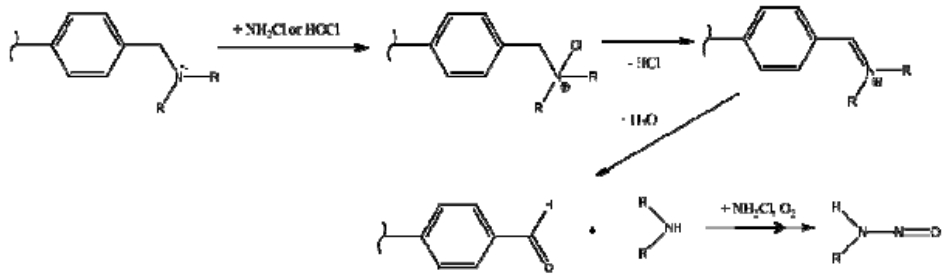

Figure 44 - Mechanism Proposed by Flowers and Singer

Our Ionomers do not have pendant dimethyl amino groups attached to an aromatic ring as is the case with polystyrene based anion resins. HG-1 is a fully aliphatic and polymeric amine. We would expect that reaction of the benzyl amine in anionic resins will be favored over reactions involving only aliphatic groups, which our polymers possess. Additionally, most of our amine groups are buried in the body of the polymer. The only "pendant" amine groups are end groups, which we could cap at the end of the reaction if required. The less reactive amine groups contained in our polymer will have a much lower propensity for chain cleavage and ultimate nitrosamine formation. We cannot rule out the possibility of nitrosamine formation from our polymers, but the formation route from ionomer appears more difficult than from traditional anion resins and we expect that any formation will be in much lower concentrations for any given time frame.

After use: We have some data on ionomer *performance* after use from adsorb-desorb experiments using HG-1. See Task 2, “Demonstration of Ionomer Re-use After Desorption”. We have not investigated if the desorbed ionomer, after a certain number of cycles, is devoid of PFAS. Further

studies could show whether, at the "end-of-useful-life," the spent ionomer could be transported as a non-hazardous waste.

Preliminary experiments showed that ~75% (350°C, 1 h, 1M NaOH) and ~85% (250°C, 2.5 h, 1M NaOH) of the HG-1 mass was retrieved following hydrothermal alkaline treatment. The amount recovered could be higher as no attempt was made to collect fine, suspended particles. The finding that HALT does not destroy the ionomer to a significant extent suggests that formation of potential nitrosamine precursors, or other undesirable decomposition products, is expected to be minimal. Future work will further test the stability of spent ionomer under HALT. Note, however, that direct treatment of PFAS-laden ionomer may not be needed, given the good desorption achieved with our all-aqueous PDP and the amenability of this solution to HALT treatment.